1984

Nonlinear finite element analysis of piles in integral abutment bridges

Pe-Shen Yang
Iowa State University

Yang, Pe-Shen

NONLINEAR FINITE ELEMENT ANALYSIS OF PILES IN INTEGRAL ABUTMENT BRIDGES

Iowa State University PH.D. 1984

Nonlinear finite element analysis of piles in integral abutment bridges

by

Pe-Shen Yang

A Dissertation Submitted to the
Graduate Faculty in Partial Fulfillment of the
Requirements for the Degree of
DOCTOR OF PHILOSOPHY

Department: Civil Engineering
Major: Structural Engineering

Approved:

Signature was redacted for privacy.

In Charge of Major Work

Signature was redacted for privacy.

For the Major Depdrtment

Signature was redacted for privacy.

For the Graduate College

Iowa State University
Ames, Iowa

1984

TABLE OF CONTENTS

LIST OF TABLES

LIST OF FIGURES

1. INTRODUCTION

1.1 Statement of the Problem

The increasing popularity of integral abutment designs for bridges has been recognized by many state highway agencies. At the present time in Iowa, theoretical piling stresses limit the maximum length of concrete bridges with integral abutments to 265 feet. Although the performance of these bridges has certainly been satisfactory, other states, e.g., South Dakota and Tennessee, have been allowing integral abutment bridges significantly longer than this with apparent success. Long bridges are particularly susceptible to damage from thermal expansion and contraction because of the relatively large displacements associated with annual temperature variations. Historically, a system of expansion joints, roller supports and other structural releases are provided on longer bridges to permit thermal expansion. However, providing expansion devices on bridges not only increases the initial cost of construction, but also increases associated maintenance costs and, frequently, they do not operate as intended.

Integral abutment bridges provide an attractive design alternative because expansion joints are not present. Thermal expansion, however, must be relieved or accounted for in some manner. In an integral abutment bridge, the piles are usually the most flexible elements and are expected to accommodate the induced movements due to thermal expansion. The maximum thermal expansion which can be allowed by the piles without reducing the vertical load carrying capacity of the pile is of primary importance in defining the safe length of integral abutment bridges. If this length

can safely be increased, the economic advantages of integral abutments can be realized for longer bridges.

Integral abutment bridges fall into two categories: nonskewed and skewed. Site conditions determine whether or not a skewed bridge is necessary. The design of a skewed bridge presents detailing and analysis problems. For skewed bridges with integral abutments, the movements caused by thermal expansion and contraction are more complex than they are for nonskewed bridges with integral abutments. These thermal-induced movements involve not only the longitudinal direction, but transverse direction as well.

1.2. Background

Prior to World War II, most bridges with an overall length of 50 feet or more were constructed with some form of expansion joints. Periodic inspection of these bridges revealed that expansion joints tended to freeze and close and did not operate as intended. Close inspection of such bridges also indicated that there was no serious distress associated with the frozen or closed expansion joints. This led to the advancement of the case for continuous construction.

Continuity in steel stringer and other types of bridges has been accepted practice since the early 1900s. In addition to the inherent economy of continuous beams, wherein negative moments over interior supports serve to reduce midspan positive moments, one line of bearing devices was automatically eliminated at each interior support. The predominant problem with these continuous bridges was at the abutments, where some kind of expansion joints were required. An example of a bridge with expansion

joints is shown in Fig. 1. The expansion joints at the abutments allowed penetration of water from the backfill and roadway into the bearing areas and onto bridge seats. The joint could then be forced closed, resulting in broken backwalls, sheared anchor bolts, damaged roadway expansion devices and other problems. Maintenance costs associated with these problems accelerated the development of integral abutments.

Fig. 2 shows an example of a bridge with integral abutments, each abutment is supported by a single row of vertical piles extending into the abutments. In addition to being aesthetically pleasing, integral abutments offer the advantage of lower initial cost and lower maintenance costs. Expensive bearings, joint material, piles for horizontal earth loads and leakage of water through the joints are all eliminated.

Today more than half of the state highway agencies have developed design criteria for bridges without expansion joint devices. These design criteria are based on years of experince. This development led to wide variations in design criteria from state to state. At this time, full-scale field testing and sophisticated rational design methods are not commonly used as a basis for increasing allowable lengths.

In 1974, the difference in maximum allowable length for concrete bridges using integral abutments between Kansas and Missouri was 200 feet [1]. A survey conducted by the University of Missouri in 1973 [2] indicated that the allowable length for integral abutment concrete bridges in some states was 500 feet while in others it was only 100 feet. Continuous steel bridges with integral abutments have performed successfully for years in the 300-foot range in such states as North Dakota, South Dakota and Tennessee. Continuous concrete structures 500-600 feet long with

integral abutments have been constructed in Kansas, California, Colorado and Tennessee [3].

1.3. Objective and Scope

The purpose of this study is to investigate the effect of thermal-induced movement of the pile on the vertical carrying capacity of the pile in integral abutment bridges.

As part of this study the highway departments of all states in the U.S. were contacted to find the extent of application of integral abutment bridges and to survey the different guidelines used for analysis and design of integral abutment bridges.

An algorithm based upon a nonlinear finite element procedure is developed to study the soil-pile interaction in integral abutment bridges. The finite element idealization consists of a one-dimensional idealization for the pile and nonlinear springs for the foundation. Incremental finite elements with an updated Lagrangian formulation and material nonlinearities are used. For the purpose of treating arbitrary large rotations in three dimensions, node orientations are described by unit vectors. Deformations are defined by the orientation of these vectors relative to a rigid body element coordinate which is along the beam chord. Updating of the element coordinates in three dimensions is also described. An incremental and iterative procedure is used for the solution of the nonlinear problem. The IAB2D and IAB3D (Integral Abutment Bridge Two- and Three-Dimensional) computer programs are developed to solve the nonlinear soil-pile interaction problems for both three- and two-

dimensional cases. A number of experimental and analytical examples are analyzed to establish their reliability.

Finally, many analytical examples are studied in which a pile is given a lateral displacement to simulate the bridge expansion. A real integral abutment bridge is used to study the effect of skew and nonskew on the vertical carrying capacity of the pile.

2. SURVEY OF CURRENT PRACTICE FOR BRIDGES WITH INTEGRAL ABUTMENTS

2.1. Objectives

As background to the theoretical investigation of bridges with integral abutments, a survey of several states was made to obtain information on the design and performances of such bridges.

2.2 Method of Investigation

Surveys concerning integral abutments have previously been conducted [1, 2]. Responses indicate that most highway department agencies establish their own limitations and criteria in designing integral abutments. The bases of these limitations and criteria are shown to be primarily empirical.

Two survey questionnaires were prepared in cooperation with the Office of Bridge Design, Highway Division, Iowa Department of Transportation, to obtain information concerning the use and design of integral bridge abutments. The first survey questionnaire was conducted by Bruce Johnson [4, 5]. The survey questions were directed at limitations in bridge length, type and skew. The states were also asked what assumptions were made in determining fixity conditions and loads for design of the piling and superstructure. The questionnaire was sent to the 50 states and Puerto Rico. A questionnaire was also sent to the Direct Construction Office, Region 15, Federal Highway Administration (FHWA). A copy of this questionnaire and response from each of these agencies are contained in Appendix A. The second survey questionnaire which was based on the responses obtained by the first survey questionnaire was prepared and conducted by Yang [6]. These survey questions concerned pile orientations

in the integral abutments. The states were also asked what structural assumptions were being made in determining fixity conditions on pile head and directions of thermal expansion and contraction of the integral abutments in skewed bridges. In addition, other questions related to the treatment of approach slab, backfill, and pile cap. This questionnaire was sent to the 28 state highway departments and the Direct Construction Office of FHWA, Region 15 who use integral abutments. A copy of this questionnaire and responses from each of these agencies are contained in Appendix B.

2.3. Trends of Responses

2.3.1. Survey conducted by Bruce Johnson

Of the 52 responses received, 29 indicated that their states use integral-type abutments. A few of these, such as New Mexico and Virginia, are just beginning to use them: their first integral abutment bridge was either recently designed or currently under construction.

Of the 23 who did not use these abutments, there were four groups having similar responses.

- Fourteen states have no plans to consider using this type of abutment.
- Five states responded that they have not previously considered the possibility of fixing the girder ends to the abutments.
- Three states have built some integral abutments or semi-integral endwalls but currently do not use them in new bridge construction.

- Three states have built some integral abutments or semi-integral endwalls but currently do not use them in new bridge construction.
- One state indicated that they were presently investigating the possibility of using integral abutments.

The following are some of the reasons given for avoiding the use of integral abutments.

- The possibility of a gap forming between the backwall and the roadway fill (two states):
- Increased substructure loads (one state);
- The possible attenuation of a bump at the ends of the bridge (one state);
- The lack of a rational method for predicting behavior (one state);
- The possible additional stress on approach pavement joints (two states); and
- Cracking of the backwall due to superstructure end span rotation and contraction (two states);

The following is a discussion, keyed to the survey question numbers, of the responses received from states using integral abutments (See Appendix A).

1. Most of the states using integral abutments do so because of cost savings. Typical designs use less piling, have simpler construction details, and eliminate expensive expansion joints.

2 and 3. Table 1 shows bridge length limitations currently being used. In summary, 70 percent or more of those states using integral abutments feel comfortable within the following range of limitations: steel, 200-300 feet; concrete, 300-400 feet; and prestressed concrete,

300-450 feet. The difference in concrete and steel length limitations reflects the greater propensity of steel to react to temperature changes. There are three states using longer limitations for each structure type. They typically have been building integral abutments longer than most states and have had good success with them. The move toward longer bridges is an attempt to achieve the good performance observed on shorter bridges for structures at the maximum practical length limit.

4. Only a few states responded to the question regarding limitations on piling. Five states use only steel piling with integral abutments. Only four of the 29 agencies indicated that the webs of steel piles were placed perpendicular to the length of the bridge. At least one state began using integral abutments with steel piling placed in the usual orientation (with the pile web along the length of the bridge). This led to distress and cracking at the beam-abutment interface, and the state eventually began to rotate the piles by 90 degrees for greater flexibility. Three others allow concrete and steel but not timber. No length limitations for timber piling were given by states other than Iowa which allows bridges less than 200 feet.

5 and 6. Twenty-two states indicated that the superstructure was assumed pinned at the abutments. Five assumed partial fixity, and one assumed total fixity. Seventeen responses noted that at the pile top a pinned assumption was made; four reported a partial fixity assumption; and five states believe the pile top is totally fixed. Six of the states

which assume a pinned condition actually use a detail designed to eliminate moment constraint at the joint.

7. Only a few states consider thermal, shrinkage, and soil pressure forces when calculating pile loads. Several states noted on the questionnaire that only vertical loads are used in design. Of those that do consider pile bending stresses, eight use thermal forces, three use shrinkage forces, and ten consider soil pressure.
8. Most states indicated that bending stresses in abutment pilings were neglected. There were three states, however, that assumed a location for a point of zero moment and used combined bending and axial stresses. Also, prebored holes were used by three states to limit bending stresses by reducing the soil pressure.
9. Most states indicated that a free-draining backfill material is used behind the abutment. Some responses, however, indicated that problems were encountered such as undermining associated with granular soils. One state said, "Have recently experienced problems with noncohesive material behind this type of abutment. Backfill material should be cohesive and free from cobbles and boulders." Six other states use common roadway fill behind the abutment.
10. All except four states rest the approach pavement on the integral abutment. One state indicated that a positive tie connection was used to connect the slab. A few states indicated that they had experienced problems when reinforced approach slabs were not used.

11. All except three states reported lower construction and maintenance costs using integral abutments. One said costs were the same, and two did not respond to the question.

The following are some isolated comments that were made about construction and maintenance problems using integral abutments:

a. Longer wingwalls may be necessary with cast-in-place, post-tensioned bridges for backwall containment;

b. The proper compaction of backfill material is critical;

c. Careful consideration of drainage at the end of the bridge is necessary;

d. Wingwall concrete should be placed after stressing of cast-in-place, post-tensioned bridges;

e. The effects of elastic shortening after post-tensioning should be carefully considered, especially on single span bridges;

f. Proper placement of piles is more critical than for conventional abutments;

g. Wingwalls may need to be designed for heavier loads to prevent cracking;

h. Adequate pressure relief joints should be provided in the approach pavement to avoid interference with the functioning of the abutment;

i. Possible negative friction forces on the piles should be accounted for in the design; and

j. Wide bridges on high skew require special consideration including strengthening of diaphragms and wingwall-to-abutment connections.

2.3.2. Survey conducted by Yang

Of the 28 responses received, 26 indicated the use of integral abutments on skewed bridges. Among these states, Virginia has designed its first integral abutment skewed bridge with a small skew (10°) and a relatively small anticipated movement at each abutment (± 3/8"). The states of Connecticut and Oklahoma indicated that they do not use integral abutments on skewed bridges. While Connecticut has not constructed any integral abutments on a skew, it has constructed one nonskewed integral abutment bridge. Oklahoma, in contrast, considered integral abutments on skews inappropriate because of integral abutment displacement.

One of the purposes of this survey was to collect methods of analysis and design details of integral abutments on skew bridges. Following is a discussion, keyed to survey question numbers, of the responses received from states using integral abutments on skewed bridges (also see Appendix B).

1. The pile orientations in integral abutments on skewed bridges shown in the first survey question can be classified into four categories: (1) the web of the pile perpendicular to roadway center line (6 states); (2) the web of the pile parallel to roadway center line (1 state); (3) The web of the pile parallel to center line of the abutment (10 states); (4) the web of the pile perpendicular to center line of the abutment (15 states). In addition, three states use circular piles in integral abutments on skewed bridges. One major difference between skewed and nonskewed integral abutment bridges is that when both are subjected to thermal expansion and contraction, the former piles will

experience biaxial bending. The responses showed that 15 of 26 states have adopted the pile orientation so that bending will be primarily about the strong axis.

Most states do not have any clear, theoretical, experimental, or empirical bases for selection pile orientations. Idaho officials assumed some creep in the soils surrounding the piles and also assumed that a redistribution of stresses will occur since thermal forces are generally applied gradually. Also, the restraint provided by the integral abutment was assumed to reduce the magnitude of the thermal movement; orienting the piles with the strong axis parallel to the center line of the bearings was assumed to give more rigidity for earthquate loads when liquification of embankment is anticipated. Vermont oriented the piles to resist the force of earth pressure from the abutment backfill rather than permit the thermal expansion. California explained its policy of orienting the web of the piles perpendicular to the center line of the abutment (see Appendix B) as follows: for a square bridge, such orientation of piles results in bending about the strong axis of the piles because of both thermal forces and active soil pressure. When the bridge is skewed, however, temperature forces act along the center line of the roadway, not parallel to the pile web, and active soil pressure acts against the strong axis of the pile. Temperature effects are somewhat compensated for by predrilling for driven piles and filling the voids with pea gravel or sand [6].

Colorado replied that they were unaware of any distress in the piling. In a few cases, with cast-in-place post-tensioned bridges

with integral abutments, cracks have been detected in the abutment wall at the intersection of the superstructure and the abutment. The state suspected that the cracks resulted primarily from movements of the superstructure caused by elastic shortening and creep from the post-tensioning forces. North Dakota has been building bridges for about 18 years using this method and so far is unaware of any problems. According to Iowa bridge engineer H. Gee cited in [6], pile orientation with the web of the pile perpendicular to the roadway center line is not considered in design because of construction work difficulty in arranging the reinforcement in the integral abutments. Thermal-induced biaxial bending stresses on piles can be avoided by using circular pipe piles. The major disadvantages are that the vertical bearing capacities of these piles are usually less than those of the steel H piles, and they are stiffer than H piles about the weak axis.

2. The second survey question revealed the following. (1): Two states indicated that a roller assumption was made at the pile top; eight reported a pinned assumption; one assumed partial fixity; and eight states assumed a totally fixed pile top. These assumptions were actually based on the restraint conditions on the pile top. In Iowa, the pile top is completely restrained by spiral reinforcement in the pile cap, and total fixity is assumed. For a pinned assumption, the top portion of piling is enclosed with a flexible material before casting in the concrete abutment [6]. (2) and (3): Only a few states consider thermal, shrinking and soil pressure forces when calculating

pile loads. Following are some of the remarks made by various states regarding thermal effects in integral abutments on skewed bridges:

- Assume that the pile is fixed a certain depth below the bottom of the pile cap and any thermal movement is accomplished by bending in the pile.
- Thermal expansion parallel to the pile cap can be resisted by the friction force between the backfill and the end wall.
- The battered piles are adopted in the integral abutments to resist thermal movement.
- Shear keys are used on the bottom of the pile cap to prevent lateral movement of the pile cap on extreme skews (40° ±).
- If the bridge design has a small skew ($\leq$ 10°) and a relatively small anticipated movement at each abutment (± 3/8"), no special consideration need be given beyond that of a 0° skew condition.

3. Most states indicated that a free-draining granular material is used as backfill behind the abutment. One state uses 1-1/2 feet of porous backfill from subgrade to the bottom of the integral abutment along with 6-inch diameter pipe underdrain. Beyond that, normal job site available material is used. Some responses, however, indicated that backfill compaction has always been something of a problem with settlement just off the end of the bridge. Several states indicated that rigid pile cap has been used, and pile was cast into a pile cap one to two feet long. Two states indicated that the pile cap is designed as a reinforced continuous beam over the piling.

The survey responses show, in general, that the approach slab can be tied to the abutment with dowels and moved back and forth with the superstructure if a construction joint is provided between the approach slab and the bridge slab. South Dakota stated that at least one approach slab panel with curb and gutter section attached to the bridge end is necessary to prevent erosion of the shoulder behind the abutment wing. One state pointed out that while an expansion joint is specified between rigid pavement and the approach slab, no special treatment is specified for flexible pavement. In Colorado, the approach slab was used if the bridge length was over 200 feet.

4. Following are some additonal comments on skewed bridges with integral abutments:

   - Some of the piles in the abutment have to be battered to resist the active earth pressure acting behind the abutment.
   - Rotational forces from the lateral earth pressure on the end walls cause a failure of anchor bolts which connected the exterior girders to the abutments.
   - For a cast-in-place bridge, the ends of steel piles may be cast into the abutment concrete which is reinforced such that it is considered essentially integral.
   - Piles may be prebored for a distance of 5 to 20 feet below the bottom of the pile cap.
   - Since the piles are oriented to allow bending about the weak axis, any stresses caused by rotation will only stress the outmost flange fibers and not the web and center portions of the flanges. When

the abutment is skewed, some twisting may be induced in the piles when the structure deflects, but this problem can be considered negligible.

2.4. Summary and Conclusions

There is wide variation in design assumptions and limitations among the various states in their approach to the use of integral abutments. This is largely due to the empirical basis for development of current design criteria. It is recognized, however, that assumptions concerning end fixity and soil reaction may substantially affect the results. A simple rational method of accurately predicting pile stresses would be valuable to the current state-of-the-art in integral abutment design.

The states that use integral abutments are generally satisifed with performance and believe they are economical. Some problems have been reported, however, concerning secondary effects of inevitable lateral displacements at the abutment. These include abutment, wingwall and pavement distress and backfill erosion. Some states reported that solutions have been developed for most of the ill effects of abutment movements. They include: (1) additional reinforcing and concrete cover in the abutment, (2) more effective permanent joints which allow thermal movements to occur, and (3) positive control of bridge deck and roadway drainage.

For integral abutments on skewed bridges, 15 states orient their piles with the web of the piles perpendicular to the center line of the

abutment so that bending will be primarily about the strong axis. Thus, thermal induced biaxial bending stresses will be introduced into the piles. The survey responses show that most states ignore the thermally induced bending stresses due to transverse and longitudinal thermal movements.

No special treatment is usually given to the backfill and pile cap on skewed bridges, and they might be constructed in the same way as nonskewed bridges. As for the approach slab, it can be tied to the abutment with dowels or an expansion joint may be provided between the approach slab and the bridge slab.

3. SOIL CHARACTERIZATION

3.1. Methods of Analysis

3.1.1. Analytical studies

Analysis and design of laterally and/or axially loaded piles is, primarily, empirical, based on data from full-scale tests of laterally and/or axially loaded piles [7 - 10]. However, in recent years, extensive research and development have been undertaken to predict theoretically the behavior of the laterally and/or axially loaded piles [11 - 16]. In general, two basic approaches have evolved: the subgrade reaction approach and the elastic approach.

The subgrade reaction was originally proposed by Winkler in 1867 when he represented the soil as a series of unconnected linear elastic springs as shown in Fig. 3. In this method, the continuous nature of the soil medium is ignored. Such factors as nonlinearity, variation of soil stiffness with depth and layering of soil profile can be incorporated into the method [13]. Several methods have been used to account for soil nonlinearity [17 - 19], including an elastic-plastic Winkler model [17]. One of the more widely used approaches has been proposed by Reese et al. [19 - 23] by using a number of soil resistance-displacement curves for the soil at various points along the pile.

The elastic approach in which the soil is considered as an elastic continuum has been described by several investigators [15, 24 - 28]. In most of these approaches, the pile is divided into a number of uniformly loaded elements, and a solution is obtained by imposing compatibility between the displacements of the pile and the adjacent soil for each

element of the pile. The elastic method can also be used to give approximate solutions for variations in soil modulus with depth and for layer systems [13].

A versatile method of analysis which permits the inclusion of all the factors mentioned above and also makes a three-dimensional formulation possible is the finite element method. A detailed description of the finite element formulation used in the study is given in Chapter 4. Input from many of the above investigators has been used in formulating the model.

3.1.2. Experimental studies

Numerous experimental research projects on piles subjected to vertical and/or lateral loading in the laboratory or field have been performed in recent years. Seed and Reese studied a small, displacement-type friction pile which was driven into a nonsensitive clay. In that study, the load-distribution curves and load-slip curves (f-z curves) for a friction pile were first defined [23]. Matlock [20], Reese and Welch [21], and Reese, Cox, and Koop [22] also performed experimental work on soft clay stiff clay, and sand, respectively, to predict lateral resistance-displacement curves (p-y curves) for laterally loaded piles. A curve describing the load-settlement behavior of the pile tip was given by Vijayvergiya [29]. Numerous methods exist for predicting these curves for different soil types. A brief discussion of some of these methods is given in [30]. Some of these results will be compared to the results from the finite element model in Chapter 6.

Many tests on instrumented piles subjected to vertical and/or lateral loading in the field or laboratory have been performed [31 - 34]. In March, 1973, a full-scale model representing the end portion of a typical highway bridge was constructed and tested in four construction stages by South Dakota State University [1]. During each stage, the test specimen was subjected to a series of predetermined longitudinal movements via hydraulic jacks to simulate expansion and contraction caused by temperature changes. In August, 1979, an operational county road bridge near Fargo, North Dakota was instrumented and monitored for temperature-induced stresses by North Dakota State University [35]. This study was being conducted by J. Jorgenson, Chairman of the Civil Engineering Department, and is sponsored by the State Highway Department. During one year of observation, monthly readings were taken on the length of the bridge, the gap between backfill and backside of the abutment, etc.

3.2. Material Idealization

3.2.1. General

The soil characteristics in the soil-pile problem can be described by three types of soil resistance-displacement models as shown in Fig. 3: lateral resistance-displacement (p-y) curves; longitudinal load-slip (f-z) curves; and pile tip load-settlement (q-z) curves. The p-y curves represent the relationship between the lateral soil pressure against the pile (force per unit length of pile) and the corresponding lateral pile displacement. The f-z curves describe the relationship between skin friction (force per unit length of pile) and the relative vertical displacement between the pile and the soil. The q-z curves describe the

relationship between the bearing stress at the pile tip and the pile tip settlement. The total pile tip force is q times the effective pile tip area. All three types of curves assume the soil behavior to be nonlinear and can be developed from basic soil parameters.

3.2.2. Modified Ramberg-Osgood model

The modified Ramberg-Osgood model [36], as shown in Eq. (3.1) in the form of a p-y curve, will be used to approximate the p-y, f-z, and q-z soil resistance-displacement curves and the material behavior of the pile (e.g., stress-strain relations).

$$p = \frac{k_h y}{\left(1 + \left|\frac{y}{y_u}\right|^n\right)^{1/n}} \tag{3.1}$$

$$y_u = \frac{p_u}{k_h} \tag{3.2}$$

in which

k_h = initial lateral stiffness

p = generalized soil resistance

p_u = ultimate lateral soil resistance

n = shape parameter (see Fig. 5)

y = generalized displacement

This model is found to be better than the procedures in which the tangent modulus is computed as the chord slope between two data points on a curve and the use of functions such as hyperbola, parabola, and splines; in fact, the model proposed herein includes hyperbola as a special case [36]. Nonlinear behavior models for symmetrical or periodic loadings have been presented by a number of workers [37-41]. The constants needed in Eq. (3.1) can be determined from equations presented in the following sections. Fig. 4 shows the modified Ramberg-Osgood curve for a typical p-y curve. Similar equations for a typical f-z curve (using f_{max}, the maximum shear stress developed between the pile and soil, and k_v, the initial vertical stiffness) or a typical q-z curve (using q_{max}, the maximum bearing stress at the pile tip, and k_q, the initial point stiffness) will be used. Fig. 5 shows the effect of the shape parameter n on the soil resistance-displacement behavior.

3.2.3. Cyclic model

Because of annual temperature changes, a bridge superstructure undergoes expansion and contraction, which in turn causes the piles in integral abutment bridges to move back and forth. A modified Ramberg-Osgood cyclic model for both symmetrical and irregular cylic loadings is proposed

$$p = p_c + \frac{k_h(y - y_c)}{\left[1 + \left(\frac{1}{c}\left|\frac{y - y_c}{y_u}\right|\right)^n\right]^{1/n}} \tag{3.3}$$

where

$$c = \pm\left|1 - \frac{p_c}{p_u}\right| \tag{3.4}$$

and also

p_c = the soil resistance at the previous reversal.

y_c = the soil displacement at the previous reversal.

The expression for the tangent modulus is obtained by differentiating Eq. (3.3) with respect to displacement y

$$k_{ht} = \frac{k_h}{\left[1 + \left(\frac{1}{c}\left|\frac{y - y_c}{y_u}\right|\right)^n\right]^{\frac{n+1}{n}}} \tag{3.5}$$

Fig. 6 illustrates a typical example of this modified Ramberg-Osgood cyclic model. In this figure, hysteresis loops that model the actual behavior of the pile and soil can be readily constructed by adopting rules presented by Pyke [41]. These rules are stated as: 1) The tangent modulus on each loading reversal assumes a value equal to the initial tangent modulus for the initial loading curves, and 2) the shape of the unloading or reloading curves is the same as that of the initial loading curve, except that the scale is enlarged by a factor of c. This is indicated in Eq. (3.4) in which the first term is negative for unloading and positive for reloading; the maximum and minimum values of the

stress or soil resistance are bounded by the ultimate (reference) stress or soil resistance.

As part of the finite element model to be presented in Chapter 4, the Ramberg-Osgood cyclic model will be required to track through several loading and unloading cycles. The determination of reversal values for loading and unloading of each load increment is obtained by adopting the flow chart in Table 2 (also illustrated in Fig. 7).

3.3. Soil Behavior

3.3.1. Analytical approximations by others

As mentioned before, the soil characteristics in the soil-pile problem can be described by three types of soil resistance-displacement curves; p-y curves; f-z curves; and q-z curves. Numerous methods exist for estimating the parameters for analytical approximations to these curves for different types of soils. A brief discussion on some of these methods follows.

3.3.1.1. Lateral resistance-displacement (p-y) curve Several investigators [20 - 22, 23] have attempted to correlate a lateral load-deflection response with laboratory soil tests. The p-y curves for clay and sand used in the study (Table 3) are believed to represent the current state of the art.

3.3.1.2. Load-slip (f-z) curve Several methods have been proposed for estimating the load-slip behavior of a single pile. The criteria used in this study are those summarized by Ha and O'Neill [42] and are believed to present the current state of the art. The analytical forms of f-z curves and their parameters for clay and sand are given in

Table 4. The factor α in Fig. 8 is used to obtain the soil/pile adhesion, given the soil cohesion. Various curves have been presented in the literature for this value [13].

3.3.1.3. Load-settlement q-z curves A curve describing the load-settlement behavior of the tip for a single pile is proposed by Vijayvergiya [29]. The analytical forms of q-z curves and their parameters for clay and sand used in this study are given in Table 5.

3.3.2. Parameters for the modified Ramberg-Osgood equation

A correspondence can be made between the analytical forms of others for the p-y, f-z and q-z curves which are presented above and a set of the modified Ramberg-Osgood models. The parameters k_n and n in Eq. (3.1) can be determined by selecting two significant points from the analytical forms of the p-y curves for clay. For example, to simulate the best approximation of the analytical p-y curve for soft clay, these two significant points can be selected as: (1) $p = 0.5\ p_u$ at $y = y_{50}$; (2) $p = 0.95\ p_u$ at $y = 8y_{50}$. Knowing these two significant points, the parameters k_n and n can be obtained by solving the nonlinear equation. A trial and error method was expedient. The values k_n and n of the modified Ramberg-Osgood models for clay are listed in Table 6. The parameters for the f-z and q-z Ramberg-Osgood curves were obtained in the same manner and are also listed. The parameters for the p-y curve for sand were obtained by a visual "best-fit" of the hyperbolic tangent. Considering the level of approximation involved in fitting these analytical approximations to

the real soil data, it was decided to round off the k and n values to those listed in Table 6.

Analytical forms by others for the p-y, f-z and q-z curves and the modified Ramberg-Osgood equations used in this study are presented in Fig. 9 for clay and sand. Two features of the analytical forms which cannot be fit by the Ramberg-Osgood equations are: (1) the infinite slope at origin and (2) the zero slope at the ultimate load. The Ramberg-Osgood equation has a finite slope, k, at the origin and asymptotically approaches the ultimate load at a rate dependent upon the shape factor n. The Ramberg-Osgood equation appears physically more realistic.

3.3.3. Typical Iowa soil

Soil properties should be investigated first by test boring at the bridge site, by measuring penetration resistance and by laboratory testing on intact samples. If a complete investigation of the soil properties is not feasible, empirical relationships may be useful. The empirical data, which is obtained from numerous test results and long-term observations, can be expected to provide reasonable and conservative values.

In consultation with engineers from the Iowa Department of Transportation, six typical Iowa soils were selected based on the blow count N, angle of friction ϕ, and cohesion c_u. Soil properties and the modified Ramberg-Osgood curves parameters for six typical Iowa soils were generated by following the criteria listed in Tables 3 to 5. They are listed in Tables 7 to 8 for clay and sand, respectively.

4. THREE-DIMENSIONAL FINITE ELEMENT PILE MODEL

4.1. Introduction

A state-of-the-art mathematical model that can be used to help evaluate the safety of piles in skewed bridges with integral abutments is described herein. Normally, for a skewed bridge with integral abutments subjected to a change in temperature, thermal movements caused by temperature changes in most cases include biaxial behavior in the pile. Thus, a three-dimensional behavior of soil-pile interaction is to be considered for all components of the system, with compatibility and equilibrium enforced throughout.

The mathematical model developed in this study was limited to defining the behavior of soil-pile interaction. A combination of a one-dimensional idealization for the piles (beam column) and an equivalent spring idealization for the soil, which includes vertical springs, lateral springs, and a point spring, are shown in Fig. 10.

4.2. Three-dimensional Beam Finite Element

Basically, two different approaches have been pursued in incremental, nonlinear finite element analysis. In the first, static and kinematic variables are referred to Eulerian (convected) coordinates in each load step. This procedure is generally called the Eulerian, convected, or moving coordinate formulation. In this approach, the geometry of the continua is updated, and the deformations are assumed to be infinitesimal; hence, the linear relations can be used. The incremental governing equations are obtained by applying the principle of virtual work or other

equivalent theorems to the continuum using its current configuration and stress [43].

In the second approach, which is generally called the Lagrangian, stationary Lagrangian, or total Lagrangian formulation, all static and kinematic variables are referred to the original configuration (Fig. 11). The advantage of the total Lagrangian formulation is the ease with which it handles the boundary conditions and nonhomogeneities. For large displacement problems, the construction of shape functions for flexural problems is quite difficult and complex if the convergence conditions of the finite element method are to be met [43]. As the rotations become large, a component originally along the coordinate axis of the beam is no longer along that axis. Therefore, the assumed shape functions in the axial (linear) and transverse (cubic) directions are not compatible. This effect restricts the rotations to moderate values.

An updated Lagrangian formulation, which reduces the efforts in computation for problems where the nonlinearities arise from material nonlinearity and finite displacement and rotation, is presented here [43]. In the updated Lagrangian formulation, the coordinates rotate and translate with the body but do not deform with it (Fig. 11). In static analysis, time is used to represent a loading parameter and not real time. Hence, $t+\Delta t$ refers to conditions after a load increment ΔF has been added. If the strains are small, this formulation linearizes the strain-displacement relations in terms of the displacements relative to the element moving chord. Strictly speaking, the updated Lagrangian formulation is a mixed procedure of the Eulerian and total Lagrangian formulations.

Derivations of the beam-column element with geometrically and materially nonlinear stiffness equations have been presented by several investigators [44-62]. A condensed description of this approach is given here to clarify the notation and approach used in the study. The following assumptions have been used in this derivation:

- The beam elements are assumed to be initially straight.
- Plane sections remain plane after deformation.
- The cross section of the beam is constant and has at least one plane of symmetry.
- Shear deformation is not considered.
- The effect of torsional deformation on normal strain is negligible (unrestrained warping).
- The beam-column can undergo large rotations, but the deformation within each element from the chord is restricted to be small.

4.2.1. Coordinate systems

In order to describe the system, three types of coordinate systems will be defined here:

1) A fixed, global set of coordinates (X, Y, Z).
2) Nodal coordinates ($\bar{x}$, $\bar{y}$, $\bar{z}$)--a set of nodal coordinates associated with each node that coincides with $\vec{b}_1$, $\vec{b}_2$, and $\vec{b}_3$ (the orthogonal base vectors), respectively, for each node. The initial orientations of the vectors $\vec{b}_i$ are chosen to coincide with the principal directions of the cross section, and since the vectors rotate with the node, they remain aligned with the principal directions.

3) Element or local coordinates (x, y, z)--a set of element coordinates associated with each element. The element coordinates rotate and translate with the end points of the element. The x, y, and z axes are associated with the orthogonal base unit vectors $\vec{e}_1$, $\vec{e}_2$, and $\vec{e}_3$, respectively, for each element. These are the updated Lagrangian coordinates described in the introduction to this chapter and illustrated in Fig. 11.

These coordinate systems are illustrated in Fig. 12. The unit vectors $\vec{b}_i$ and $\vec{e}_i$ define the rotational transformation for any vector components between the coordinate systems.

4.2.2. Strain-displacement relationship

In the updated Lagrangian formulation, consider a generic beam-column element with Node I and J (or 1 and 2) at the endpoints. The element has six degree of freedoms per node; three displacements and three rotations. The nodal displacement vectors in global and element coordinates are designated as D_1 to D_{12} and d_1 to d_{12}, respectively. The positive directions are given by the righthand rule. The element coordinate system (x, y, z) for the beam-column element is defined so that the x axis is updated to remain coincident with a line joining the endpoints of the element, while the y and z axes can be defined by a third node which lies in the positive x-y plane (K node). In general, the third node translates as the average of the two end nodes. In addition, it rotates about the local axis of the beam (x axis) an amount equal to the average of the twisting rotations at the ends [63].

Consistent with the updated Lagrangian approach, the element coordinate system is temporarily visualized as remaining stationary at x^t, y^t, z^t (Fig. 11) as the beam moves during Δt. The neutral axis displacements relative to x^t, y^t, z^t are given by cubic shape functions to describe bending deformations and linear shape functions to specifiy axial and torsional deformations as

$$\begin{Bmatrix} u_{na} \\ v_{na} \\ w_{na} \\ \phi_{na} \end{Bmatrix} = \left[\begin{array}{cccccc:cccccc} 1-\xi & 0 & 0 & 0 & 0 & 0 & \xi & 0 & 0 & 0 & 0 & 0 \\ 0 & 1-3\xi^2+2\xi^3 & 0 & 0 & 0 & \ell^t(\xi-2\xi^2+\xi^3) & 0 & 3\xi^2-2\xi^3 & 0 & 0 & 0 & \ell^t(-\xi^2+\xi^3) \\ 0 & 0 & 1-3\xi^2+2\xi^3 & 0 & \ell^t(-\xi+2\xi^2-\xi^3) & 0 & 0 & 0 & 3\xi^2-2\xi^3 & 0 & \ell^t(\xi^2-\xi^3) & 0 \\ 0 & 0 & 0 & 1-\xi & 0 & 0 & 0 & 0 & 0 & \xi & 0 & 0 \end{array}\right] \begin{Bmatrix} d_1 \\ d_2 \\ d_3 \\ d_4 \\ d_5 \\ d_6 \\ d_7 \\ d_8 \\ d_9 \\ d_{10} \\ d_{11} \\ d_{12} \end{Bmatrix}$$

$$= [N]\{d\} \qquad (4.1)$$

where

$$\xi = \frac{x}{\ell^t} \qquad (4.2)$$

ℓ^t = the length of the element at time t.

The u_{na}, v_{na}, w_{na} and ϕ_{na} are neutral axis displacements which include rigid body motion, measured relatively to the current stationary

element coordinate system as shown in Fig. 11 (e.e., the moving chord which connects the endpoints).

Following the usual Euler-Bernoulli beam assumptions that normals to the midline remain straight and normal, the deformation displacement at each point of the beam element may be written as

$$u = u_{na} - y \frac{\partial v_{na}}{\partial x} - z \frac{\partial w_{na}}{\partial x} \tag{4.3}$$

$$v = v_{na} - z\phi_{na} \tag{4.4}$$

$$w = w_{na} + y\phi_{na} \tag{4.5}$$

From the previous assumptions, the effect of torsional deformation on normal strain is neglected and shear deformation is not considered. The relationship between the beam normal strains and the displacements is

$$\varepsilon = \frac{\partial u}{\partial x} + \frac{1}{2}\left(\frac{\partial v}{\partial x}\right)^2 + \frac{1}{2}\left(\frac{\partial v}{\partial x}\right)^2 \tag{4.6}$$

The equation is valid as long as $(\partial v/\partial x)^2$ and $(\partial w/\partial x)^2$ are large compared to $(\partial u/\partial x)^2$. Although this condition is similar in appearance to that of moderate rotation theories, it is far less restrictive because v and w are the displacements relative to the updated element coordinate x. By reducing the size of the element, v and w can be made as small as necessary [64].

From Eqs. (4.1) to (4.6), the strain and displacement can be related as

$$\varepsilon = ([B_L] + \frac{1}{2}[B_{NL}])\{d\} \tag{4.7}$$

where

$$[B_L] = [\frac{-1}{\ell^t},\ \frac{-\eta}{\ell^t}(12\xi-6),\ \frac{-\rho}{\ell^t}(12\xi-6),\ 0,\ \rho(6\xi-4),\ -\eta(6\xi-4)\ \vdots$$

$$\frac{1}{\ell^t},\ \frac{\eta}{\ell^t}(12\xi-6),\ \frac{\rho}{\ell^t}(12\xi-6),\ 0,\ \rho(6\xi-2),\ -\eta(6\xi-2)] \quad (4.8)$$

$$[B_{NL}] = \{d\}^T([G_z]^T[G_z] + [G_y]^T[G_y]) \quad (4.9)$$

$$[G_z] = [0,\ \frac{1}{\ell^t}\Psi_3(\xi),\ 0,\ \rho,\ 0,\ \Psi_1(\xi),\ 0,\ \frac{-1}{\ell^t}\Psi_4(\xi),\ 0,\ -\rho,\ 0,\ \Psi_2(\xi)] \quad (4.10)$$

$$[G_y] = [0,\ 0,\ \frac{1}{\ell^t}\Psi_3(\xi),\ -\eta,\ -\Psi_1(\xi),\ 0,\ 0,\ 0,\ \frac{-1}{\ell^t}\Psi_4(\xi),\ \eta,\ -\Psi_2(\xi),\ 0] \quad (4.11)$$

$$\Psi_1(\xi) = 1 - 4\xi + 3\xi^2 \quad (4.12)$$

$$\Psi_2(\xi) = -2\xi + 3\xi^2 \quad (4.13)$$

$$\Psi_3(\xi) = -6\xi + 6\xi^2 \quad (4.14)$$

$$\eta = \frac{y}{\ell^t},\ \rho = \frac{z}{\ell^t} \quad (4.15)$$

For general nonlinear problems, the solution algorithm (Newton-Raphson method) is based upon the application of a small load increment. For this technique, it is necessary to relate the rate of change of force with displacement, that is, the tangent stiffness. From Eq. (4.7) that rate of strain $\Delta\varepsilon$ can be found as [60]

$$\Delta\varepsilon = ([B_L] + [B_{NL}])\ \{\Delta d\} \quad (4.16)$$

or

$$\Delta\varepsilon = [B]\{\Delta d\} \tag{4.17}$$

Once the strains are known, the stresses are computed by the constitutive laws [65]. The nonlinear stress-strain relationship of the beam material will be approximated by the modified Ramberg-Osgood cyclic model (see Sec. 3.2.3). The incremental stress-strain relationship of the beam-column element is expressed as

$$\Delta\sigma = E_T \Delta\varepsilon \tag{4.18}$$

where E_T is the tangent modulus of elasticity of the stress-strain curve. If the thermal strains are considered, Eq. (4.18) is modified to

$$\Delta\sigma = E_T(\Delta\varepsilon - \Delta\varepsilon_T) \tag{4.19}$$

$$\Delta\varepsilon_T = \alpha\Delta T \tag{4.20}$$

in which

ΔT = temperature above an arbitrary reference temperature

α = coefficient of thermal expansion

4.2.3. Tangent stiffness matrix in element coordinate system

The theorem of virtual work will be used to obtain the equation of equilibrium. The nodal forces are found as

$$\{f\} = \int_V [B]^T \sigma dV \tag{4.21}$$

where V is the volume of the element. In the updated Lagrangian formulation, the incremental form of Eq. (4.21) will be used to obtain the tangent stiffness matrix of the beam-column element in the element coordinate system. The incremental form of Eq. (4.21) is

$$\{\Delta f\} = \int_V [\Delta B]^T \sigma dV + \int_V [B]^T \Delta\sigma dV \tag{4.22}$$

The following definitions are introduced

$$\int_V [B]^T \Delta\sigma dV = ([k_0] + [k_L])\{\Delta d\} \tag{4.23}$$

$$\int_V [\Delta B]^T \sigma dV = [k_G]\{\Delta d\} \tag{4.24}$$

where

$$[k_0] = \int_V [B_L]^T E_T [B_L]\, dV \tag{4.25}$$

$$[k_L] = \int_V ([B_L]^T E_T [B_{NL}] + [B_{NL}]^T E_T [B_L] + [B_{NL}]^T E_T [B_{NL}])dV \tag{4.26}$$

and on can show, with some manipulations, that

$$[\Delta B]^T = ([G_z]^T [G_z] + [G_y]^T [G_y])\{\Delta d\} \tag{4.27}$$

The matrix $[k_0]$ is the conventional stiffness matrix; $[k_G]$ is the initial stress matrix (or the geometric stiffness matrix), which depend linearly on the nodal displacements $\{d\}$; and $[k_L]$ represents the large displacement stiffness matrix, which depends on quadratic terms of the nodal displacements $\{d\}$. The updated Lagrangian strain approach

makes the strains and rotations in the element system small enough (for reasonably small element sizes and small load steps, Δt) that $[k_L]$ can be omitted [60]. Eq. (4.22) can then be reduced to

$$\{\Delta f\} = ([k_0] + [k_G])\{\Delta d\}$$

$$= [k]_T\{\Delta d\} \tag{4.28}$$

The following definitions are made in order to obtain the expressions for $[k_0]$ and $[k_G]$:

$$P_i = \int_A \sigma dA \tag{4.29}$$

$$M_i^y = \int_A \sigma z dA \tag{4.30}$$

$$M_i^z = -\int_A \sigma y dA \tag{4.31}$$

$$M_i = \frac{1}{\ell^t} \int_A \sigma(y^2 + z^2)dA \tag{4.32}$$

$$(EA)_{Ti} = \int_A E_T dA \tag{4.33}$$

$$(EK^y)_{Ti} = \int_A E_T z dA \tag{4.34}$$

$$(EK^z)_{Ti} = \int_A E_T y dA \tag{4.35}$$

$$(EI^y)_{Ti} = \int_A E_T z^2 dA \tag{4.36}$$

$$(EI^{z})_{Ti} = \int_{A} E_T y^2 dA \tag{4.37}$$

$$(EI^{yz})_{Ti} = \int_{A} E_T yz dA \tag{4.38}$$

where i = I and J denotes ξ = 0 and 1, respectively, and A refers to the beam cross-sectional area. The integrals in Eqs. (4.29) to (4.38) must be evaluated numerically since the cross section may be partially plastic. Numerical methods are introduced to calculate the current strains and stresses (which are functions of η and ρ) at different points of the cross section. In Eqs. (4.29) to (4.38), σ is the current stress correspond to the current strain ε (Eq. 3.3) and E_T is the tangent modules of elasticity of the stress-strain curve correspond to the current strain ε (Eq. 3.5). The cross-sectional area is correspondingly divided into a number of subelements over the depth and width as shown in Fig. 13. The number of layers used in two directions must be sufficient to describe the variation of material properties and stresses over the depth and width. Each subelement is assumed to have uniform material properties, and the strain is evaluated at the centroid of the subelement. The stress is assumed constant and equal to the stress calculated at the centroid of the subelement. The quantities obtained from Eq. (4.29) to Eq. (4.38) are assumed to vary linearly between I and J; for example,

$$P(\xi) = (P_J - P_I)\xi + P_I \tag{4.39}$$

$$M^{y}(\xi) = (M^{y}_J - M^{y}_I)\xi + M^{y}_I \tag{4.40}$$

$$M^z(\xi) = (M_J^z - M_I^z)\xi + M_I^z \tag{4.41}$$

$$M(\xi) = (M_J - M_I)\xi + M_I \tag{4.42}$$

The conventional matrix stiffness is obtained by evaluating the integral [See Eq. (4.25)]. Using the definition of Eqs. (4.33) to (4.38) gives the explicit form of $[k_0]$ as

$[k_0] =$

$$\begin{bmatrix}
k_1^0 & -k_2^0 & -k_3^0 & 0 & k_4^0 & -k_5^0 & -k_1^0 & k_2^0 & k_3^0 & 0 & -k_6^0 & k_7^0 \\
 & k_8^0 & k_9^0 & 0 & -k_{10}^0 & k_{11}^0 & k_2^0 & -k_8^0 & -k_9^0 & 0 & -k_{12}^0 & k_{13}^0 \\
 & & k_{14}^0 & 0 & -k_{15}^0 & k_{13}^0 & k_3^0 & -k_9^0 & -k_{14}^0 & 0 & -k_{16}^0 & k_{12}^0 \\
 & & & k_{17}^0 & 0 & 0 & 0 & 0 & 0 & -k_{17}^0 & 0 & 0 \\
 & & & & k_{18}^0 & -k_{13}^0 & -k_4^0 & k_{10}^0 & k_{15}^0 & 0 & k_{20}^0 & -k_{21}^0 \\
 & & & & & k_{22}^0 & k_5^0 & -k_{11}^0 & -k_{13}^0 & 0 & -k_{21}^0 & k_{23}^0 \\
 & & & & & & k_1^0 & -k_2^0 & -k_3^0 & 0 & k_6^0 & -k_7^0 \\
 & & \text{sym.} & & & & & k_8^0 & k_9^0 & 0 & k_{12}^0 & -k_{13}^0 \\
 & & & & & & & & k_{14}^0 & 0 & k_{16}^0 & -k_{12}^0 \\
 & & & & & & & & & k_{17}^0 & 0 & 0 \\
 & & & & & & & & & & k_{24}^0 & -k_{25}^0 \\
 & & & & & & & & & & & k_{26}^0
\end{bmatrix}$$

(4.43)

where

$$k_1^0 = \frac{1}{\ell^t}\left(\frac{1}{2}(EA)_{TI} + \frac{1}{2}(EA)_{TJ}\right)$$

$$k_2^0 = \frac{1}{(\ell^t)^2}\left((EK^z)_{TI} - (EK^z)_{TJ}\right)$$

$$k_3^0 = \frac{1}{(\ell^t)^2}\left((EK^y)_{TI} - (EK^y)_{TJ}\right)$$

$$k_4^0 = \frac{1}{\ell^t}(EK^y)_{TI}$$

$$k_5^0 = \frac{1}{\ell^t}(EK^z)_{TI}$$

$$k_6^0 = \frac{1}{\ell^t}(EK^y)_{TJ}$$

$$k_7^0 = \frac{1}{\ell^t}(EK^z)_{TJ}$$

$$k_8^0 = \frac{1}{(\ell^t)^3}\left(6(EI^z)_{TI} + 6(EI^z)_{TJ}\right)$$

$$k_9^0 = \frac{1}{(\ell^t)^3}\left(6(EI^{yz})_{TI} + 6(EI^{yz})_{TJ}\right)$$

$$k_{10}^0 = \frac{1}{(\ell^t)^2}\left(4(EI^{yz})_{TI} + 2(EI^{yz})_{TJ}\right)$$

$$k_{11}^0 = \frac{1}{(\ell^t)^2}\left(4(EI^z)_{TI} + 2(EI^z)_{TJ}\right)$$

$$k_{12}^0 = \frac{1}{(\ell^t)^2}\left(2(EI^{yz})_{TI} + 4(EI^{yz})_{TJ}\right)$$

$$k_{13}^{0} = \frac{1}{(\ell^t)^2}\left(2(EI^z)_{TI} + 4(EI^z)_{TJ}\right)$$

$$k_{14}^{0} = \frac{1}{(\ell^t)^3}\left(6(EI^y)_{TI} + 6(EI^y)_{TJ}\right)$$

$$k_{15}^{0} = \frac{1}{(\ell^t)^2}\left(4(EI^y)_{TI} + 2(EI^y)_{TJ}\right)$$

$$k_{16}^{0} = \frac{1}{(\ell^t)^2}\left(2(EI^y)_{TI} + 4(EI^y)_{TJ}\right)$$

$$k_{17}^{0} = (GJ)_T/\ell^t$$

$$k_{18}^{0} = \frac{1}{\ell^t}\left(3(EI^y)_{TI} + (EI^y)_{TJ}\right)$$

$$k_{19}^{0} = \frac{1}{\ell^t}\left(3(EI^{yz})_{TI} + (EI^{yz})_{TJ}\right)$$

$$k_{20}^{0} = \frac{1}{\ell^t}\left((EI^y)_{TI} + (EI^y)_{TJ}\right)$$

$$k_{21}^{0} = \frac{1}{\ell^t}\left((EI^{yz})_{TI} + (EI^{yz})_{TJ}\right)$$

$$k_{22}^{0} = \frac{1}{\ell^t}\left(3(EI^z)_{TI} + (EI^z)_{TJ}\right)$$

$$k_{23}^{0} = \frac{1}{\ell^t}\left((EI^z)_{TI} + (EI^z)_{TJ}\right)$$

$$k_{24}^{0} = \frac{1}{\ell^t}\left((EI^y)_{TI} + 3(EI^y)_{TJ}\right)$$

$$k_{25}^{0} = \frac{1}{\ell^t}\left((EI^{yz}) + 3(EI^{yz})_{TJ}\right)$$

$$k_{26}^{0} = \frac{1}{\ell^t}\left((EI^{z})_{TI} + 3(EI^{z})_{TJ}\right) \qquad (4.44)$$

The linear term $(GJ)_T/\ell^t$ has been inserted into Eq. (4.43) even though it does not result from axial (normal) strain. It should be noted that for a conventional stiffness matrix this term is used to resist the applied torsion.

The geometric (initial stress) stiffness matrix $[k_G]$ is obtained by evaluating the integral of Eq. (4.24) with the definition in Eqs. (4.29) to (4.32) and (4.35) to (4.42). The explicit form of $[k_G]$ is

$$[k_G] = 1/\ell^t$$

$$\begin{bmatrix}
0 & 0 & 0 & 0 & 0 & 0 & 0 & 0 & 0 & 0 & 0 & 0 \\
 & k_1^G & 0 & -k_2^G & 0 & k_3^G & 0 & -k_1^G & 0 & k_2^G & 0 & k_4^G \\
 & & k_1^G & -k_5^G & -k_3^G & 0 & 0 & 0 & -k_1^G & k_5^G & -k_4^G & 0 \\
 & & & k_6^G & k_7^G & -k_8^G & 0 & k_2^G & k_5^G & -k_6^G & -k_7^G & k_8^G \\
 & & & & k_9^G & 0 & 0 & 0 & k_3^G & -k_7^G & k_{10}^G & 0 \\
 & & & & & k_9^G & 0 & -k_3^G & 0 & k_8^G & 0 & k_{10}^G \\
 & & & & & & 0 & 0 & 0 & 0 & 0 & 0 \\
 & & & & & & & k_1^G & 0 & -k_2^G & 0 & -k_4^G \\
 & & \text{sym.} & & & & & & k_1^G & -k_5^G & k_4^G & 0 \\
 & & & & & & & & & k_6^G & k_7^G & -k_8^G \\
 & & & & & & & & & & k_{11}^G & 0 \\
 & & & & & & & & & & & k_{11}^G
\end{bmatrix} \qquad (4.45)$$

$$k_1^G = \frac{1}{60}(36P_I + 36P_J) \qquad k_2^G = \frac{1}{2}(M_I^y + M_J^y)$$

$$k_3^G = \frac{\ell^t}{60}(6P_J) \qquad k_4^G = \frac{\ell^t}{60}(6P_I)$$

$$k_5^G = \frac{1}{2}(M_I^z + M_J^z) \qquad k_6^G = \ell^t(\frac{1}{2}M_I + \frac{1}{2}M_J)$$

$$k_7^G = \frac{\ell^t}{12}(M_J^z - M_I^z) \qquad k_8^G = \frac{\ell^t}{12}(M_J^y - M_I^y)$$

$$k_9^G = \frac{(\ell^t)^2}{60}(6P_I + 2P_J) \qquad k_{10}^G = \frac{(\ell^t)^2}{60}(-P_I - P_J)$$

$$k_{11}^G = \frac{(\ell^t)^2}{60}(2P_I + 6P_J) \qquad (4.46)$$

4.2.4. Three-dimensional transformation matrix and coordinate updating

Consider the motion of a beam-column element in a fixed Cartesian coordinate system (global system) as shown in Fig. 14. In Eq. (4.28), the incremental equilibrium equations of a beam-column element are derived by first evaluating the finite element matrices corresponding to the element coordinate system (see Fig. 14). The resulting matrices can next be transformed to the global Cartesian coordinate axes prior to the element assemblage process [43]. The transformation matrix [T], which relates displacements measured in the element system at the current configuration (at time t) to the displacements measured in the global coordinate system, is obtained by a vector transformation between the element and global coordinate system. The direction cosines for the element unit vectors $\vec{e}_i^t$ are

$$\overset{t}{e}_1 = \frac{\overset{t}{X}_{IJ}}{\left|\overset{t}{X}_{IJ}\right|} = \ell_1^t \overset{t}{I} + m_1^t \overset{t}{J} + n_1^t \overset{t}{K} \tag{4.47}$$

$$\overset{t}{e}_3 = \frac{\overset{t}{X}_{IJ} \times \overset{t}{X}_{IK}}{\left|\overset{t}{X}_{IJ} \times \overset{t}{X}_{IK}\right|} = \ell_3^t \overset{t}{I} + m_3^t \overset{t}{J} + n_3^t \overset{t}{K} \tag{4.48}$$

$$\overset{t}{e}_2 = \overset{t}{e}_3 \times \overset{t}{e}_1 = \ell_2^t \overset{t}{I} + m_2^t \overset{t}{J} + n_2^t \overset{t}{K} \tag{4.49}$$

where $\overset{t}{I}$, $\overset{t}{J}$, $\overset{t}{K}$ are unit vectors in the global coordinate system and

$$\overset{t}{X}_{IJ} = \overset{t}{X}_J - \overset{t}{X}_I \text{ , etc.} \tag{4.50}$$

Incremental nodal displacements in the element and global coordinates are related by an orthogonal transformation

$$\{\Delta d\} = [T]\{\Delta D\} \tag{4.51}$$

where

$$[T] = \begin{bmatrix} [T_{EG}] & & & \\ & [T_{EG}] & & \\ & & [T_{EG}] & \\ & & & [T_{EG}] \end{bmatrix} \tag{4.52}$$

$$[T_{EG}] = \begin{bmatrix} \ell_1^t & m_1^t & n_1^t \\ \ell_2^t & m_2^t & n_2^t \\ \ell_3^t & m_3^t & n_3^t \end{bmatrix} \tag{4.53}$$

The tangent stiffness of the beam-column element in the global coordinate system is

$$\{\Delta F\} = [K_T]\{\Delta D\} \tag{4.54}$$

where

$$[K_T] = [T]^T [k]_T [T] \tag{4.55}$$

As mentioned before, the unit vectors $\vec{e}_i^t$, $\vec{b}_{Ii}^t$, and $\vec{b}_{Ji}^t$ (i = 1, 3) must be updated to $\vec{e}_i^{t+\Delta t}$, $\vec{b}_{Ii}^{t+\Delta t}$, $\vec{b}_{Ji}^{t+\Delta t}$, after each incremental load in order to track the element and nodal coordinate systems. For the purpose of tracking the unit vectors $\vec{e}_i^t$, $\vec{b}_{Ii}^t$, and $\vec{b}_{Ji}^t$ at the current stage, start from the initial stage (at time 0) when the unit vectors $\vec{e}_i^0$, $\vec{b}_{Ii}^0$, and $\vec{b}_{Ji}^0$ are the same. After the first incremental load is applied, the incremental displacements $\{\Delta D^t\}$ are obtained in the global coordinate system from the solution of Eq. (4.54)

$$\{\Delta D^t\} = \begin{Bmatrix} \{\Delta D_{TI}^t\} \\ \{\Delta D_{\theta I}^t\} \\ \{\Delta D_{TJ}^t\} \\ \{\Delta D_{\theta J}^t\} \end{Bmatrix} \tag{4.56}$$

where

$\{\Delta D_{TI}^t\}$ = translation at node I in X, Y, and Z directions

$\{\Delta D_{\theta I}^t\}$ = rotation at node I in X, Y, and Z directions

At the initial stage, the third node K is defined as a point in the positive x-y plane as shown in Fig. 14. At the current stage, nodes I and J are displaced to the new position $\vec{X}_I^t$ and $\vec{X}_J^t$, respectively.

$$\vec{X}_I^t = \vec{X}_J^0 + \Delta\vec{D}_{TI}^t \tag{4.57}$$

$$\vec{X}_J^t = \vec{X}_J^0 + \Delta\vec{D}_{TJ}^t \tag{4.58}$$

where

$\vec{X}_I^t$ = position vector of node I at time t

$\vec{X}_I^0$ = position vector of node I at time 0

The third node (K node) translates as the average of the two end nodes. In addition, it rotates about the axis of the beam on the average of the twisting rotations. Since the incremental displacements $\{\Delta D^t\}$ are assumed to be small, the new position of the K node is obtained as

$$\vec{X}_K^t = \vec{X}_{TK}^t + \Delta\vec{D}_{\theta K}^t \times \left(\vec{X}_{TK}^t - \vec{X}_M^t\right) \tag{4.59}$$

where

$$X_{TK}^t = \vec{X}_K^0 + \frac{1}{2}\left(\Delta\vec{D}_{TI}^t + \Delta\vec{D}_{TJ}^t\right) \tag{4.60}$$

is the translation term. The small rotation about the beam axis is

$$\Delta\vec{D}_{\theta K}^t = \left[\frac{1}{2}\left(\Delta\vec{D}_{\theta I}^t + \Delta\vec{D}_{\theta J}^t\right) \cdot \vec{e}_1^t\right]\vec{e}_1^t \tag{4.61}$$

The quantity in parentheses in Eq. (4.59) is the radius vector from the midpoint M to K, in which

$$\vec{X}_M^t = \frac{1}{2}\left(\vec{X}_I^t + \vec{X}_J^t\right) \tag{4.62}$$

Now, for the nodal coordinate system, the unit vectors $\vec{b}_{Ii}^t$ and $\vec{b}_{Ji}^t$ are also updated since they rotate with the nodes. From the assumption that the incremental rotations $\{\Delta\vec{D}_{\theta I}^t\}$ and $\{\Delta\vec{D}_{\theta J}^t\}$ are small, the incremental vectors can be obtained by taking the cross product of the two vectors, $\Delta\vec{D}_I^t$ and $\vec{b}_{Ii}^0$, and updating

$$\vec{b}_{Ii}^t = \vec{b}_{Ii}^0 + \Delta\vec{D}_{\theta I}^t \times \vec{b}_{Ii}^0 \tag{4.63}$$

$$\vec{b}_{Ji}^t = \vec{b}_{Ji}^0 + \Delta\vec{D}_{\theta J}^t \times \vec{b}_{Ji}^0 \tag{4.64}$$

These current updated vectors must be normalized to obtain the direction cosines for the current updated unit vectors. For the next increment, t = 0 refers to the previous increment.

4.2.5. Nodal forces computation

In the updated Lagrangian formulation, the incremental nodal displacements $\{\Delta D^t\}$ which are obtained from the applied incremental load (Eq. 4.54) are updated to find the new position. The nodal forces are then evaluated in this updated element coordinate system ($x^{t+\Delta t}$, $y^{t+\Delta t}$, $z^{t+\Delta t}$ in Fig. 11). In the following updating procedure, the superscript 0 refers to the previous step and superscript t refers to the updated position, i.e., $t+\Delta t$ is replaced by t. Once the coordinates have been updated, the nodal displacements $\{d^t\}$ account for only the displacements

due to straining. That is, the rigid body motion has already been included in the coordinate updating (i.e., $d_1^t = d_2^t = d_3^t = d_4^t = d_8^t = d_9^t = 0$). The displacement due to material straining in the axial direction is determined by

$$d_7^t = \Delta_{IJ} = \left|\left(\vec{x}_J^t - \vec{x}_I^t\right)\right| - \left|\left(\vec{x}_J^0 - \vec{x}_I^0\right)\right|$$

$$= \frac{1}{(\ell^t + \ell^0)} \left[2 \left(X_{JI}^0 D_{71} + Y_{JI}^0 D_{82} + Z_{JI}^0 D_{93} \right) + (D_{71})^2 + (D_{82})^2 + (D_{93})^2 \right] \qquad (4.65)$$

where

ℓ^0, ℓ^t = the length of the element at time 0 and t, respectively.

$X_{JI}^0 = X_J^0 - X_I^0$, $D_{71} = D_7 - D_1$, etc.

Δ_{IJ} = elongation

For the purpose of computing the relative rotations at time t, d_5^t, d_6^t, d_{10}^t, d_{11}^t and d_{12}^t, nodal unit vectors for node I and J are defined by $\vec{b}_{Ii}^t$, $\vec{b}_{Ji}^t$, respectively (i = 1, 3). Element unit vectors (x, y, z) are denoted by $\vec{e}_i^t$. Since the nodal vectors $\vec{b}_{Ii}^t$ and $\vec{b}_{Ji}^t$ rotate with the nodes, the angle between $\vec{b}_{Ii}^t$ and $\vec{e}_i^t$ indicates the magnitude of the deformation at node I. For example, the cross product of the two vectors $\vec{e}_1^t$ and $\vec{b}_{I1}^t$ is a vector perpendicular to the plane which contains these two vectors. The magnitude of this vector is equal to the sine of the angle between $\vec{e}_1^t$ and $\vec{b}_{I1}^t$. With the assumption of small

deformation within the updated coordinate system, the bending deformation rotation $d_5^{t+\Delta t}$ can be obtained by projecting this vector ($\vec{e}_1^{t+\Delta t} \times \vec{b}_{I1}^{t+\Delta t}$) on the current y axis. This is illustrated in Fig. 12 and the mathematical expressions are given below.

$$d_5^{t+\Delta t} = \theta_I^y = (\vec{e}_1^{t+\Delta t} \times \vec{b}_{I1}^{t+\Delta t}) \cdot \vec{e}_2^{t+\Delta t} \tag{4.66}$$

$$d_6^{t+\Delta t} = \theta_I^z = (\vec{e}_1^{t+\Delta t} \times \vec{b}_{I1}^{t+\Delta t}) \cdot \vec{e}_3^{t+\Delta t} \tag{4.67}$$

$$d_{11}^{t+\Delta t} = \theta_J^y = (\vec{e}_1^{t+\Delta t} \times \vec{b}_{J1}^{t+\Delta t}) \cdot \vec{e}_2^{t+\Delta t} \tag{4.68}$$

$$d_{12}^{t+\Delta t} = \theta_J^z = (\vec{e}_1^{t+\Delta t} \times \vec{b}_{J1}^{t+\Delta t}) \cdot \vec{e}_3^{t+\Delta t} \tag{4.69}$$

where

θ_I^y, θ_I^z, θ_J^y, θ_J^z = bending deformation rotation at ends I and J.

The torsional deformation is found by taking the cross product of $\vec{b}_{I2}^{t+\Delta t}$ and $\vec{b}_{J2}^{t+\Delta t}$ and projecting this vector on the current axis of the beam (x axis). This yields

$$d_{10}^{t+\Delta t} = \theta_{IJ}^x = (\vec{b}_{I2}^{t+\Delta t} \times \vec{b}_{J2}^{t+\Delta t}) \cdot \vec{e}_1^{t+\Delta t} \tag{4.70}$$

where

θ_{IJ}^x = torsional deformation rotation

The strain ε which is caused by these displacements relative to the updated element coordinates is now calculated (Eq. 4.7). The current

stress σ which corresponds to the current strain ε can be obtained from Eq. (3.3). The nodal forces in the updated element coordinate system (Eq. 4.21) will be evaluated numerically first by performing area integral in Eqs. (4.29) through (4.33) and assuming they are varied linearly between node I and J [Eqs. (4.39) to 4.42)], then performing length integrals to obtain the nodal forces in closed form as

$$\{f^t\} = \{A_L\} + \{A_{NL}\} \tag{4.71}$$

where

$$\{A_L\} = [R]^T \{f_L\} \tag{4.72}$$

$$\{A_{NL}\} = [R]^T \{f_{NL}\} \tag{4.73}$$

$$[R] = \begin{bmatrix} -1 & 0 & 0 & 0 & 0 & 0 & 1 & 0 & 0 & 0 & 0 & 0 \\ 0 & 0 & 0 & -1 & 0 & 0 & 0 & 0 & 0 & 1 & 0 & 0 \\ 0 & 0 & \frac{-1}{\ell^t} & 0 & 1 & 0 & 0 & 0 & \frac{1}{\ell^t} & 0 & 0 & 0 \\ 0 & \frac{1}{\ell^t} & 0 & 0 & 0 & 1 & 0 & \frac{-1}{\ell^t} & 0 & 0 & 0 & 0 \\ 0 & 0 & \frac{-1}{\ell^t} & 0 & 0 & 0 & 0 & 0 & \frac{1}{\ell^t} & 0 & 1 & 0 \\ 0 & \frac{1}{\ell^t} & 0 & 0 & 0 & 0 & 0 & \frac{-1}{\ell^t} & 0 & 0 & 0 & 1 \end{bmatrix} \tag{4.74}$$

$$\{f_L\} = \begin{Bmatrix} 1/2(P_I + P_J) \\ M_{IJ} \\ -M_I^y \\ -M_I^z \\ M_J^y \\ M_J^z \end{Bmatrix} \tag{4.75}$$

$$\{f_{NL}\} = \begin{Bmatrix} 0 \\ (\frac{1}{2} M_I + \frac{1}{2} M_J)\theta^x_{IJ} + \frac{1}{12}(M^z_J - M^z_I)(\theta^y_J - \theta^y_I) + \frac{1}{12}(M^y_J - M^y_I)(\theta^z_I - \theta^z_J) \\ \frac{-1}{12}(M^z_J - M^z_I)\theta^x_{IJ} + \frac{\ell^t}{60}(6P_I + 2P_J)\theta^y_I + \frac{\ell^t}{60}(-P_I - P_J)\theta^y_J \\ \frac{1}{12}(M^y_J - M^y_I)\theta^x_{IJ} + \frac{\ell^t}{60}(6P_I + 2P_J)\theta^z_I + \frac{\ell^t}{60}(-P_I - P_J)\theta^z_J \\ \frac{1}{12}(M^z_J - M^z_I)\theta^x_{IJ} + \frac{\ell^t}{60}(-P_I - P_J)\theta^y_I + \frac{\ell^t}{60}(2P_I + 6P_J)\theta^y_J \\ \frac{-1}{12}(M^y_J - M^y_I)\theta^x_{IJ} + \frac{\ell^t}{60}(-P_I - P_J)\theta^z_I + \frac{\ell^t}{60}(2P_I + 6P_J)\theta^z_J \end{Bmatrix} \tag{4.76}$$

The first term on the righthand side of Eq. (4.71) is the linear approximation to the nodal forces and, hence, is not dependent on the deformation. The second term introduces the additional contribution as a result of a deformation. The linear term is given by

$$M_{IJ} = \frac{GJ}{\ell^t}\ \theta^x_{IJ} \tag{4.77}$$

where G is the shearing modulus, and J is a torsional constant expressed as a function of the element cross section [62]. This linear term M_{IJ}, has been added to Eq. (4.75), even though it does not result from normal axis stress.

The nodal forces and displacements in the global system can be related to the updated system by

$$\{F^t\} = [T]^T \{f^t\} \tag{4.78}$$

in which $\{F^t\}$ are internal forces due to the internal stresses of the element.

4.3. Soil Spring Finite Element

4.3.1. Soil model description

The basic assumptions employed for the treatment of the three-dimensional soil model are as follows:

(1) Torsional soil resistance is not considered in the soil-pile interaction [5].

(2) There is no coupling between the axial and lateral soil resistance. That is, the deformation modes for an isolated soil spring are independent of each other. Parker and Reese [66] have reported that the relationship between axial load and displacements of the soil is not significantly affected by the presence of lateral deflections of the soil, and vice versa. Soil behavior can thus be divided into axial and lateral parts as described in Section 3.3.

(3) The behavior of the soil at a particular depth is independent of the soil behavior at another depth [67].

(4) The lateral soil behavior is assumed to be independent in the two orthogonal lateral directions. That is, the soil resistance in the y direction is not affected by the soil resistance in the z direction. Two independent lateral springs will be placed in the y and z directions, respectively.

The soil displacements and forces are calculated on the basis of the displacements in the element coordinate system as shown in Fig. 15.

4.3.2. Soil springs

If nonlinear behavior is considered, the soil spring stiffness is not a constant and instead is a function of displacement. Only the lateral spring element in the y direction will be discussed here, since the other soil spring would follow the same derivations. As discussed in the previous section, the soil resistance directly opposes the lateral displacement in the y direction. The lateral soil resistance per unit length of the pile p is assumed to be linearly distributed along the pile element (Fig. 15). A set of p-y curves is represented by the modified Ramberg-Osgood cyclic model (see Sec. 3.2.3). In this figure, p, y, and k_{yt} (the lateral soil tangent stiffness) are in the updated element y direction. The relationship between incremental soil resistance and displacement can be expressed following Eq. (3.5) as

$$\Delta p_y = k_{yt} \Delta y \tag{4.79}$$

The quantities Δy, k_{yt}, and p_y are assumed to be linear functions of ξ,

$$\Delta y = [1 - \xi, \xi] \begin{Bmatrix} \Delta d_2 \\ \Delta d_8 \end{Bmatrix} = [N_s]\{\Delta d\} \tag{4.80}$$

$$k_{yt} = [1 - \xi, \xi] \begin{Bmatrix} k_{ytI} \\ k_{ytJ} \end{Bmatrix} \tag{4.81}$$

$$p_y = [1 - \xi, \xi] \begin{Bmatrix} p_{yI} \\ p_{yJ} \end{Bmatrix} \tag{4.82}$$

By the principle of virtual work

$$\{\Delta f\} = [k_y]_T\{\Delta d\} \tag{4.83}$$

where

$$[k_y]_T = \int_0^{\ell} [N_s]^T k_{yt} [N_s] dx \tag{4.84}$$

The explicit form of soil lateral tangent stiffness for y motions is

$$[k_y]_T = \ell^t \begin{bmatrix} 1/4\ k_{ytI} + 1/12\ k_{ytJ} & 1/12\ k_{ytI} + 1/12\ k_{ytJ} \\ \text{sym} & 1/12\ k_{ytI} + 1/4\ k_{ytJ} \end{bmatrix} \tag{4.85}$$

The total nodal forces $\{f\}$ can be obtained by using the principle of virtual work as

$$\{f\} = \int_0^{\ell} [N_s]^T p_y \, dx \tag{4.86}$$

or, explicitly, since degree-of-freedom 2 and 8 are for the y displacements of the beam element,

$$\begin{Bmatrix} f_2 \\ f_8 \end{Bmatrix} = \ell^t \begin{Bmatrix} 1/3\ p_{yI} + 1/6\ p_{yJ} \\ 1/6\ p_{yI} + 1/3\ p_{yJ} \end{Bmatrix} \tag{4.87}$$

The tangent stiffness of the nonlinear springs for the other cases (lateral z spring, vertical spring, and point spring) can be obtained in a similar manner (see Fig. 10). The matrix $[k_s]_T$ represents the

tangent stiffness for the soil model, which is added to the beam stiffness $[k]_T$ to form the tangent stiffness of the soil-pile interaction model.

4.3.3. Backwall soil model

Figure 16 shows the backwall soil model which is considered in integral bridge abutments. Longitudinal bridge movements may cause parts of the backwall to come into contact with or separate from the soil. In the idealized backwall soil model, it can be assumed that the backwall soil is attached to the backwall, so that the soil spring properties of the backwall soil can be treated the same as the soil springs attached to the pile.

4.4. Two-Dimensional Version

4.4.1. Specialization from the three-dimensional model

The general features of the two-dimensional are similar to the three-dimensional version, except the out of plane displacements are zero ($D_3 = D_4 = D_5 = D_9 = D_{10} = D_{11} = 0$), that is, three degrees of freedoms per node in the X-Y plane. The tangent stiffness matrices, $[k_0]$ and $[k_G]$, transformation matrix [T], and the displacements due to straining have much simpler forms than the three-dimensional version [5].

5. BASIC NONLINEAR SOLUTION TECHNIQUES

In the previous chapter, the finite element model which is used to predict the nonlinear behavior of soil-pile interaction has been described. The general incremental tangent stiffness equations for the beam-column and soil spring elements are the major results. In this section, these equations become the basis from which a general incremental nonlinear solution procedure is formulated.

5.1. The Incremental Load Technique

The conditions of equilibrium for a given structure are satisfied by solving the structural stiffness equations for the unknown generalized (global) displacements given a known applied loading. In a linear analysis environment, this solution procedure is straightforward because all of the stiffness parameters are constant, that is, independent of displacement and expressed in closed form. This is not the case in a nonlinear analysis environment where the stiffness parameters are themselves dependent on the state of total displacement, total stress, and material properties, and may not be conveniently expressed in closed form. In this case, the most suitable approach to analysis is to apply the total load in a series of small finite-sized increments. For each load increment, the resulting increment of displacement is determined from the incremental stiffness equations where the stiffness parameters are evaluated to reflect the instantaneous state of the total displacement, total stress, and material characteristics that exist just prior to the application of the load increment. The total displacement after the

load increment has been applied is evaluated by adding the computed displacement increment to the total displacement that exists prior to the application of the load increment.

This type of solution is a piecewise linear solution, a physical representation of which is illustrated in Fig. 17. This figure shows three load-displacement (F - d) curves for a single degree-of-freedom system. Curve A represents the linear behavior which would result by solving the governing stiffness equation for the total load applied in one increment; curve B is the piecewise linear solution which would result by applying the total load in several increments; and curve C represents the exact nonlinear behavior. It is clear that as the size of the load increment approaches zero (or the number of load increments approaches infinity), the piecewise linear curve approaches the true curve. Since load increments of infinitesimal order are impossible to achieve, a reasonable number of moderately sized load increments will be applied.

5.2. Newton-Raphson Iteration Method

As indicated in Fig. 17, it is desirable for the structural solution procedure to come as close to curve C with as few load increments as possible to obtain the desired analytical accuracy. This can be achieved by employing the Newton-Raphson method to satisfy equilibrium iteratively.

This approach is characteristic of the tangent stiffness technique where, in a given load increment, the Newton-Raphson iteration method is applied so that the element nodal displacements are successively

corrected until joint equilibrium is satisfied. These displacement corrections are computed using element tangent stiffness matrices, which are successively computed to reflect the most current state of total displacement, total stress, and material properties.

The basic characteristics of this technique are illustrated in Fig. 18 for a single degree-of-freedom system which is characterized by the following parameters:

σ = element stress

f = element force

F = applied external load

d = element displacement (in this case for a single degree-of-freedom, this is the same as the global displacement D)

E_T = element material property parameter--the instantaneous slope of the element stress-strain relationship

$k_T = k_T(d, \sigma, E_T)$ the tangent stiffness--a function of total element displacement d, total element stress σ, and the state of the element material property parameter E_T.

At a particular level of applied load, given by F_j, the total element stress is given by σ_j, the total element force is given by f_j, the total element displacement is given by d_j, and the current tangent stiffness is given by k_{Tj}. This state, which is indicated by point 1 on Fig. 18, is reached after the application of several load increments.

At this level of applied load F_j, the description of the Newton-Raphson iteration begins with the application of an increment of external load ΔF. To satisfy equilibrium, the following relationship must be true:

$$f_j + (K_{Tj})\,\Delta d = F_j + \Delta F \tag{5.1}$$

Equation (5.1) is a representation of the linearized incremental analysis wherein the structure is assumed to behave linearly during the application of an incremental load ΔF. Equation (5.1) also establishes the analysis at point 2 of Fig. 18. This increment of displacement Δd_j^1, which results from the application of ΔF, is computed by rearranging Eq. (5.1) and solving for Δd_j^1 as follows:

$$\Delta d_j^1 = k_{Tj}^{-1} (F_j + \Delta F - f_j) \tag{5.2}$$

The increment of displacement is added to the previous total displacement d_j to form the new total displacement

$$d_j^1 = d_j + \Delta d_j^1 \tag{5.3}$$

where

d_j^1 = the new total displacement

Note that the subscript denotes the load increment number and the superscript denotes the iteration number within this load step.

The analysis is still at point 2 on Fig. 18, where a new material property parameter E_{Tj}^1 and a new state of element stress σ_j^1 are computed in order to reflect the new displacement d_j^1. Since the element stiffness k_T is dependent on σ, d, and E_T, it is recomputed to reflect σ_j^1, d_j^1, and E_{Tj}^1 as follows:

$$k_{Tj}^{1} = k_T \left(\sigma_j^1, d_j^1, E_{Tj}^1\right) \tag{5.4}$$

The stiffness parameter k_{Tj}^{1} is the tangent stiffness at point 3 on the actual load-displacement curve of Fig. 18.

The internal force due to the new displacement d_j^1 and the new state of element stress σ_j^1 is computed in the following manner:

$$f_j^1 = f(\sigma_j^1, d_j^1) \tag{5.5}$$

where

f_j^1 = the new total internal force

Equation (5.5) establishes the analysis at point 3 of Fig. 18. At this point, equilibrium is satisfied if and only if the following relationship is true:

$$F_j + \Delta F - f_j^1 = 0 \tag{5.6}$$

However, because of nonlinear behavior, it is clear that equilibrium at point 3 is not satisifed exactly by Eq. (5.6) because Δd_j^1 and d_j^1 were computed on the basis of the previous tangent stiffness k_{Tj}, while f_j^1 was computed on the basis of the new state of σ_j^1 and d_j^1. This established the need for a solution technique like the Newton-Raphson method, which attempts to modify f_j^1 in such a way as to satisfy the equilibrium equation [Eq. (5.6)] at the new applied load level $F_j + \Delta F$.

Since Eq. (5.6) is not satisfied, it is more suitably expressed in the following form:

$$\Delta F_j^1 = F_j + \Delta F - f_j^1 \tag{5.7}$$

where ΔF_j^1 is called the residual or unbalanced force, which results from the changing stiffness. The Newton-Raphson method thus attempts to find an equilibrium solution for an increment of external load ΔF, by forcing the residual ΔF_j^1 to be as close to zero as possible through a series of iterations.

The next step in the iteration method is to attain a new equilibrium solution by assuming that the residual is applied as an external load

$$\begin{aligned} \Delta d_j^2 &= \left(k_{Tj}^1\right)^{-1} \left(F_j + \Delta F - f_j^1\right) \\ &= \left(k_{Tj}^1\right)^{-1} \left(\Delta F_j^1\right) \end{aligned} \tag{5.8}$$

where Δd_j^2 represents a new displacement increment, which is a displacement correction to d_j^1, in order to adjust equilibrium to compensate for the residual. The analysis is now at point 4 of Fig. 18. This Δd_j^2 is added to d_j^1 and a new total displacement d_j^2 is obtained. Following the same procedures, one computes σ_j^2, E_{Tj}^2, k_{Tj}^2, and f_j^2. If this iteration is convergent, then this new residual is smaller than the previous residual and the true equilibrium solution is approached. Solution of the displacement for the next load increment can proceed by the same processes as before.

5.3. Convergence Criteria

If the equilibrium is ultimately satisfied for a particular load increment, this method must result in a series of residuals which tend toward zero. It will be assumed that the iteration converges and equilibrium is satisfied when the most recently computed displacement increment and/or residual is less than or equal to some user-prescribed tolerance [59]. The convergence criterion used herein for a single degree-of-freedom is

$$\frac{\left|\Delta d_j^{i+1}\right|}{\left|d_j^i\right|} \leq \text{tolerance} \tag{5.9}$$

where Δd_j^{i+1} is the most recently computed displacement increment and d_j^i is the current state of total displacement just before Δd_j^{i+1} is added to form a new total displacement. If Eq. (5.9) is satisfied, then the convergence is indicated, equilibrium is sufficiently satisfied, the iteration stops, and the analysis proceeds to the next increment of applied load. This stage of the analysis is indicated by point 6 of Fig. 18.

In the event that convergence is not satisfied, it may be that the displacement increments are diverging, which indicates that the iteration process cannot find an equilibrium solution for the given increment of applied load. Divergence can be caused by a numerical instability because of the stiffness changing too rapidly within the load increment. In the event of such behavior, a smaller load increment may produce more stable behavior.

On the other hand, if the load increment is already reasonably small, divergence may signify that the structural stiffness is tending toward zero, which indicates instability of the structure. In any case, if divergence is detected, the Newton-Raphson process and the total analysis are terminated.

The Newton-Raphson process and the total analysis are terminated on the basis of one additonal mechanism. It is a safety mechanism and is employed in order to prevent excessive iterations. Thus, the iterative process is terminated and the total analysis is terminated if the number of iterations exceed a user-specified maximum.

5.4. The Complete Solution Procedure in Detail

The basic properties of load incrementation and Newton-Raphson iteration described in the previous sections are combined to form the basis of the total nonlinear solution procedure. In this nonlinear solution procedure, the most current information available concerning the structure is used to calculate the incremental quantities at any step. In other words, the tangent stiffness matrix at the start of each iteration is used to estimate the next incremental quantities. It requires the formation of the element tangent stiffness transformed into global coordinates at the start of each iteration.

Suppose that current $\{\varepsilon_j^i\}$, $\{\sigma_j^i\}$, $\{P_j^i\}$, $\{M_j^i\}$, $\{M_j^{yi}\}$, $\{M_j^{zi}\}$, $\{r_j^i\}$, $\{F_j^i\}$, $\{X_j^i\}$, $\{b_j^i\}$, $\{e_j^i\}$, $\{D_j^i\}$, $\{d_j^i\}$, $\{A_{L_j}^i\}$, and $\{A_{NL_j}^i\}$ are given at the jth increment and the ith iteration. The condition i = 1 and j = 1 is the initial stage in the nonlinear problem. Thus, except for $\{X_1^1\}$,

b_1^1 , and e_1^1 , the above vectors are null. To generate the i + 1 iteration by the updated Lagrangian method, the following steps will be followed:

Step 1: Calculate the current unbalanced forces in the global system

$$\{\Delta F_j^{i+1}\} = \{F_{j+1}\} - \{F_j^i\} \tag{5.10}$$

where

$\{F_{j+1}\}$ = forces for j + 1 load increment

$\{F_j^i\}$ = forces from previous iteration i

Step 2: Establish the current element coordinates $\{x_j^i\}$ for the element at hand by formulating the transformation matrix $[T_j^i]$ from the current global coordinates $\{X_{Ij}^i\}$, $\{X_{Jj}^i\}$, and $\{X_{Kj}^i\}$.

Step 3: Generate the structural tangent stiffness in current coordinates $\{X_j^i\}$

(a) Establish E_T at each integration point through the cross section (with current strain deformation); that is, Eq. (3.5) is used to calculate E_T for static and cyclic loading.

(b) Perform $(EA)_T$, $(EK^y)_T$, $(EK^z)_T$, $(EI^y)_T$, $(EI^z)_T$, and $(EI^{yz})_T$ integrals at each end from Eqs. (4.33) to (4.38).

(c) Determine $[k_{0j}^i]$ [from Eq. (4.43)]; also with current $\{P_j^i\}$, $\{M_j^i\}$, $\{M_j^{yi}\}$, and $\{M_j^{zi}\}$ [from Eqs. (4.29 to (4.32)] find $[k_{Gj}^i]$ from Eq. (4.45).

(d) Generate $[k_j^i]_T$ by adding $[k_{sj}^i]_T$ [from Eq. (4.85)].

(e) Transform $[k_j^i]_T$ into global coordinates through the transformation matrix $[T_j^i]$ (Eq. 4.52) to get $[K_j^i]_T$ (Eq. 4.55).

(f) Assemble $[K_j^i]_T$ into the structural tangent stiffness $\Sigma [K_j^i]_T$.

Step 4: Solve for the incremental displacements with the current unbalanced forces

$$\{\Delta D_j^{i+1}\} = [\Sigma K_j^i]_T^{-1} \{\Delta F_j^{i+1}\} \tag{5.11}$$

Step 5: Update coordinates and forumlate $[T_j^{i+1}]$

(a) Update coordinates for node I, J, and K from Eqs. (4.57) to (4.58).

(b) Update displacements, $\{D_j^{i+1}\} = \{D_j^i\} + \{\Delta D_j^{i+1}\}$.

(c) Update nodal unit vectors $\{b_j^{i+1}\}$ from Eqs. (4.63) to (4.64).

(d) From the updated coordinates in (a), find the unit vectors $\{e_j^{i+1}\}$ in element coordinate system from Eqs. (4.47) to (4.49) to formulate $[T_j^{i+1}]$.

Step 6: Calculate updated strains and stresses

(a) Use the unit vectors $\{b_j^{i+1}\}$, $\{b_j^{i+1}\}$, and $\{e_j^{i+1}\}$ to find $\{d_j^{i+1}\}$ from Eqs. (4.65) to (4.70).

(b) Compute $\{\varepsilon_j^{i+1}\}$ from Eq. (4.7).

(c) Compute $\{\sigma_j^{i+1}\}$ from Eq. (3.3).

Step 7: Compute element nodal forces in the element system

(a) Perform numerical integration from Eqs. (4.29) to (4.32) and use Eqs. (4.72) and (4.73) to find $\{A_{Lj}^{i+1}\}$ and $\{A_{NLj}^{i+1}\}$.

(b) Compute $\{f_j^{i+1}\}$ from Eq. (4.71).

Step 8: Find the equilibrium external nodal forces in global coordinates

$$\{F_j^{i+1}\} = \Sigma [T_j^{i+1}] \{f_j^{i+1}\} \tag{5.12}$$

Step 9: Test for convergence. If not satisfied; return to Step 1. Otherwise, store these stresses and strains and go to the next increment load $\{F_{j+2}\}$. Each step of this algorithm is tangent to the load-versus-displacement curve, as suggested before. The process is interpreted graphically in Fig. 19.

5.5 Guidelines for Program Usage

The basic philosophy of the finite element method is to analyze a piecewise approximation to the structure. Specifically, the structure or body is divided into finite elements; simple functions, usually polynomials, are assumed to approximate the displacements within each element. The greater the number of terms included in the approximation, the more closely the exact solution is represented [65]. For example, in the beam-column element the displacement functions (shape functions) are assumed to be a linear polynomial in the longitudinal direction and a cubic polynomial in the transverse direction.

In the region of high curvature gradients, a finer mesh is necessary to obtain a satisfactory solution. For a beam on an elastic foundation, four to eight elements in a one-half wave of the deflected shape will provide satisfactory results [5]. For elastic problems, the length of one-half wave is π/β [68] where

$$\beta^4 = \frac{k_y \ell^4}{EI} \tag{5.13}$$

where

k_y = the lateral stiffness of the soil

ℓ = length of the pile

EI = the flexural rigidity of the pile

For inelastic problems, high curvature gradients occur in the region of a plastic hinge and a finer mesh is required to achieve comparable accuracy. The experience of the authors indicates that the change in curvature between elements should be no more than 0.0001 rad./in.

Mesh sizes must be sufficiently fine to model changing soil and pile properties such as layered soil or tapered piles.

Load step sizes are controlled by the relative amount of nonlinear behavior. For example, convergence can become a numerical problem in the plastic region due to the difference between loading and unloading moduli. This problem can usually be overcome by reducing the load or displacement increment.

Mesh size and convergence problems are encountered in all types of finite element analysis. Usually, these problems are solved by

reducing the mesh (or load increment) size until no significant change occurs in the structural response.

6. ANALYTICAL AND EXPERIMENTAL VERIFICATIONS

Based on the theory outlined in Chapters 4 and 5, two computer programs, IAB2D and IAB3D (Integral Abutment Bridge Two- and Three-Dimensional Finite Element Computer Programs) have been developed to solve the nonlinear soil-pile interaction problems for both two- and three-dimensional cases. A number of examples have been analyzed to establish their reliability.

6.1. Analytical Verification

6.1.1. Two-dimensional analytical verification

Several numerical example problems are solved using the two-dimensional computer program IAB2D. These problems were also solved with IAB3D to confirm the validity of the three-dimensional computer program. A beam-column problem and a short, thick column problem were first used to check geometric and material nonlinearity, respectively. Additional problems were analyzed, such as: (a) snap-through problem, (b) Williams' toggle problem, (c) two-dimensional frame problem, (d) thermal problem, and (e) soil problem.

6.1.1.1. Beam-column problem Figure 20 shows a beam-column (HP 14 x 73) with a concentrated lateral load, Q, acting on the midspan. Only geometric nonlinearity was considered here. The theoretical displacement at the midspan can be evaluating by solving the classic differential equation for a beam-column [69] (refer to Fig. 20). Fig. 20 shows the relation between P and δ, if P is allowed to increase. The

load-displacement relation is not linear. This is true regardless of whether Q remains constant (solid line) or increases proportionally with P (dashed curve). The displacement of a beam-column is, thus, a linear function of Q but a nonlinear function of P. The results obtained by running the IAB2D computer program (two beam elements) are also plotted in Fig. 20. Significant differences between these results and the classical beam column solution occur only when P approaches P_{cr}.

6.1.1.2. Short column problem Figure 21 shows a short thick column with negligible geometric nonlinearities. Simple plastic theory assumes that a member subjected to pure bending will sustain a certain limiting bending moment value, M_p. If a member is subjected to the combined action of bending moment and axial forces, the maximum moment capacity is reduced [70-72]. Three different applied load cases are analyzed in this example:

Proportional Loading

Case (1) $e = \frac{M}{P} = \infty$ (pure moment)

Case (2) $e = 0.467'$

Nonproportional Loading

Case (3) θ increased to θp and Δ held equal to zero, then Δ increased as θ is held constant.

The results obtained from the above load cases are plotted in Fig. 21. Theoretical values are also shown. The computer program gives satisfactory agreement with theoretical values. Case (3) illustrates that the moment decreases as the rotation is held constant and the axial deformation is increased.

6.1.1.3. Snap-through problem Figure 4.22 shows a simple symmetric truss with a concentrated load at the top. This type of problem can be solved by incrementing the deflections (rather than loads). The load-deflection curve is shown in Fig. 4.22. Several positions can be used to check the results. When the truss has a deflection where Δ equals 1.2 in. (the truss is in the horizontal position), the truss resists no load. If the truss has a deflection where Δ equals 2.4 in. (the truss is below horizontal by 1.2 in.), the strain is zero and, hence, the bar forces are zero. If Δ is greater than 2.4 in., the truss members are in tension and the load increases.

6.1.1.4. Williams' toggle problem The Toggle shown in Fig. 23 is the same problem as the previous section except the ends are fixed. The load-deflection curve can be obtained by using specified load or displacement as shown in Fig. 23. A similar problem with different material and geometric properties was first analyzed and tested by Williams [73]. The load-deflection curve in Fig. 23 shows that the shape is compatible to the Williams' test results.

6.1.1.5. Two-dimensional frame problem A two-dimensional square portal frame subjected to two vertical loads and a small horizontal load is shown in Fig. 24. The theoretical buckling loads for the side-sway mode are: P_{cr} (fixed base) 4605 kips, and P_{cr} (hinged base) 1170 kips [74]. The horizontal load for the finite element analysis is quite small (0.001 P) but is sufficient to initiate geometrically nonlinear behavior. The load-deflection curves for both cases (fixed base and

hinged base) are shown in Fig. 24. The numerical results show that a lower bound on the critical load for the fixed base is 4600 kips and for the hinged base is 1150 kips.

6.1.1.6. Thermal problems Several thermal problems were used to check thermal strain caused by temperature changes: (a) cantilever beam, subjected to uniform and gradient temperature changes; and (b) fixed-end beam, subjected to uniform and gradient temperature changes. The results, although not shown here, compared exactly with theoretical solutions.

6.1.1.7. Soil problems Soil models were also tested in the two-dimensional computer program by checking the lateral and axial behavior of the soil springs. A rigid pile was analyzed with IAB2D by specifying loads and displacements in the axial and lateral directions to observe soil responses. The theoretical displacements should follow the p-y, f-z, and q-z curves. The numerical results were identical to the theoretical answers and are not shown here [5].

6.1.2. Three-dimensional analytical verification

Three sample problems were analyzed with the three-dimensional program: (a) large deflection analysis of a shallow arch; (b) large displacement, three-dimensional analysis of a 45° bend; (c) a simple soil problem to check soil nonlinearity and cyclic behavior.

6.1.2.1. Large deflection analysis of a shallow arch The clamped circular arch with a single static load at the apex was analyzed

for buckling using the beam-column element, as shown in Fig. 25. The material of the arch was assumed to be isotropic linear elastic. One half of the arch was idealized using six equal beam-column elements.

This arch was also analyzed by Bathe and Bolourchi, who used 6, 12, and 18 equal beam elements and 8 six-node isoparametric elements with 2 x 2 Gauss integration [43]. Mallet and Berke used 4 "equilibrium-based" elements [75]. Dupuis et al. [76] analyzed the same arch using curved beam elements. In addition, the experiment results given by Gjelsvik and Bodner [77] are also shown in Fig. 25.

Fig. 25 shows the predicted load-deflection curve of the arch obtained by using IAB3D. In this analysis, the use of beam-column elements is quite effective, and the numerical results match the experimental results.

6.1.2.2. Large displacement three-dimensional analysis of a 45° bend The large displacement response of a cantilevered 45° bend beam subjected to a concentrated end load, as shown in Fig. 26, was calculated. The concentrated tip load is applied in the positive Y direction. The material was assumed to be linearly elastic.

The linear and nonlinear solution of this curved beam subjected to a tip load was given by Bathe and Bolourchi [43] by using 8 equal straight beam elements and 16 sixteen-node, three-dimensional solid elements. Fig. 26 shows the tip deflection predicted by ADINA using the two finite element models [78]. The ADINA solution, obtained with a large number of elements and load steps, should be regarded as the most correct answer.

The numerical results obtained by using the IAB3D computer program with eight equal, straight beam-column elements is also shown in Fig. 26. The predicted tip deflections match with ADINA solutions. Fig. 27 also shows the deflected shapes of the bend at various load levels.

6.1.2.3. Soil problems Several soil problems were analyzed to check the soil material nonlinearity and cyclic behavior. Since the vertical, lateral, and point springs are assumed to be similar and uncoupled, only the lateral springs are considered here. For example, suppose an HP 14 x 73 pile was embedded below the ground as shown in Fig. 28. The soil responses can then be observed by specifying loads and displacements in the Y and Z directions. Theoretical displacements and soil resistance follow the p-y curve path. For a specified load, the displacement will be obtained from the Newton-Raphson solution algorithm. For a specified cyclic load and displacement, the soil response will follow the modified Ramberg-Osgood cyclic curves. Figs. 29 and 30 show the soil response for specified cyclic loads in Y, Z, and YZ directions, respectively.

Fig. 29 shows that the maximum displacement in Y and Z directions are the same (1.5 in.). Since the length of the web and flange for the H pile are very close, both directions have identical p-y curves. The maximum displacement in the YZ direction (Fig. 30) is not the same as it is in the Y and Z directions (Fig. 29), even though the total applied forces are equal. Since the soil springs in the Y and Z directions are assumed to be independent, the total applied force in YZ direction can be resolved into Y and Z components (707 kips). These forces produce maximum displace-

ments in both the Y and Z directions at 0.9 in. or a total of 1.3 in. in the YZ direction which is less than the maximum displacement for Y and Z cases.

6.2. Experimental Verification

The results from four experimental pile tests will now be compared to results from the IAB2D program. The experimental tests consist of an axial load test on an end-bearing H pile, lateral load tests on drilled concrete piers and on timber piles, and axial and combined load tests on a timber pile. Preliminary investigations of the first two examples were conducted by Yang et al. [5]. The revised investigations of these two examples and the two final examples were conducted by Edmunds [79]. The results are summarized herein for completeness, i.e., to document the analytical method and the associated computer program.

6.2.1. Load transfer in end-bearing steel H piles

In Ref. [80], the increase in the load-carrying capacity of an end-bearing pile due to load transferred to the surrounding soil by friction was experimentally studied. Site conditions, pile driving, and instrumentation were examined. The strain-gage readings were analyzed to determine the distribution of the load transferred by friction along the piles. The piles were loaded and unloaded in increments to 150 kips, 300 kips, 450 kips, and 600 kips. From the plots of pile load as a function of depth, the true elastic shortening can be obtained, and the total displacements at each point of the pile can be calculated by adding the accumulated elastic shortening to the observed tip displacements [5]. Two sets of f-z and q-z curves (one set for each pile) can be constructed

[30]. Since all the pile load tests were held at the same site, the final set of f-z curves was taken as the average of the f-z cufves from the HP 14 x 89 and HP 14 x 117. Soil parameters for the modified Ramberg-Osgood cyclic curves are obtained by approximately fitting the irregular shape of the average f-z curves and q-z curves. The pile is subdivided into eight elements of unequal length. The Ramberg-Osgood parameters used in the analysis are given in Tables 9 and 10. The load-settlement curves for the HP 14 x 117 pile, both observed and predicted values, are plotted in Fig. 31. The results calculated from the computer solution (IAB2D) are a fairly good approximation to the results obtained in the experiment.

6.2.2. Lateral load tests on drilled piers in stiff clay

Two drilled piers were selected from the laterally loaded pile tests conducted by Bhushan et al. [81]. Measurements of horizontal ground line displacements were made for two piers. Soil properties, as determined by borings at each test site, are summarized in Table 11. The two piers were constructed with a spacing of about 20 ft. and were loading by jacking between them. Displacements of the piers were measured by the dial gauges located one ft. above ground surface. The properties of Table 11 are consistent with a very stiff clay. Thus, the p-y curve was approximated using the Ramberg-Osgood parameters for very stiff clay given in Table 3.

The displacements at the top of the pier are plotted in Fig. 32 (Pier No. 1) and Fig. 33 (Pier No. 2). A comparison between the predicted values obtained from IAB2D and the experimental results shows

that the results are within limits usually expected with this type of analysis (30 percent approximately). The error in the initial stiffness in these figures is caused by the approximation of the initial slope of the p-y curves.

6.2.3. Lateral load tests on timber piles

Lateral load tests were conducted by Alizadeh [82] on four instrumented, Class B timber piles at two sites approximately 1000 ft. apart. The two piles at each test site were seven ft. apart. The soils at Test Site 1 consisted of four ft. of sand and gravel underlaid by layers of clay. The soils at Test Site 2 consisted of a layer of "fat clay" over layers of silt and "lean clay." At both sites, the clay soils had a soft to medium consistency. The timber piles used were 43 ft. long and were slightly tapered (one ft. diameter near the ground surface and 0.8 ft. diameter near the tip). The modulus of elasticity of each pile was determined from calibration tests and is given in Table 12 [82]. For the clay and silt soils, average undrained cohesion values of 620 psf at Test Site 1 and 670 psf at Test Site 2 were used. For determining the Ramberg-Osgood parameters in Table 3, these soils were assumed to be soft clay. The sand and gravel layer at Test Site 1 was assumed to be a medium sand. A constant pile diameter equal to the average diameter of the upper half of the embedded portion of the pile was used. The ultimate strength of the timber was estimated to be 7230 psi [83].

The experimental results and the results obtained with the finite element program are compared in Figs. 34 to 36. For the smaller loads,

the results from the program for piles 1-A and 1-B are close to the experimental values, but for the 20 kip applied load, there is quite a difference (Figs. 34 and 36). The computed results were not as close to the experimental results for piles 2-A and 2-B. The discrepancies are mainly due to inadequate modeling of the soil, that is, the variation of soil properties with depth was not clearly defined. Better computed results could be obtained if more information on the variation of soil properties with depth were available. Some accuracy is also lost by approximating the soil resistance-displacement curves with the Ramberg-Osgood equation.

6.2.4. Pile response to axial and lateral loading

Combined axial and lateral load tests were conducted on three pile groups and on a single pile by Stevens et al. [84]. The experimental data for the single pile will be compared to values predicted by the finite element program. The soil profile at the test site is shown in Fig. 37. A schematic diagram of the pile is also shown in Fig. 37. The piles used in the test were untreated green Douglas fir piles. The modulus of elasticity and ultimate strength of the timber were taken to be 2000 ksi and 3615 psi, respectively [83]. The piles had initial lengths of 43 to 45 ft.

The piles were subject to four types of tests: cyclic preloading, pile driving effects, axial load testing, and combined load testing. The results of the axial and combined load tests will be presented here. For the axial load tests, the loads were applied in 60 kip increments until failure. For the combined load test, an axial load of 60 kips

was first applied to the pile. Then, a lateral load was applied to the pile 28 in. above the ground surface in increments of 12 kips until failure. The lateral deflection was measured 33 in. above the ground surface.

For the finite element program, the 20-ft.-thick layer of sand near the surface was assumed to be medium sand. The silty clay and sandy silt layers were modeled as stiff clay and the layer of sand near the bottom of the pile was assumed to be dense sand. The curve parameters for each layer were determined from the equations in Tables 3, 4, and 5. A constant pile diameter of 11.75 in. was used for the computer analysis. The boundary conditions used in the computer analysis are shown in Fig. 37. The pile was assumed to be pinned at the top of the vertical hydraulic jack. The pile cap and hydraulic jack were modeled as a single rigid element.

The results of the experimental tests and the computer analysis are shown in Figs. 38 and 39. These figures show that the results obtained using the finite element program are close to the observed values, although the finite element program does predict a lower ultimate load for the axial load test.

7. PILE BEHAVIOR IN INTEGRAL ABUTMENT BRIDGES

7.1. Introduction

An idealized mathematical model of an integral abutment bridge is shown in Fig. 3. In the soil-pile interaction problem, the pile will take a shape similar to the solid line in Fig. 40, as the pile is subjected to the specified lateral displacement Δ_h (to simulate induced thermal expansion or contraction) and no rotation (since the bridge is much stiffer than the pile) at the pile top. As the vertical load V (to simulate the bridge load) is applied, the pile deflects as illustrated by the dashed line. As can be seen, some of the soil springs will be subjected to load reversals (cyclic loading). Similarly, some of the pile moments are reversed during this loading history. A modified Ramberg-Osgood cyclic model (see 3.2.3) for soil and pile cyclic behavior has been adopted. A typical pile (HP 10 x 42) in an integral abutment bridge with an embedded length of about 40 feet will be used to evaluate the ultimate vertical load capacity after the specified lateral displacement has occurred. Timber and concrete piles are also included in this study. Six typical Iowa soils (Tables 7 and 8) were selected to study the soil-pile interaction in integral abutment bridges.

7.2. Steel Piles in Nonskewed Bridges

7.2.1. Friction and end-bearing piles

The effect of the horizontal pile top displacement on the pile capacity for friction and end-bearing piles bending about the weak axis

will be analyzed. The point spring resistance in the end-bearing piles is taken to be large to simulate stiff rock. In the IAB2D program, the total displacement Δ_h is applied in increments of 0.5 in., while V is held equal to zero. Once the total Δ_h is achieved (0, 1, 2, or 4 in.) V is increased in increments of 5 kips or 10 kips until the vertical capacity of the pile is reached.

Results obtained by running the IAB2D program will be presented here to show the behavior of a steel H pile embedded in Iowa soils. (Chapter 3 summarizes the soil properties.) Sets of vertical load-settlement curves with specified lateral displacements (see Fig. 40) for a friction pile in very stiff clay and end-bearing piles in soft clay and loose sand are shown in Fig. 41 through 43 respectively. These are typical of the other cases. The ultimate vertical load V_u is determined from a load-displacement diagram using the following procedures. For piles whose load-displacement curve exhibit a definite maximum load, this maximum load is taken as the ultimate load. For all other piles, a line with a slope of AE/L is drawn through the origin of the load-displacement curve. A second line, which intersects the settlement axis at (0.15 + 0.1b) inches, is drawn parallel to the first line. The value b is the diameter or width of the pile in feet. The intersection of the second line and the load-displacement curve gives the ultimate vertical load [5, 85]. Nondimensional forms of the ultimate pile load ratio V_u/V_{uo} versus the specified lateral displacement Δ_h for friction piles and end-bearing piles in different types of Iowa soils are shown in Figs. 44 and 45,

respectively. The value V_{uo} represents the ultimate load when there is no induced lateral displacement.

Fig. 44 shows that a lateral movement up to 4 in. has no effect on the vertical load capacity of friction piles. These results indicate that for friction piles, the failure mechanism (slip mechanism) occurs when the soil fails and pile slips through the soil. The load capacity of the pile for the slip mechanism is equal to the sum of the load carried by skin friction along the length of the pile and the load carried by end-bearing at the pile tip.

In the end-bearing piles the failure mode is dominated by the yield load of the pile. The slip mechanism does not occur. Fig. 45 (a and b) shows that the ultimate load-carrying capacity of the pile is reduced in soft clay and loose sand. Since the lateral stiffness of the soil in soft clay and loose sand is relatively small, the pile is permitted to deflect laterally under vertical load and the lateral failure mode eventually develops. For the stiff soils, the full yield load of the pile is developed before lateral motions are permitted.

7.2.2. Effect of cyclic lateral displacements

Two cases are presented here to illustrate the effect of cyclic lateral displacements on pile capacity: friction piles in very stiff clay and end-bearing piles in soft clay. These are the cases most likely to be affected by cyclic loading. The specified lateral displacement is cyclically applied; for example, Δ_h is cycled from +1.0 in. to -1.0 in. to +1.0 in. The vertical load V is then applied.

The resultant set of vertical load-settlement curves, after the specified cyclic lateral displacements for a friction pile in very stiff clay and end-bearing pile in soft clay, are identical to those shown in Figs. 41 and 42 respectively. These results show that the vertical load capacity is not significantly affected by the cyclic lateral displacements.

7.2.3. Effect of pinned pile top

The condition at the pile top, which is embedded in the concrete abutment, depends on the relative stiffness of the superstructure and the abutment. The top of the pile can be assumed to be (a) fully restrained without rotation (fixed pile head), (b) partially restrained allowing some degree of rotation, or (c) pinned, allowing complete rotation freedom (pinned pile head). The friction and end-bearing piles with fixed pile heads in very stiff clay and soft clay have been discussed in Section 7.2.1. The friction and end-bearing piles with pinned pile heads in very stiff clay and soft clay will be presented here. Results obtained from IAB2D computer program shows that the load capacity of the friction pile is not affected by the boundary condition on the pile top. In both cases, the failure mechanism is controlled by slip. Fig. 46 shows the nondimensional forms of the ultimate vertical load ratio versus specified lateral displacements of end-bearing piles with pinned pile heads in very stiff clay and soft clay. In the case of the end-bearing pile with a pinned head, the load capacity is reduced more in soft clay than in very stiff clay (Fig. 45a. and Fig. 46). The failure mechanism in both cases is controlled by the lateral mechanism, which is affected by the

number of plastic hinges and the lateral soil resistance. The fixed head requires an additional plastic hinge to form before failure. The reduced lateral resistance of soft clay more easily permits the lateral mode.

7.3. Nonskewed Bridge Example

7.3.1. Bridge studied

A nonskewed bridge located at State Avenue over U.S. 30, Story County, Ames, Iowa, was chosen as an example to investigate the behavior of an integral abutment bridge subjected to thermal expansion and contraction. Plan and elevation views of the bridge are shown in Fig. 47. It is a 245-ft.-long, prestressed concrete bridge with integral abutments and piers. There are no expansion joints on the bridge; however, expansion joints are located in the approach slab about 20 ft. from each end of the bridge.

A section through the bridge deck is shown in Fig. 48. Pretensioned, prestressed concrete beams were used to support a poured-in-place concrete deck. The beams and deck were designed to act as a monolithic unit, even over the piers. The steel piles, pier cap, diaphragm, concrete beam, and concrete deck were all reinforced to behave as a single unit. A section through the abutment is shown in Fig. 49. The pile is oriented with its strong axis along the roadway center line (bending about the weak axis) and is reinforced within the abutment cap and diaphragm to transmit the full plastic moment of the pile (HP 10 x 42).

More details about the State Avenue bridge can be found in Iowa Department of Transportation design sheets, File No. 22616 and Design No. 267.

7.3.2. Mathematical model of the bridge

The proposed mathematical model of the State Avenue bridge is shown in Fig. 50(a). Two types of prestressed concrete beams, C30-50 and C80, are used in this bridge. A simplified two-dimensional model of the bridge, which contains one concrete beam, a section of the abutment and pile cap, and one pile as shown in Fig. 50(b), was used. The cross-sectional properties have been calculated based upon this idealization. Note also that the bridge was assumed to be symmetrical about the mid-length. Fig. 51 shows the section through the abutment and the soil profile. The granular backfill is considered as dense sand. The abutment pile was driven in an 8-ft. deep, oversized hole through the fill. Voids around the pile are assumed to be still empty. The finite element model is shown in Fig. 52. Six beam-column elements, each 20 ft. long, are used to represent the concrete beam; two beam-column elements, each 3.75 ft. long, are used to represent the abutment and pile cap; and 12 elements with unequal length are used to represent the pile. There are no vertical soil springs along the abutment and the predrilled oversized hole. No lateral soil springs are attached within the predrilled oversized hole. Soil properties based on the Iowa soils are calculated. The temperature change is taken as -60° F to +60°F from the construction temperature [35].

7.3.3. Numerical results

Several cases have been investigated in order to fully understand the behavior of the integral abutment bridges with thermal expansion and contraction. These are: (a) no thermal changes, (b) with +60°F temperature changes, (c) without backfill, with +60°F temperature changes, (d) with a complete cycle of temperature changes (-60°F to +60°F), and (e) without concrete bridge model, but with specified lateral displacements equal to the displacements in case (b). After each of these loadings, a vertical load is applied at the top of the pile until failure (Fig. 52).

Vertical load-settlement curves obtained with IAB2D program are shown in Fig. 53. Case (e) is actually a single pile with an abutment attached to it, very similar to the cases in Sec. 7.2. It fails by the slip mechanism when the applied load exceeds the friction force of the soil springs. The rest of the cases do not fail at this level, since the pile is part of the bridge model. As the pile moves downward, the concrete bridge beams carry some load as a cantilever type structure. Cases (a) and (b) have noticeably different load-settlement curves. In case (b), the +60°F temperature change expands the beams and activates the passive soil pressure behind the abutment. (See diagram in Fig. 54.) Since the beam and abutment are not colinear, a moment M and shear V_s are introduced into the concrete beam. The shear V_s, equal to about 20 kips in this case, is applied to the pile. In other words, the pile is subjected to a 20-kips downward load before the vertical live load is applied. From Fig. 53, cases (a) and (b) do have a 20-kips

difference in ultimate load. This is also confirmed by case (c), which is identical to case (b) except that the backfill is removed. In this case, the initial 20-kip pile load is not introduced and the load-settlement curve is about the same as case (a). A comparison of cases (b) and (d) shows that there is no difference in load-settlement curves for cyclic and noncyclic thermal changes.

7.4. Steel Piles in Skewed Bridges

As illustrated in Appendix B, pile orientations for steel H piles in integral abutment, skewed bridges can be classified into four types: the web of the pile perpendicular (Type 1) or parallel (Type 2) to the roadway center line, and the web of the pile parallel (Type 3) or perpendicular (Type 4) to the center line of the abutment. In addition, some states use circular piles (Type 5) in integral abutments on skewed bridges. In each of these types, the pile is bending about its weak axis, strong axis, or a combination of both. Bending of piles about the weak axis was discussed in Sec. 7.2. Before proceeding to an actual bridge, individual piles displaced laterally about the strong axis and at 45° to the strong and weak axis will be studied.

7.4.1. Bending about the strong axis

For H piles bent about the strong axis (displaced along the weak axis), the analysis procedure is the same as in Sec. 7.2.1., except the pile cross-sectional properties are rotated 90°. The two-dimensional program IAB2D can still be used for this case. A set of nondimensional curves of the ultimate pile load ratio (V_u/V_{uo}) versus the specified

lateral displacement (Δ_h, in the direction of the weak axis), for end-bearing piles in different types of Iowa soils, are shown in Fig. 55. The pile heads are fixed against rotation in these figures.

Results obtained from the IAB2D computer program show that a lateral movement of up to four in. has no effect on the vertical load capacity for friction piles. This is not true for end-bearing piles, since the failure mode is dominated by the yield load of the pile. The slip mechanism does not occur. Fig. 55(a) shows that end-bearing piles with a fixed pile head and bending about the strong axis have a significantly reduced ultimate load capacity in very stiff clay.

Fig. 56 shows the vertical load-settlement curves of end-bearing piles with fixed pile head displaced four in. laterally for soft clay, stiff clay, and very stiff clay. These curves show that the peak load (point of zero slope) for very stiff clay is greater than for stiff clay, which is greater than for soft clay. The peak load is not affected by the residual stresses which, in this case, are due to the plastic hinges formed by the initial lateral motion [76]. However, as Fig. 56 clearly shows, residual stresses do affect the load-settlement curve. For the very stiff clay, two plastic hinges formed in the pile during the four in. lateral displacement. For soft clay and stiff clay, only one plastic hinge formed. This plastic hinge formation does significantly affect the load-settlement curve of the very stiff clay pile; the tangent stiffness is noticeably reduced at point A in Fig. 56. Hence, the ultimate load for the very stiff clay case, as determined by the offset displacement method, is less than for soft clay and stiff clay.

7.4.2. Friction and end-bearing piles bending about the 45° axis

If pile orientations of types 3 and 4 are adopted for construction convenience, the thermal expansion or contraction along the roadway center can be divided into components parallel and perpendicular to the pile web (see Appendix B). Thus, the piles in integral abutment skewed bridges will be subjected to biaxial bending resulting from thermal movement. Piles displaced at 45° from the major axes will be analyzed in this section to illustrate the effect of biaxial bending. The same loading procedure is used as in Sec. 7.4.1. except that the specified lateral displacement Δ_h is measured in a direction 45° from the principal axes (See Fig. 28). The three-dimensional computer program IAB3D is used to calculate the load capacities of friction and end-bearing piles.

For friction piles, results obtained from the IAB3D program show that the load capacity of friction piles is not affected by applying the specified lateral displacement Δ_h (0, 1, 2, or 4 in.) in the 45° direction for all Iowa soils, since failure is controlled by the slip mechanism. This agrees with the results obtained from the previous sections.

The ultimate vertical load ratio for end-bearing piles with specified displacement Δ_h (0, 1, 2, or 4 in.) in the direction of 45° axis is shown in Fig. 57. In this case, the load capacity of end-bearing piles is affected by the specified movements at the top, since failure is controlled by the lateral mechanism. It is interesting to note that the load capacity of end-bearing piles bent about the 45° axis is between the load capacity of end-bearing piles bent about the weak

and strong axis (Sec. 7.2.1. and 7.4.1.). The upper bound and lower bound on the load capacity of end-bearing piles can be estimated from the weak or strong axis bending. As an expendient solution, analysis can be accomplished by a simplified two-dimensional analysis.

7.4.3. Effect of pinned pile top

In this section, the effect of a pin at the pile top on friction and end-bearing piles bent about the strong axis will be demonstrated. Piles in very stiff clay and soft clay will be studied. Results obtained from the IAB2D show that the load capacity of the friction piles is not affected by the boundary condition at the pile top. In both cases (fixed and pinned), the failure mechanism is controlled by the slip mechanism. This is not true in the case of an end-bearing pile (compare Figs. 55(a) and 58). For pinned piles displaced four in. laterally, the tangent stiffness of the load-settlement curve in very stiff clay is not reduced as significantly as it was at point A in Fig. 56 for fixed piles. Hence, the vertical load capacity, as determined by the offset displacement method, is not noticeably reduced.

7.5. Skewed Bridge Example

In this section, a skewed bridge with integral abutments is used to investigate the behavior of the piles under temperature changes. The bridge in Sec. 7.3. is used as a skewed bridge in which the skew angle is 30° (see Fig. 59). The pile orientations are classified into four different types as mentioned in Sec. 7.3. These four different types of pile orientations, as shown in Appendix B, will be discussed here.

Since the same bridge is used in this example, the properties of prestressed concrete beams, abutments, piles, and soil profiles are the same as in Sec. 7.3. The mathematical model for this skewed bridge is also similar to the one used in Sec. 7.3. except that a three-dimensional model is required to account for the effect of the skew. This three-dimensional model includes a concrete beam, abutment, and pile. Only one-half of the bridge in this model is analyzed by taking advantage of the symmetry about the midline of the bridge. The global coordinates as shown in Fig. 59 are selected to impose the symmetry requirement. Rotations about the global X-axis at the abutments and piers are considered to be restrained because of the diaphragm underneath the concrete beam.

Four types of pile orientations in the abutment are considered and are loaded with the following cases: (a) without thermal changes, (b) with +60°F temperature changes, and (c) without bridge beam and with Δ_h for +60°F temperature changes. Results obtained from the IAB3D program show that there is no significant difference in the load-settlement curves for different pile orientations, that is, the load-settlement curves will not be affected by the pile orientations (see Fig. 60). This agrees with the results in the previous sections which indicate that bending about weak, strong, and 45° axes do not affect the vertical load capcity of friction piles which fail by the slip mechanism. As in the two-dimensional case, as the applied load exceeds the pile friction resistance, the excess load will be carried by the concrete beams as a cantilever type structure. Hence, case (a) continues to carry an increasing load beyond case (c). Cases (a) and (b) have a noticeable

difference because of the pile pre-load induced by the thermal expansion, as illustrated in Fig. 54.

The deflected shape of the skewed bridge (in the plan view) after thermal expansion is also shown in Fig. 59. If the soil springs acting on the abutment in the tangential direction, which respresent the friction resistance of the backfill, did not exist, the bridge would move toward the upper right.

7.6. Timber and Concrete Piles

Piles are available in a variety of sizes, shapes, and materials to suit many special requirements, including economic competition. Piles can be classified by the principal materials of which they consist, for example, timber, concrete, and steel piles. Steel H piles have been discussed in Secs. 7.2. and 7.4. Circular timber and concrete piles will be investigated in this section.

Timber piles are probably the most commonly used type. Under many circumstances, they provide dependable, economical foundations. Their length is limited by the height of available trees; piles 20 to 40 ft. long are common, but longer ones cannot be obtained economically in all areas.

Since concrete piles were initially used shortly before 1900, several types of concrete piles have been devised. Today, an engineer may choose those best suited to a particular project. Concrete piles may be divided into two principal categories, cast-in-place and precast

piles. The cast-in-place piles may be further divided into cased and uncased piles.

A Douglas fir timber pile and a cast-in-place concrete pile, both one ft. diameter and 20 ft. long will be investigated here. Table 13 shows the material properties of timber and concrete piles [84]. The stress-strain relationship of the timber pile can be represented by the modified Ramberg-Osgood cyclic model. For concrete piles, reinforcing bars are used to resist the tensile force for the internal moment. The beam element in the current program does not have the capability of modeling the post-cracking behavior of reinforced concrete piles. The representation of the bond/anchorage/cracking behavior of reinforced concrete is a complex phenomenon which has not been completely solved by state-of-the-art methods. The scope of this project did not permit incorporation of such behavior. In addition, since the pile is predominantly in axial compression, the compression characteristics of the material will dominate. The compression stress-strain relation of the concrete pile is idealized by the modified Ramberg-Osgood cyclic model.

Using the same procedure as in Sec. 7.2.1., results indicate that the vertical load capacity of timber and concrete friction piles with fixed pile heads in six types of Iowa soils is not reduced by a lateral movement of up to two in. The failure for both timber and concrete friction piles with vertical loads is by the slip mechanism. Point bearing timber and concrete piles are not analyzed.

As described above, these analyses are based upon a Ramberg-Osgood representation of the timber and concrete materials, which implies unlimited ductility. This is not necessarily true. Hence, the above conclusion that the capacity of a friction pile is unaffected by lateral displacements of up to two in. will be true only if the pile has the ductility to develop a full plastic moment and, subsequently, to behave as a plastic hinge for the required rotations. The results of the finite element analysis indicate that, for a two in. lateral displacement, the plastic hinge rotation required at the top of a pile is approximately 0.04 radians over a 24 in. length in timber and over a 12 in. length in concrete.

8. SUMMARY, CONCLUSIONS, AND FURTHER WORK

8.1. Summary

The highway departments of all fifty states were contacted to find the extent of application of integral abutment bridges, to survey the different guidelines used for analysis and design of integral abutment bridges, and to assess the performance of such bridges through the years. The survey showed a wide variation in design assumptions and limitations among the various states in their approach to the use of integral abutments. The survey also showed that the variations among the different states are due largely to the empirical basis of current design criteria, thereby underscoring the need for a simple, rational method of accurately predicting pile stresses.

The states that use integral abutments indicated that they were generally satisfied with the performance of the bridges and these bridges were economical. Some problems have been reported, however, concerning secondary effects of inevitable lateral displacements at the abutment. These include abutment, wingwall and pavement distress and backfill erosion. Only a few states noted that any difficulty had been encountered. Other states reported that solutions have been developed for most of the ill effects of abutment movements.

Survey responses also indicated that 26 states use integral type abutments on skewed bridges. Most states design integral abutments on skewed bridges on the basis of empirical experience, and no theoretical analysis is introduced in design. Fifteen states orient their piles

with the web of the piles perpendicular to centerline of the abutment so that bending will be primarily about the strong axis. However, the survey responses showed that most states ignore thermally-induced bending stresses caused by transverse and longitudinal movement. No special treatment is given to backfill and pile cap on skewed bridges. As for approach slab, it might be tied to the abutment with dowels, or an expansion joint may be provided between the approach slab and the bridge slab.

The parameters needed to describe the behavior of the soil are given in Chapter 3. Three types of soil resistance-displacement curves were developed: lateral, vertical, and pile tip. The parameters needed for each curve are the initial stiffness, the ultimate soil resistance, and a shape parameter. Each of these curves was approximated using a modified Ramberg-Osgood model. This model was expanded to include cyclic loadings. The constants used in the modified Ramberg-Osgood model for clay and sand were determined by approximating analytical expressions of others. Six typical Iowa soils were identified for the use of numerical examples.

An algorithm based upon a nonlinear finite element procedure was developed to study the soil-pile interaction in integral abutment bridges. The finite element idealization consists of a one-dimensional idealization for the pile and nonlinear spring for the foundation. Incremental finite elements with an updated Lagrangian formulation and material nonlinearities were used. For the purpose of treating arbitrarily large rotations, node orientations were described by unit vectors. The nodal

forces were evaluated by numerical integration through the cross section. Explicit forms of the tangent stiffness in the element coordinate are presented. Updating of the element coordinates in three dimensions is also described. The numerical techniques available for the solutions of the nonlinear equations are reviewed, and the incremental and iterative techniques used in the study are discussed in detail. Two computer programs, IAB2D and IAB3D (Integral Abutment Bridge Two- and Three-Dimensional Finite Element Computer Programs) have been developed to solve the nonlinear soil-pile interaction problems for both two- and three-dimensional cases. A number of analytical and experimental examples have been analyzed to establish their reliability.

In Chapter 7, many analytical examples are presented in which a pile was given a lateral displacement to simulate the bridge expansion. A vertical load was then applied until failure occurred. These examples showed that for the cases studied in Iowa soils, friction H piles experienced no decrease in load-carrying capacity for lateral displacements up to four in. This was true whether the pile was bent about the strong axis, weak axis, or 45° from either axis. This was also true for timber and concrete piles displaced up to two in. All of these cases failed by a slip mechanism. However, end-bearing piles did show significant reductions in load-carrying capacity for similar lateral displacements and for bending about all three axies. These cases failed by a lateral mehcanism. Other examples showed that the cyclic behavior had no effect. Examples with skewed and nonskewed bridges showed no effect on the pile

capacity since these piles were friction piles. However, the longitudinal expansion of the bridges introduced a preload on the pile which reduced the effective pile capacity.

8.2. Conclusions

The ultimate load capacity for friction piles was not affected by lateral displacements of up to four in. for H piles and up to two in. for timber and concrete piles. However, the ultimate load capacity was significantly reduced for lateral displacements greater than two in. for end-bearing piles. Pile orientation of friction piles does not reduce the load capacity of the piles for lateral displacements up to four in., but it does reduce the load capacity of the piles for end-bearing piles. The load capacity of friction piles is not affected by cyclic loadings.

A vertical preload was introduced on the pile by the thermal expansion of the bridge as it pushed the abutment against the backfill. The load capacity of the pile was, thus, effectively reduced.

For the time being, the maximum allowable length for bridges with integral butments can not be determinted precisely. The safe length of the bridge not only depends on the properties of the soil and piles, but also on the backwall soil model, approach slab, etc. An approximation of determining the bridge safe length based on the thermal expansion and contraction on the structural integrity of the piles is

$$L_b = \frac{2\Delta_h}{\alpha\Delta T} \tag{8.1}$$

where L_b is the length of the bridge, α is the coefficient of thermal expansion for the material in the bridge superstructure, ΔT is the average temperature change, and Δ_h is allowable thermal movement.

It is important to note that analysis presented herein was for the structural integrity of the piles only. Other factors, notably the effects of the abutment movement on the approach slab and fill and the effects of the induced axial stresses in the superstructure, must also be considered. While these factors have a relatively small effect on shorter bridges, as longer bridges with integral abutments are built these problems will become of greater importance.

8.3. Further Work

1) A scale model of a pile in in integral abutment bridge could be set up and tested in the laboratory. The experimental results can be compared to the results obtained from the analytical methods.
2) An actual bridge could be instrumented to monitor thermal movements and piling stresses during temperature change.
3) A study of the backfill and the approach slab under cyclic thermal movements would determine the most suitable type of approach slab to be used with the integral abutment type of bridges.
4) A study of the effects of the pile preload caused by the thermal expansion of the bridge is needed.
5) The effects of the abutment movement on the approach slab and fill and the effects of the induced axial stresses in the superstructure need further consideration.

Table 1. Integral abutment bridge length limitations (1981)

Maximum Length	Number of States		
	Steel	Concrete	Prestressed
800		1	1
500		1	2
450		1	3
400	2	3	4
350	1	3	1
300	8	8	8
250	2	1	
200	5	1	2
150	1		
100		1	

Table 2. Flow chart for determining the reversal values of loading and unloading

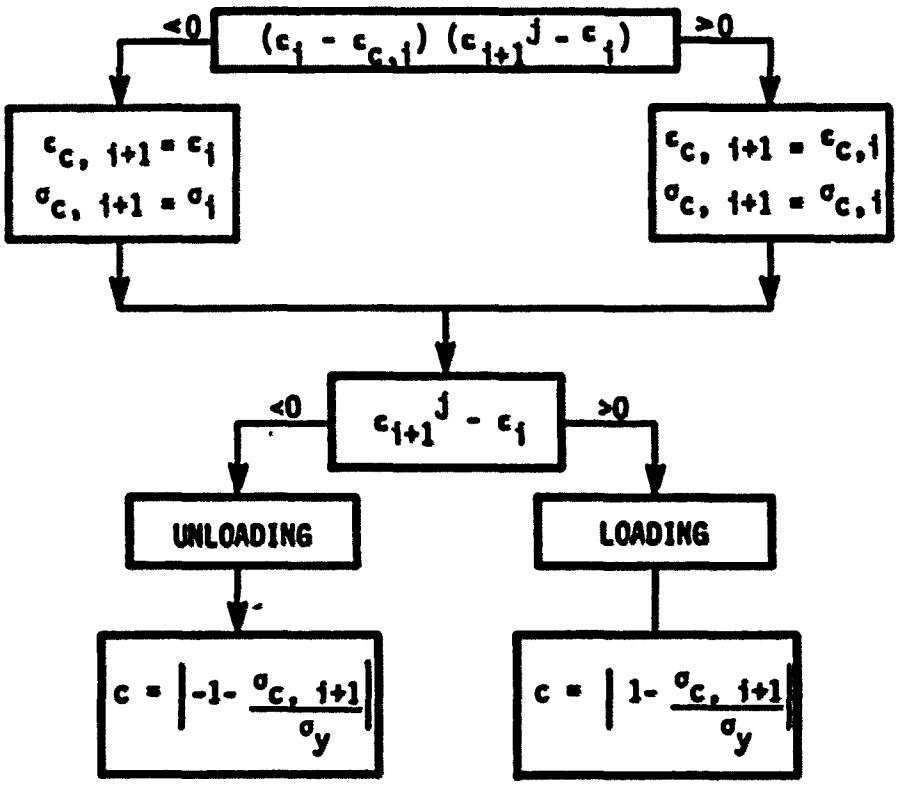

ε_i = THE CONVERGED STRAIN OF THE PREVIOUS INCREMENT i,

σ_i = THE CONVERGED STRESS OF THE PREVIOUS INCREMENT i,

$\varepsilon_{c,i}$ = THE REVERSAL STRAIN OF THE PREVIOUS INCREMENT i,

$\sigma_{c,i}$ = THE REVERSAL STRESS OF THE PREVIOUS INCREMENT i,

ε_{i+1}^j = THE UPDATED STRAIN OF THE CURRENT INCREMENT i+1,

σ_{i+1}^j = THE UPDATED STRESS OF THE CURRENT INCREMENT i+1,

$\varepsilon_{c,i+1}$ = THE UPDATED REVERSAL STRAIN OF THE CURRENT INCREMENT i+1,

$\sigma_{c,i+1}$ = THE UPDATED REVERSAL STRESS OF THE CURRENT INCREMENT i+1.

Table 3. Analytical forms of p-y curves

Case	Basic p-y Curves Equations	p_u (use lesser value)	Esi
Soft Clay, Static Load	$p/p_u = 0.5\,(y/y_{50})^{1/3}$	$p_u = 9\,c_u B$	—
		$p_u = (3 + \frac{\gamma}{c_u}x + \frac{0.5}{B}x)c_u B$	
Stiff Clay, Static Load	$p/p_u = 0.5(y/y_{50})^{1/4}$	$p_u = 9\,c_u B$	
		$p_u = (3 + \frac{\gamma}{c_u}x + \frac{0.5}{B}x)c_u B$	—
Very Stiff Clay, Static Load	$p/p_u = 0.5(y/y_{50})^{1/2}$	$p_u = 9\,c_u B$	
		$p_u = (3 + \frac{\gamma}{c_u}x + \frac{2.0}{B}x)c_u B$	—
Sand, Static Load	$p/p_u = \tanh(E_{si}y/p_u)$	$p_u = \gamma x\,[B(k_p - k_a) +$	$J\gamma x/1.35$
		$x\,k_p \tan\alpha\,(\tan\beta) +$	
		$x\,k_o \tan\beta\,(\tan\phi - \tan\alpha)]$	
		$p_u = \gamma x(k_p^3 + 2k_p^2 k_o \tan\phi - k_a)B$	

Table 3. (continued)

Parameter	Evaluation
ε_{50}	From laboratory triaxial test, or use = 0.02 for soft clay = 0.01 for stiff clay = 0.005 for very stiff clay (Axial strain at 0.5 times peak stress difference)
c_u	Undrained cohesion indicated for an unconsolidated undrained laboratory test
B	Pile width
γ	Effective unit soil weight
x	Depth from soil surface
ϕ	Angle of internal friction
k_p	$= \tan^2 (45° + \frac{\phi}{2})$
k_a	$= \tan^2 (45° - \frac{\phi}{2})$
k_o	$= 1 - \sin\phi$

Table 3. (continued)

Parameter	Evaluation
α	$= \frac{\phi}{2}$ for dense or medium sand
	$= \frac{\phi}{3}$ for loose sand
β	$= 45° + \frac{\phi}{2}$
J	= 200 for loose sand
	= 600 for medium sand
	= 1500 for dense sand
y_{50}	Displacement at one-half ultimate soil reaction
	$= 2.5\ B\varepsilon_{50}$ for soft and stiff clay
	$= 2.0\ B\varepsilon_{50}$ for very stiff clay

Table 4. Analytical forms of f-z curves and parameters

Case	Basic f-z Curve Equations	f_{max}, klf H Piles	f_{max}, klf Others
Clay (Static Load)	$\frac{f}{f_{max}} = (2\sqrt{z/z_c} - z/z_c)$	The least of:	The lesser of:
		$2(d+b_f)c_u$	$\ell_g c_a$
		$2(d+2b_f)c_a$	$\ell_g c_u$
		$2(dc_u+b_f c_a)$	
Sand (Static Load)	$\frac{f}{f_{max}} = (2\sqrt{z/z_c} - z/z_c)$	$0.02N(2(d+2b_f))$	$0.04N\ell_g$

α = Shear strength reduction factor (see Fig. 8.)

c_u = Undrained cohesion of the clay soil

= 97.0N + 114.0 (psf)

c_a = Adhesion between soil and pile

= αc_u (psf)

N = Average standard penetration blow count

z_c = Relative displacement required to develop f_{max}

= 0.4 in. (0.033 ft.) for sand

= 0.25 in. (0.021 ft.) for clay

ℓ_g = Gross perimeter of the pile (ft.)

d = Section depth of H pile or diameter of pipe pile (ft.)

b_f = Flange width of H pile (ft.)

Table 5. Analytical forms of q-z curves and parameters

Case	Basic q-z Curve Equation	q_{max}, ksf
Clay (Static case)	$\frac{q}{q_{max}} = (z/z_c)^{1/3}$	$9c_u$
Sand (Static case)	$\frac{q}{q_{max}} = (z/z_c)^{1/3}$	$8N_{corr}$

N_{corr} = Corrected standard penetration test (SPT) blow count at depth of pile tip

= N (uncorrected) if $N \leq 15$

= $15 + 0.5(N-15)$ if $N > 15$

c_u = Undrained cohesion of the clay soil

= $97.0N + 114.0$ (psf)

z_c = Relative displacement required to develop q_{max}

= 0.4 in. (0.033 ft.) for sand

= 0.25 in. (0.021 ft.) for clay

N = Average standard penetration blow count

Table 6. Parameters used in the modified Ramberg-Osgood models for clay and sand

Soil Type	p-y Calculated k_h	p-y Calculated n	p-y Used k_h	p-y Used n
Soft Clay	$0.669 \frac{p_u}{y_{50}}$	1.5	$\frac{p_u}{y_{50}}$	1.0
Stiff Clay	$0.915 \frac{p_u}{y_{50}}$	1.07	$\frac{p_u}{y_{50}}$	1.0
Very Stiff Clay	$0.539 \frac{p_u}{y_{50}}$	2.56	$\frac{p_u}{2y_{50}}$	2.0
Sand			$\frac{J\gamma x}{1.35}$	3.0

Soil Type	Calculated k	Calculated n	Used k	Used n
f-z (All Soils)	$7.32 \frac{f_{max}}{z_c}$	1.33	$10 \frac{f_{max}}{z_c}$	1.0
q-z (All Soils)	$7.32 \frac{q_{max}}{z_c}$	1.33	$10 \frac{q_{max}}{z_c}$	1.0

Table 7. Soil properties and curve parameters for sand

	Typical Value For Loose Sand	Typical Value For Medium Sand	Typical Value For Dense Sand
Soil Properties:			
Blow count, N	5	15	30
Unit weight, γ (pcf)	110	120	130
Angle of friction, ϕ	30°	35°	40
p-y Curve Parameters:			
n	3.0	3.0	3.0
p_u (klf)	$0.14x^2 + 0.29Bx$ for $x \leq 23B$ $3.5Bx$ for $x > 23B$	$0.31x^2 + 0.41Bx$ for $x \leq 21B$ $7.0Bx$ for $x > 21B$	$0.51x^2 + 0.57Bx$ for $x \leq 27B$ $14Bx$ for $x > 27B$
k_h (ksf)	16x	53x	140x
f-z Curve Parameters:			
n	1.0	1.0	1.0
f_{max} (klf)*	0.5	1.5	3.0
k_v (ksf)*	150	450	900

q-z Curve Parameters

n	1.0	1.0	1.0
q_{max} (ksf)	40	120	180
k_q (kcf)	12,000	36,000	55,000

*These values are for a HP10x42 pile.

B = pile width (ft.)

x = depth from soil surface (ft.)

Table 8. Soil properties and curve parameters for clay

	Typical Value For Soft Clay	Typical Value For Stiff Clay	Typical Value For Very Stiff Clay
Soil Properties:			
Blow count, N	3	15	50
Unit weight, (pcf)	100	120	130
Undrained cohesion c_u (psf)	405	1569	5000
p-y Curve Parameters:			
n	1.0	1.0	2.0
p_u (klf) (use lesser value)	3.6B or 1.2B+0.10Bx+0.20x	14B or 4.7B+0.12Bx+0.78x	45B or 15B+0.13Bx+10x
k_h (ksf) (use lesser value)	73 or 24+2x+4.1x/B	560 or 190+4.8x+31x/B	2250 or 750+6.5x+500x/B
f-z Curve Parameters:			
n	1.0	1.0	1.0
f_{max} (klf)*	1.34	3.86	6.22

k_v (ksf)*	640	1850	2960
q-z Curve Parameters:			
n	1.0	1.0	1.0
q_{max} (ksf)	3.6	14	45
k_q (kcf)	1700	6700	21,000

*These values are for a HP10x42 pile.

Table 9. Ramberg-Osgood parameters for f-z curve

Depth below surface (ft.)	k_y (ksi)	f_{max} (k/in.)	n
0.0 to 3.0	2.19	0.39	0.85
3.0 to 9.0	3.11	0.42	0.75
9.0 to 14.66	3.37	0.21	1.69
14.66 to 21.0	0.81	0.18	1.55
21.0 to 26.0	3.03	0.95	1.34
26.0 to 31.0	5.56	0.29	0.95
31.0 to 36.0	10.42	0.53	0.65
36.0 to 44.5	6.74	0.11	1.55

Table 10. Ramberg-Osgood parameters for q-z curve

Depth below pile top (ft.)	k_q (kci)	q_{max} (ksi)	n
44.5	115.74	3.47	0.50

Table 11. Soil characteristics

Pier No.	Site No.	Soil Type	Total Unit Wt.--lbs/ft^3	Avg. undrained shear strength lbs/ft.^{2}	ϵ_{50} %	Depth ft.
1	A	Sandy Clay (CL-CH)	130	5500	0.96	0 ~ 9
2	B	Sandy Clay (CL)	130	4750	0.72	0 ~ 16

Table 12. Modulus of elasticity for timber piles

Test Site	Pile	Avg. Modulus of Elasticity, E(ksi)
1	1-A	2000
	1-B	2500
2	2-A	1900
	2-B	2000*

*Assumed, as no calibration test was made on this pile.

Table 13. Material properties of timber and concrete piles

Piles	Modulus of Elasticity ksi	Yield Stress ksi
Douglas fir timber pile	2000	7.5
Concrete pile	4300	4.0

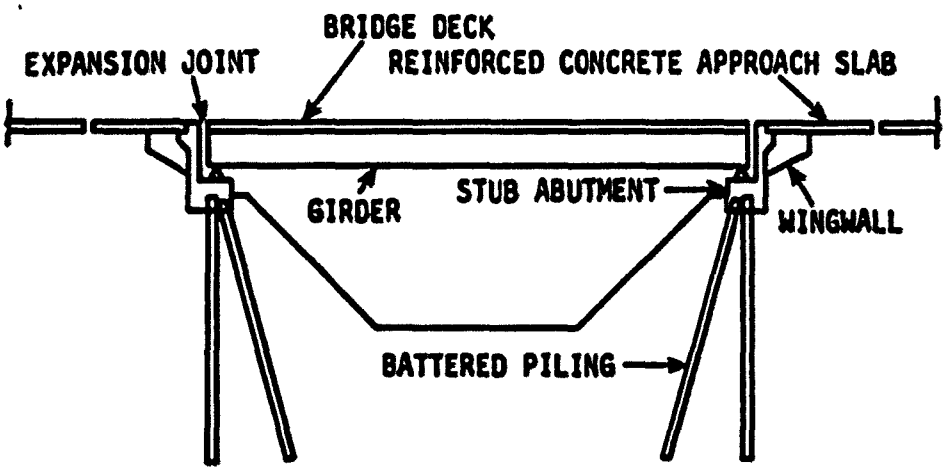

Fig. 1. Cross-section of a bridge with expansion joints

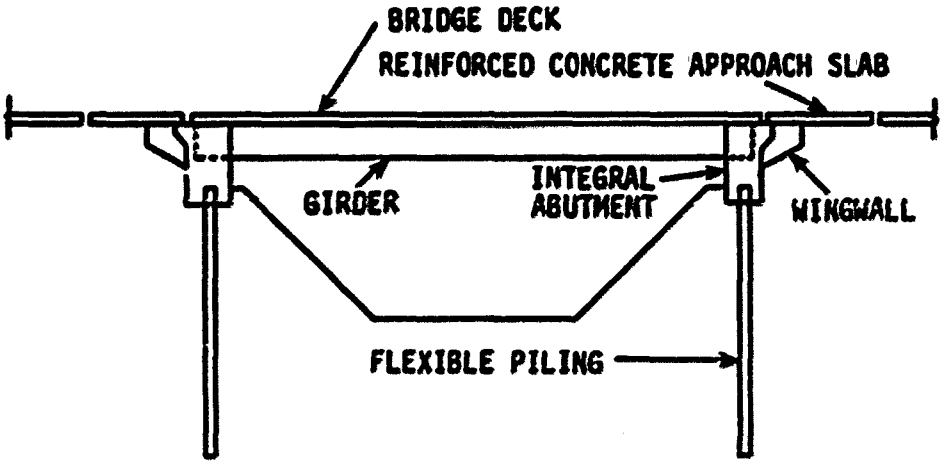

Fig. 2. Cross-section of a bridge with integral abutments

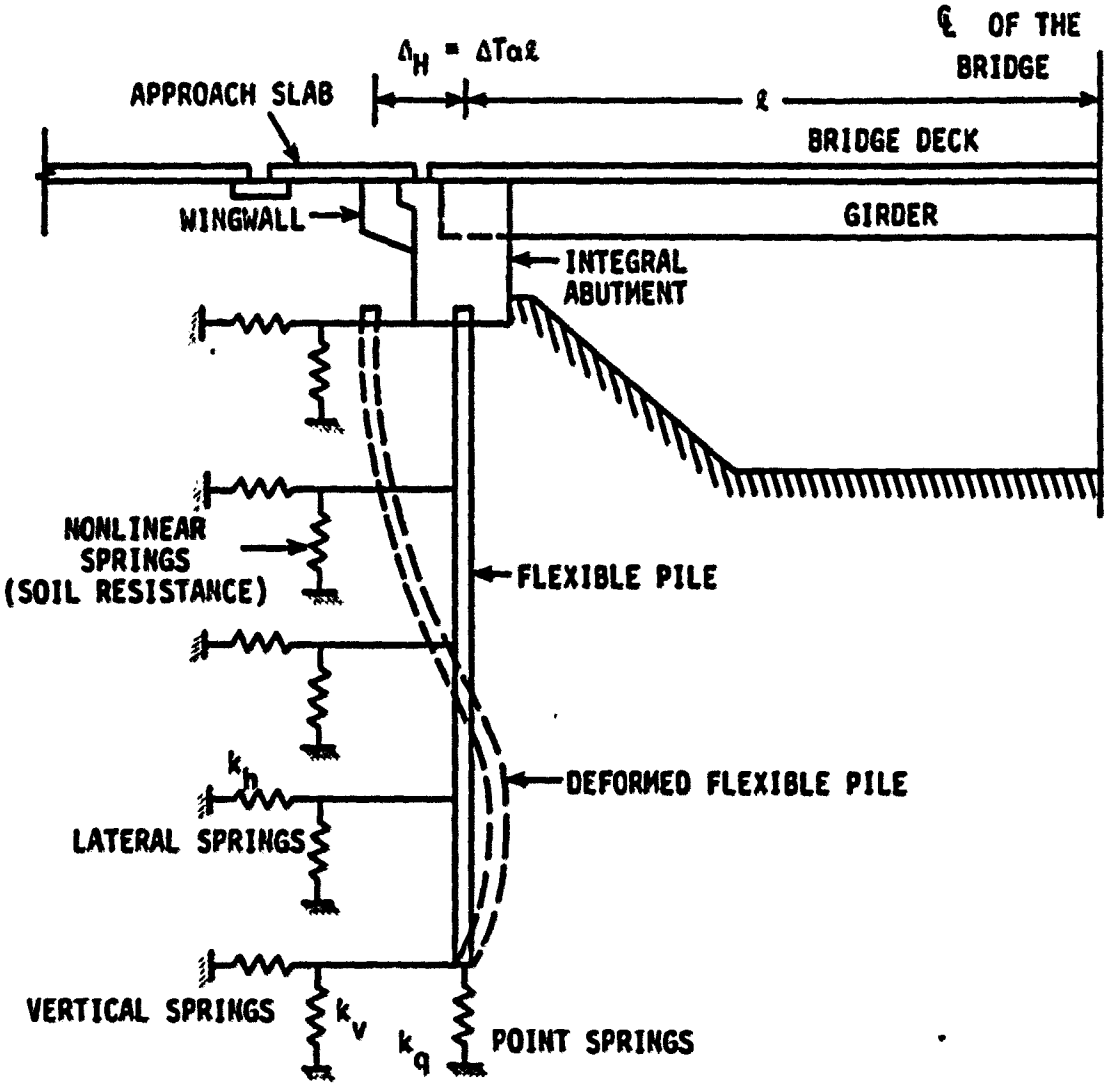

Fig. 3. Cross-section of the integral abutment bridge with soil-pile interaction

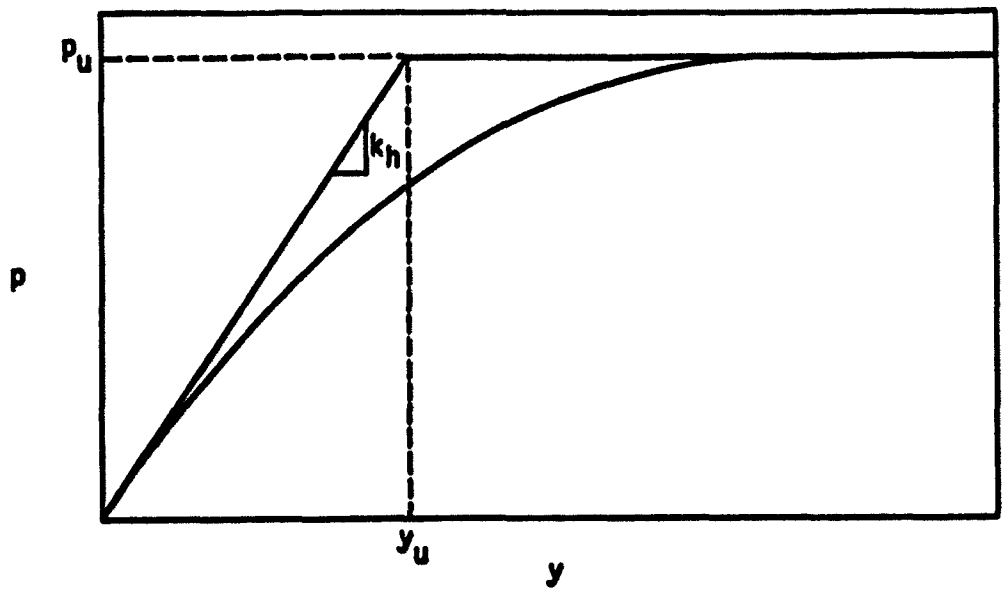

Fig. 4. Typical p-y curve with Ramberg-Osgood constants

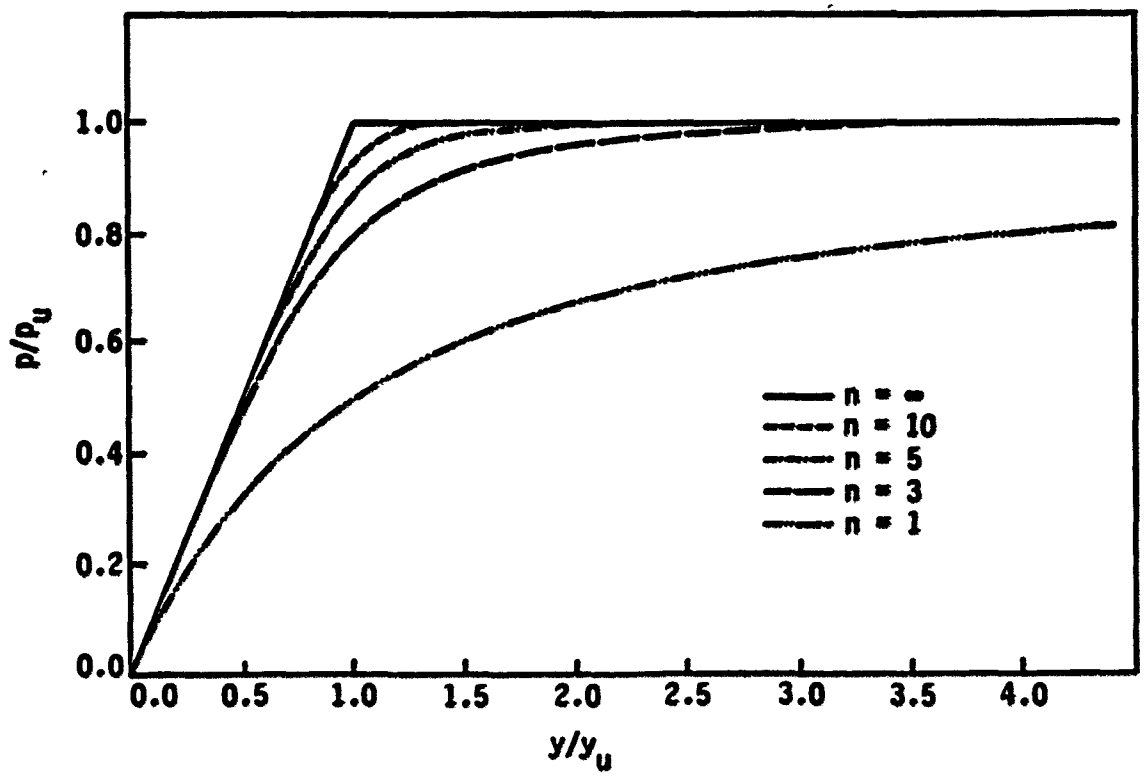

Fig. 5. Nondimensional form of the modified Ramberg-Osgood equation

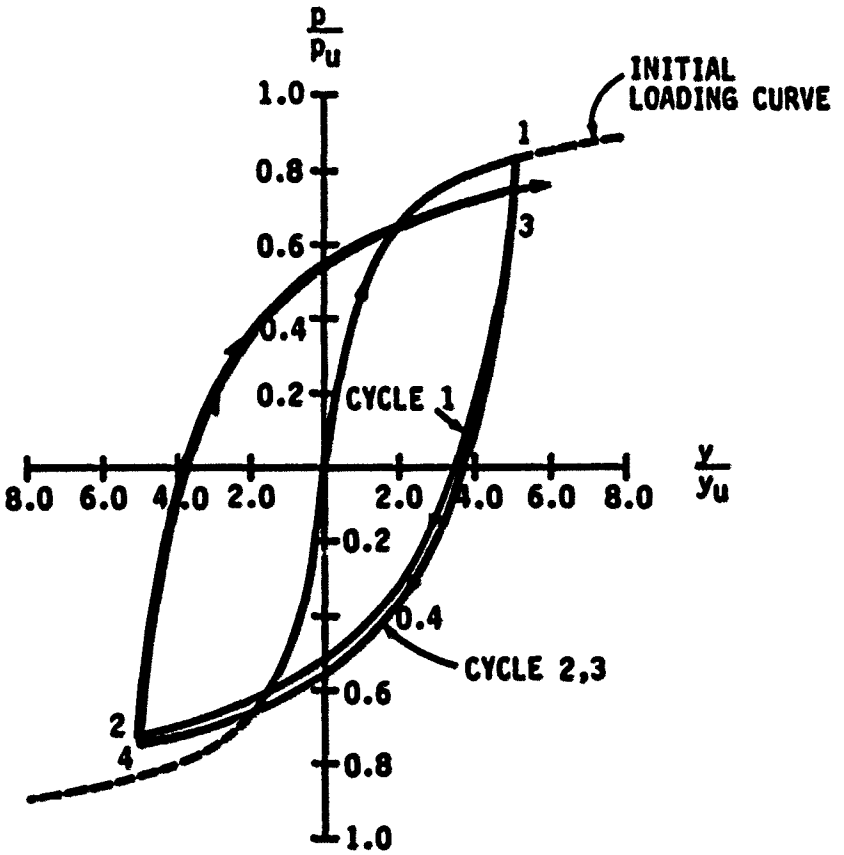

Fig. 6. Hysteresis loops in accordance with modified Ramberg-Osgood cyclic model with n = 1.0

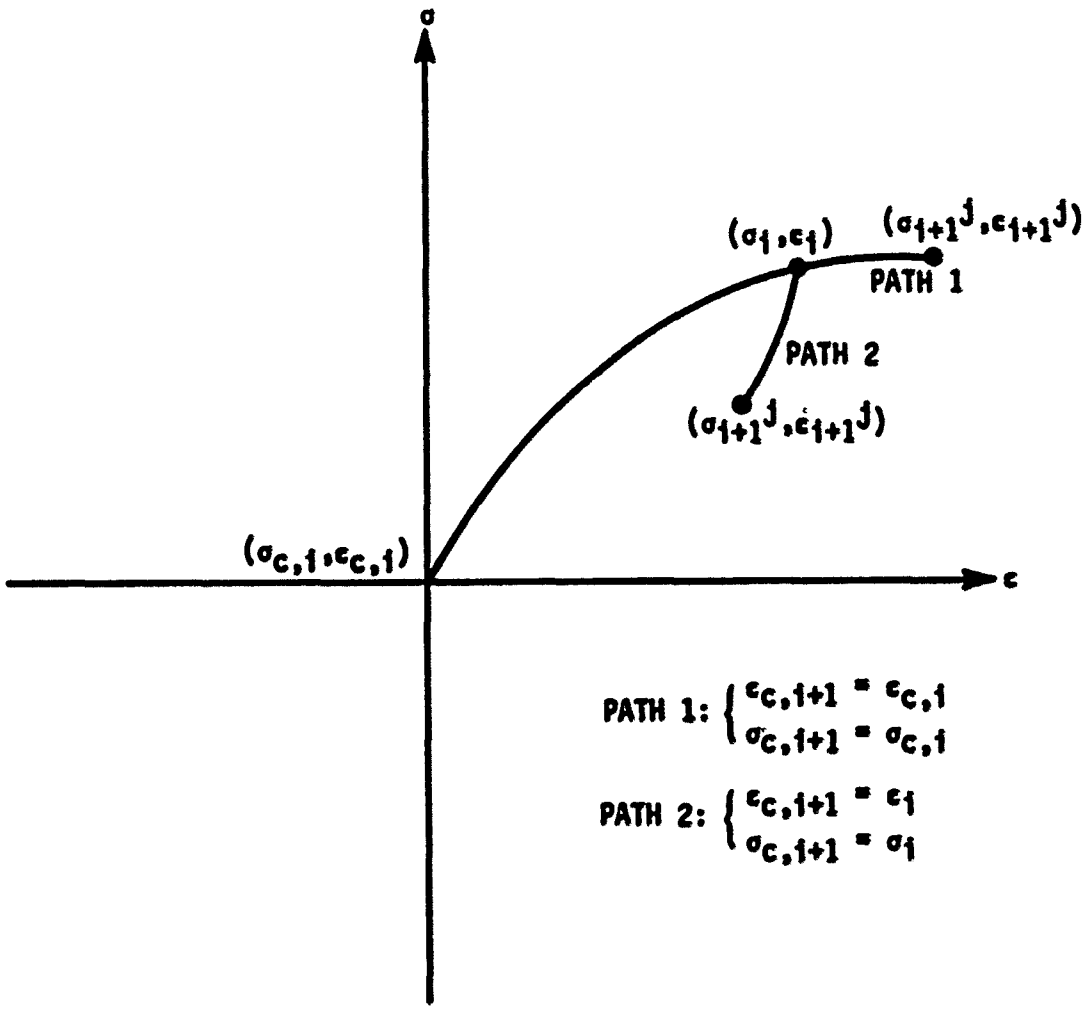

Fig. 7. The determination of reversal values for loading and unloading

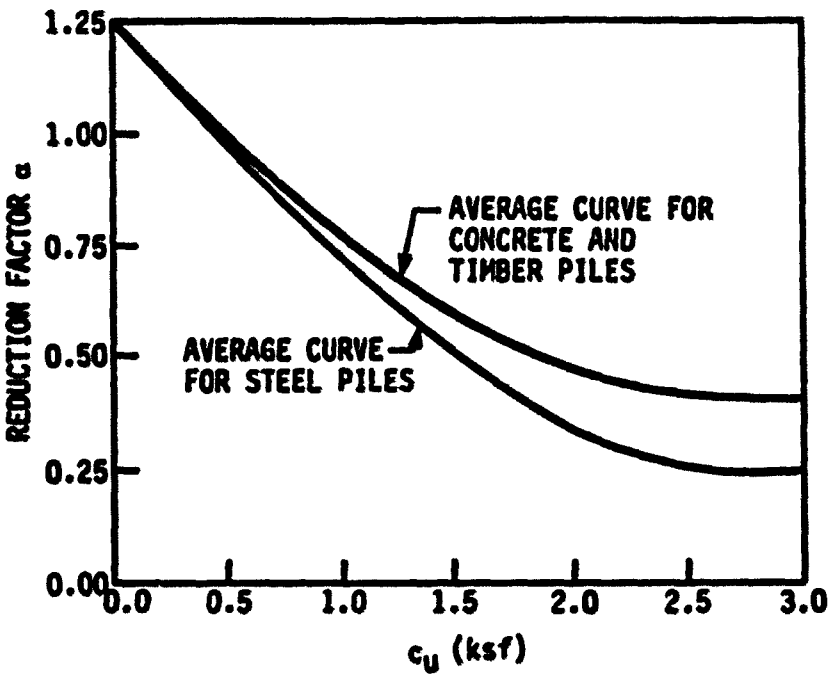

Fig. 8. Reduction factor α [13]

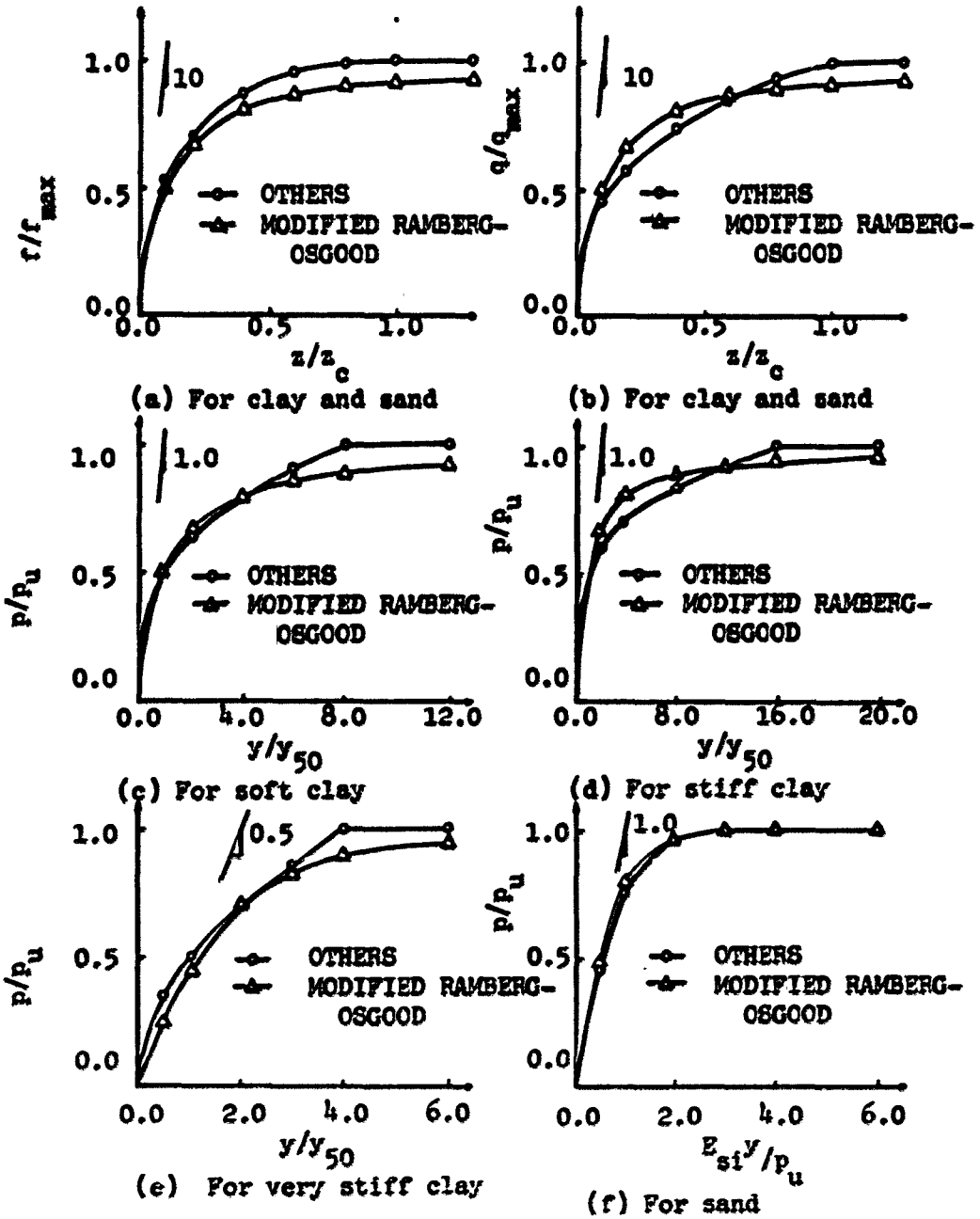

Fig. 9. Comparison between the analytical forms of the p-y, f-z, and q-z curves by others and the modified Ramberg-Osgood models

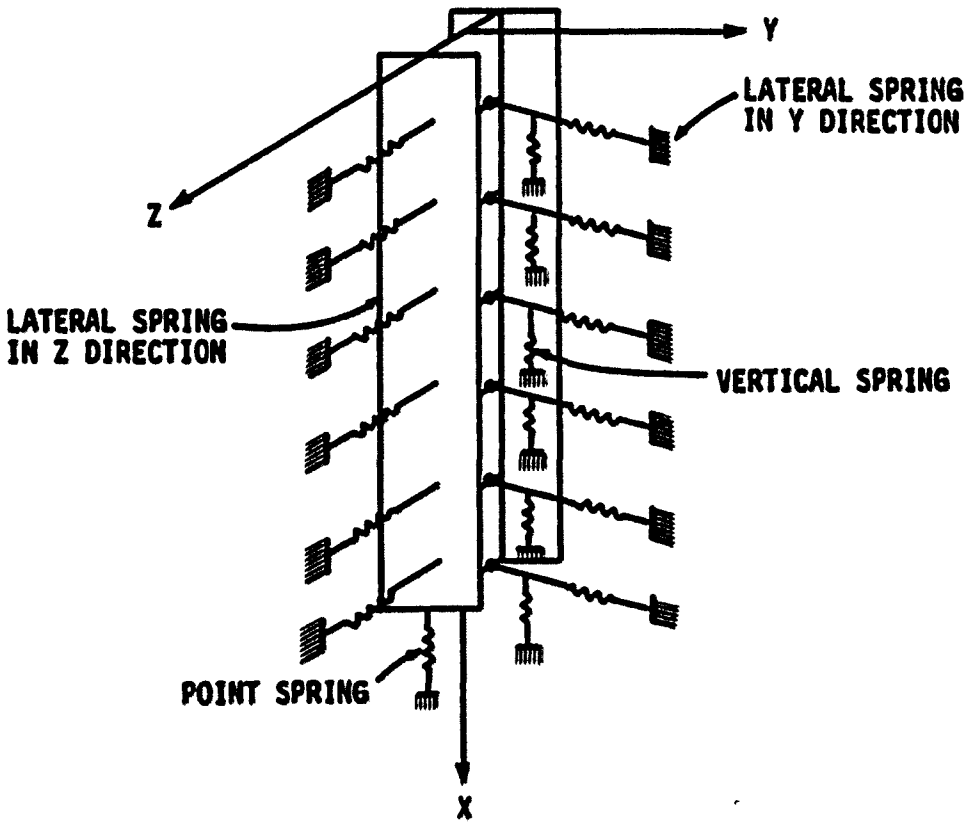

Fig. 10. A combination of a one-dimensional idealization for the pile and an equivalent nonlinear spring idealization for the soil

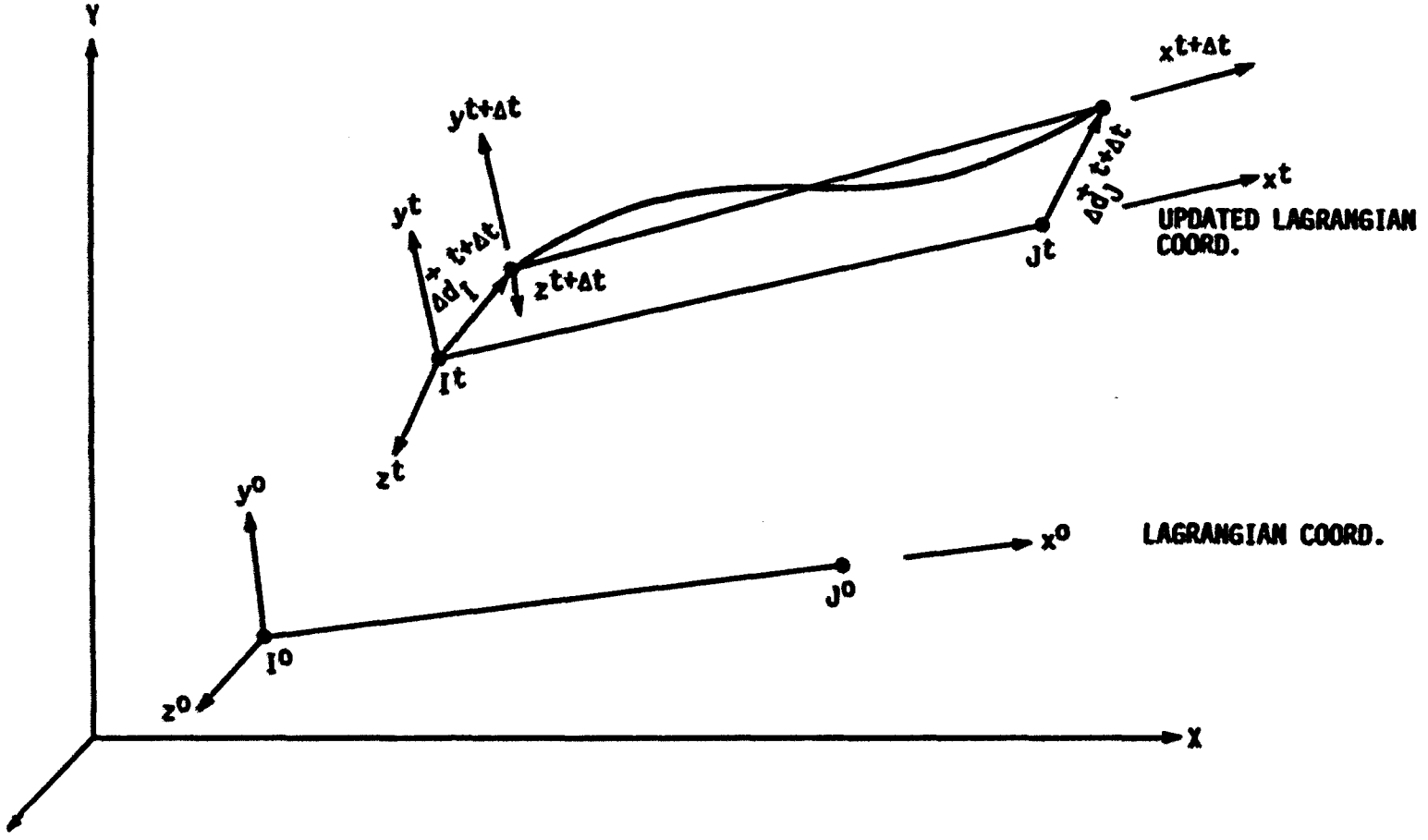

Fig. 11. Nonlinear finite element analysis approaches: (a) Eulerian approach, (b) Lagrangian approach, (c) updated Lagrangian approach

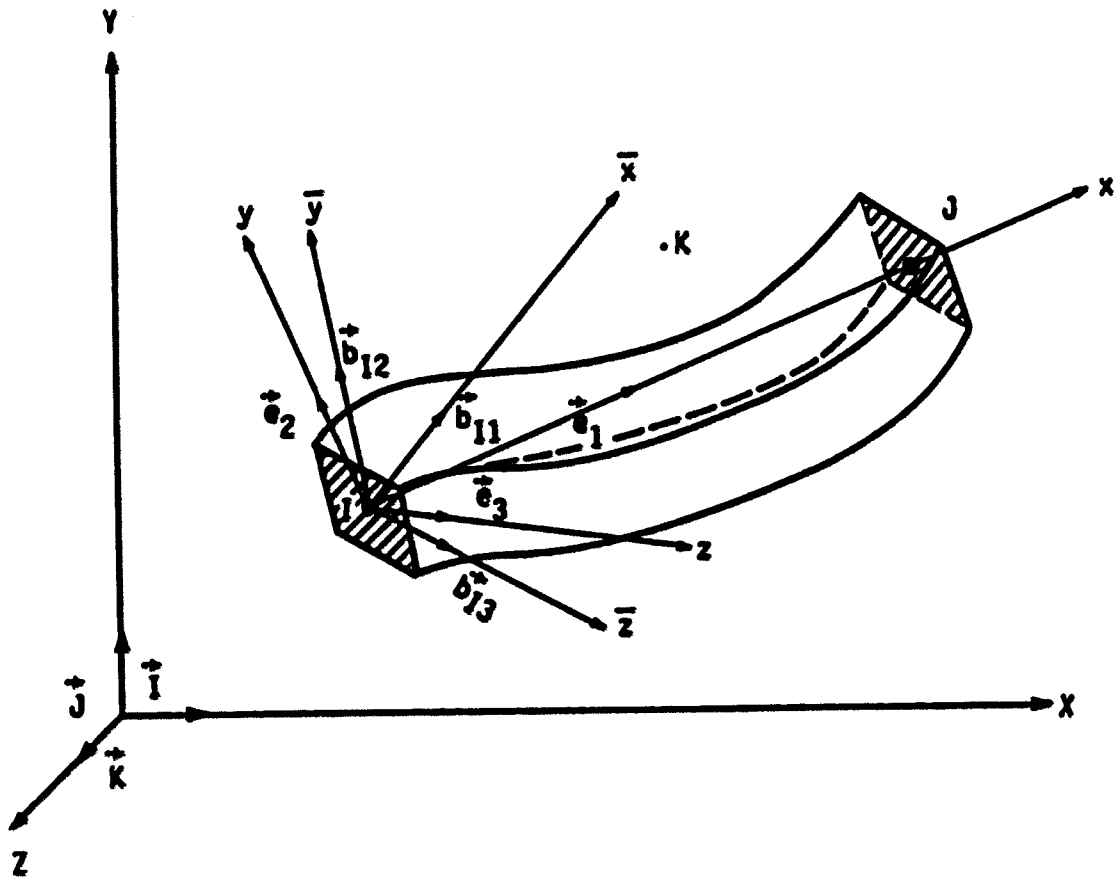

Fig. 12. Coordinate systems and nomenclature

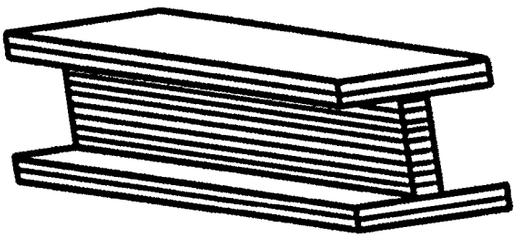

Fig. 13a. Element layering for two-dimensional analysis

Fig. 13b. Element layering for three-dimensional analysis

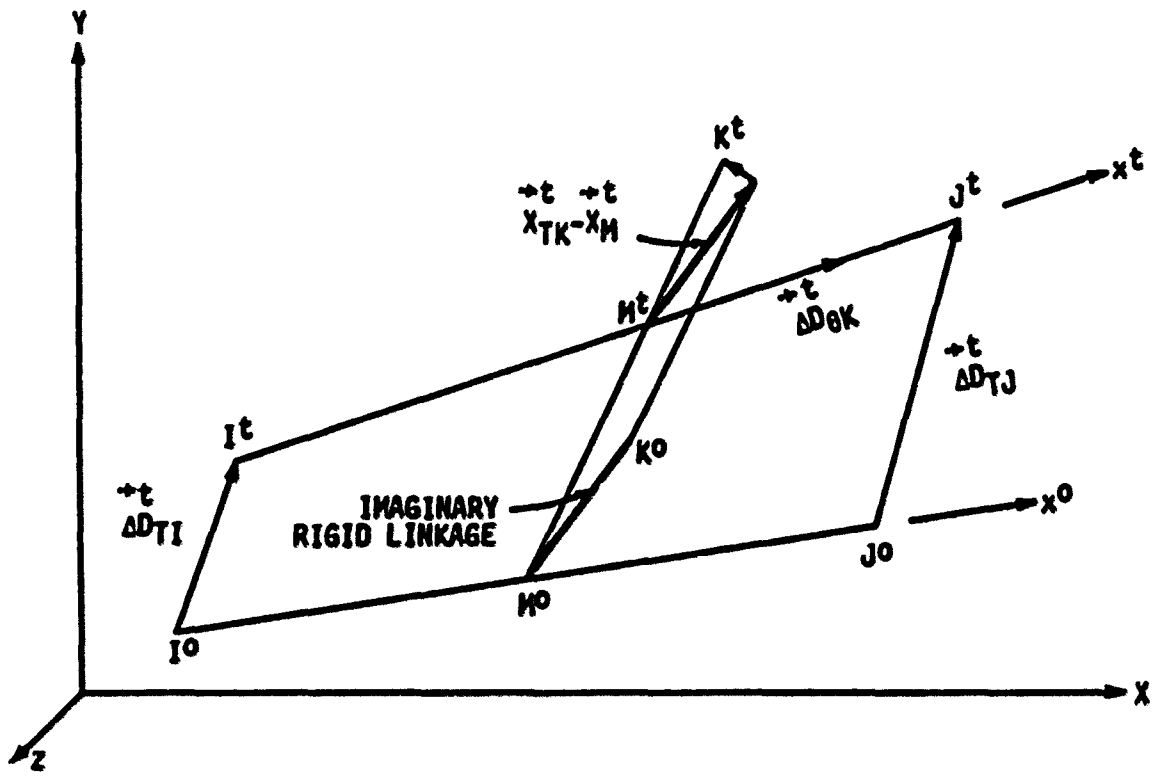

Fig. 14. The coordinate updating of K node in three-dimensional beam-column element

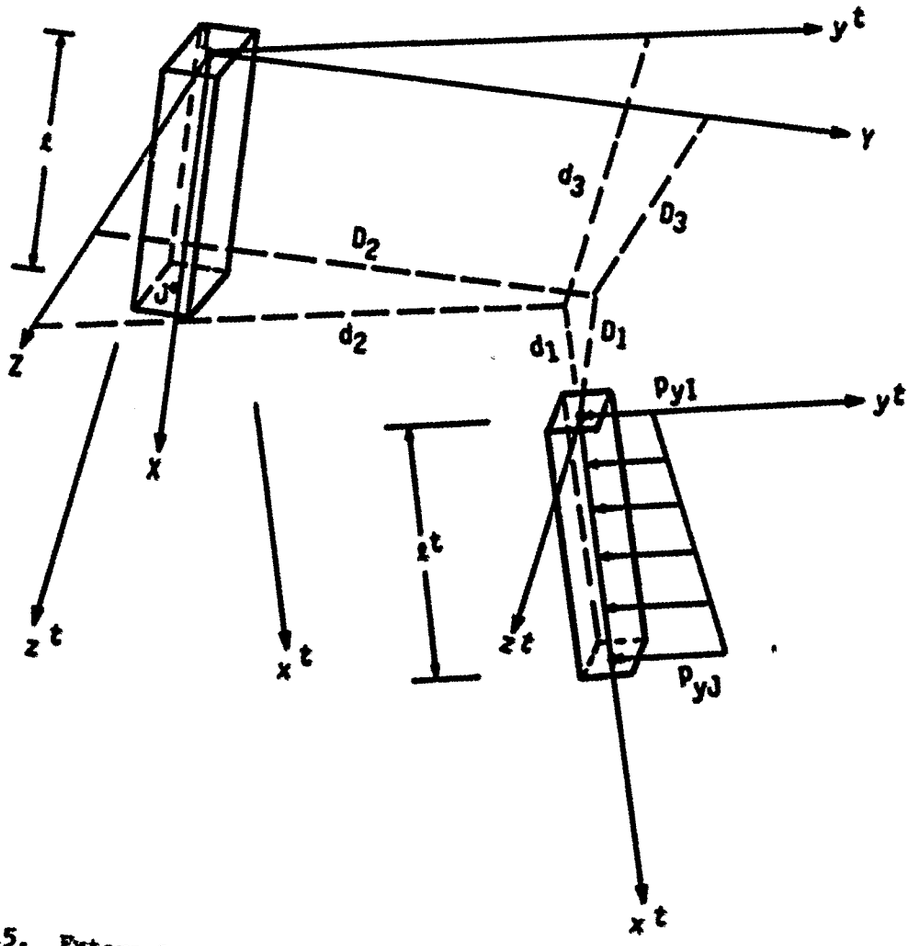

Fig. 15. External and internal forces and displacements acting on the pile element

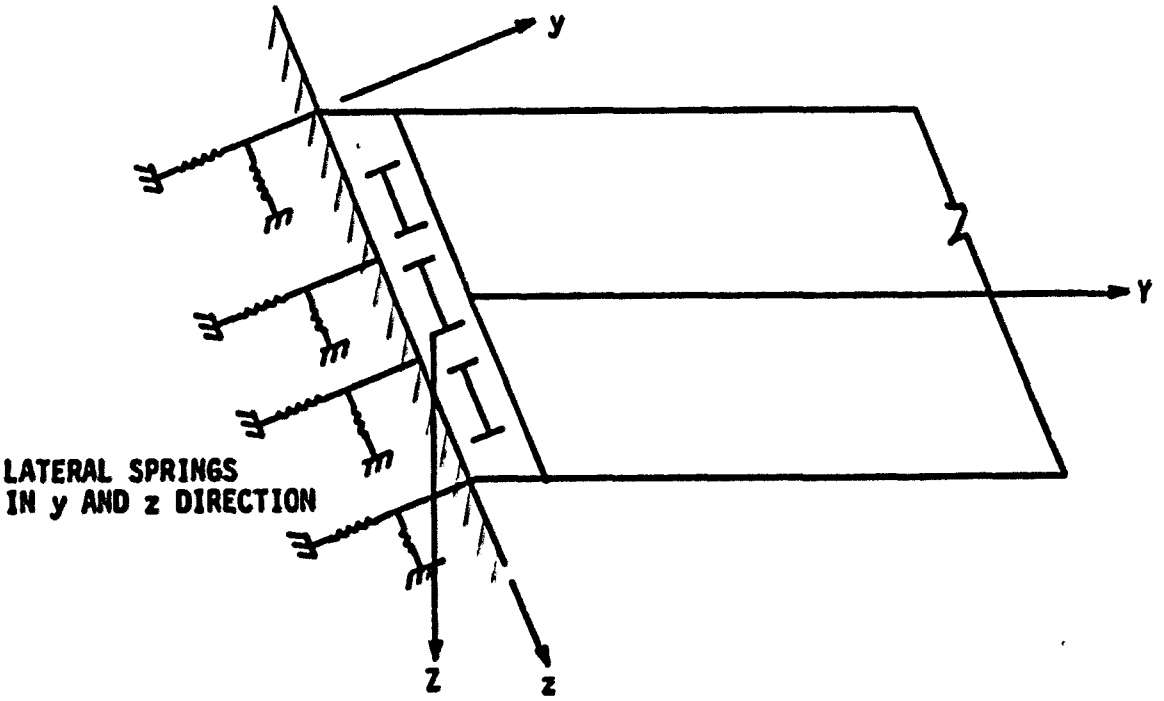

Fig. 16a. Idealized backwall soil model in integral bridge abutments

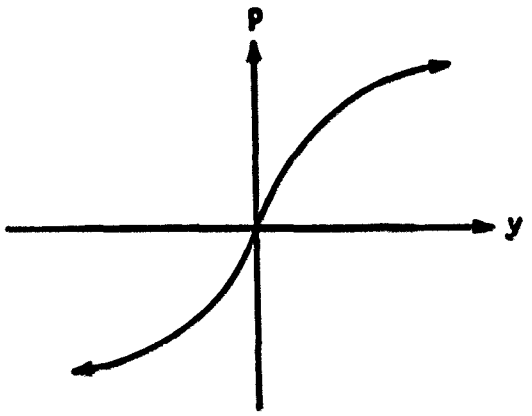

Fig. 16b. p-y curve for backwall soil model in element y direction

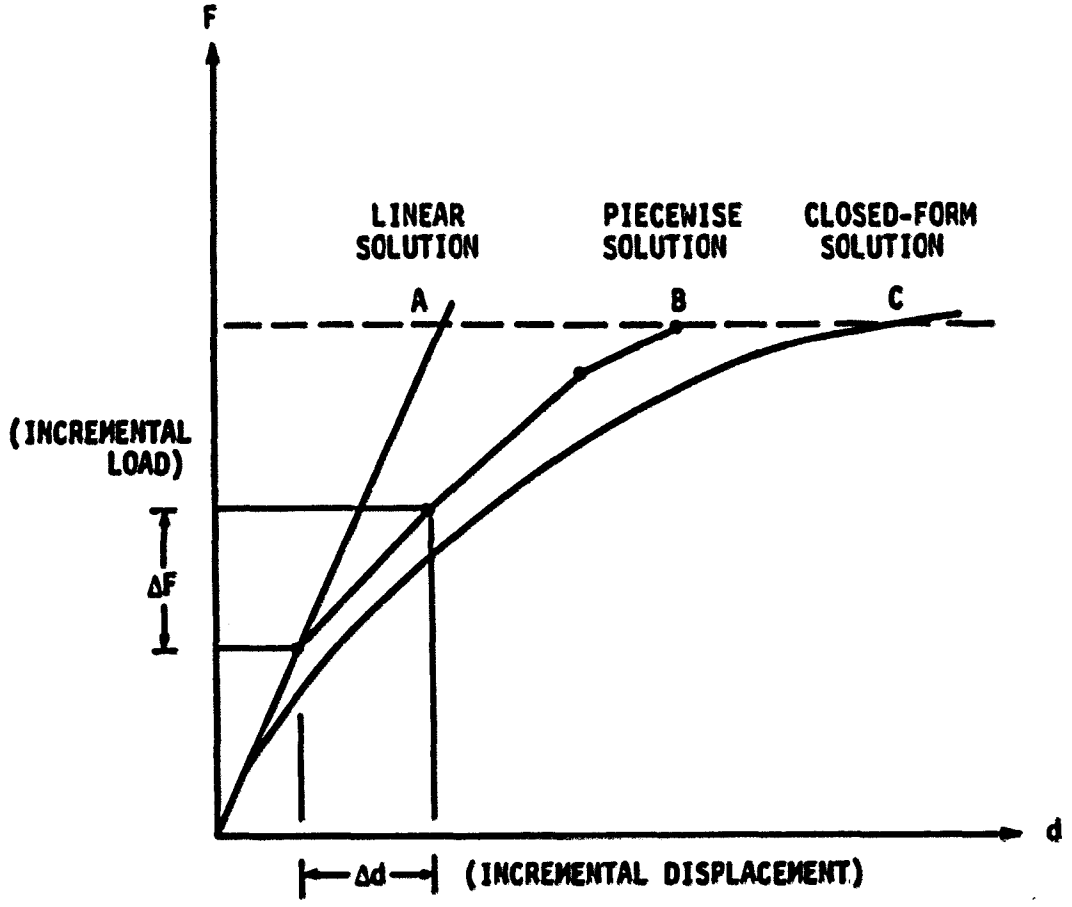

Fig. 17. Piecewise linear solution for a single degree-of-freedom system

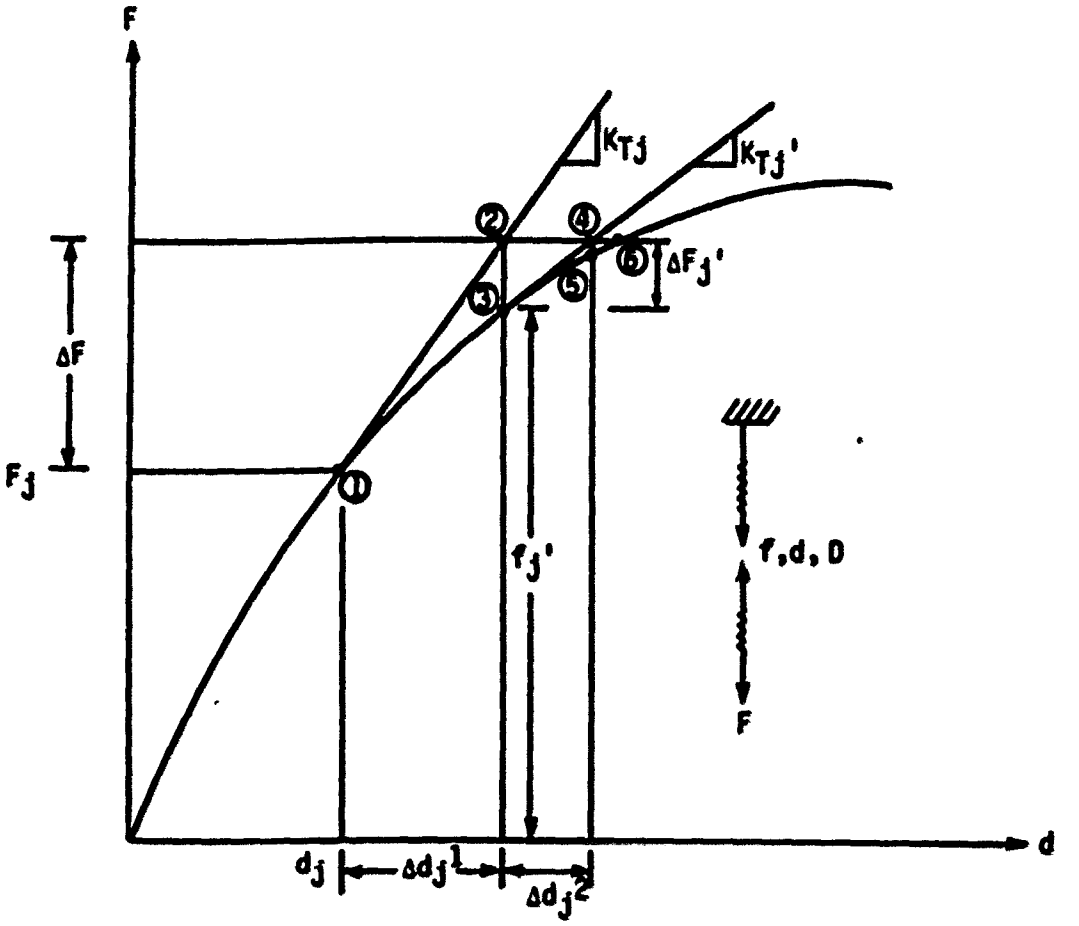

Fig. 18. Characteristics of Newton-Raphson iteration in a simple one-degree-of-freedom

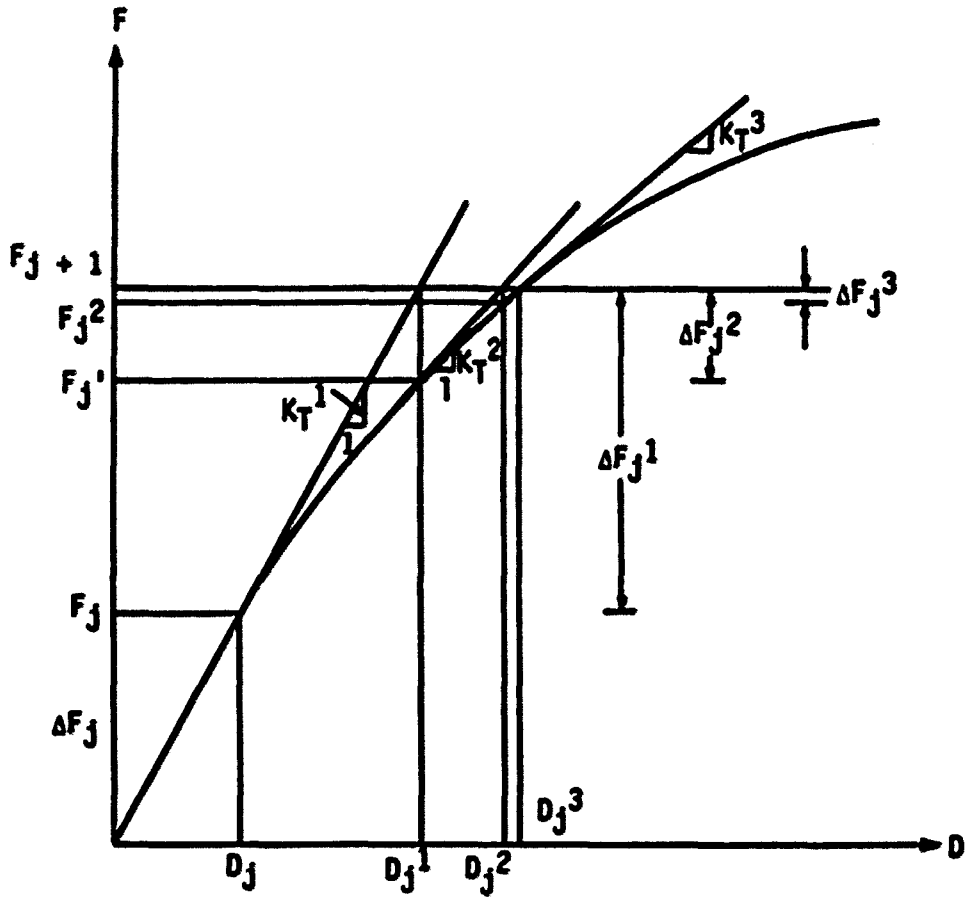

Fig. 19. Increment-iteration or mixed procedure in a multi-degree-of-freedom structure (Newton-Raphson solution of the equation $F = f(D)$)

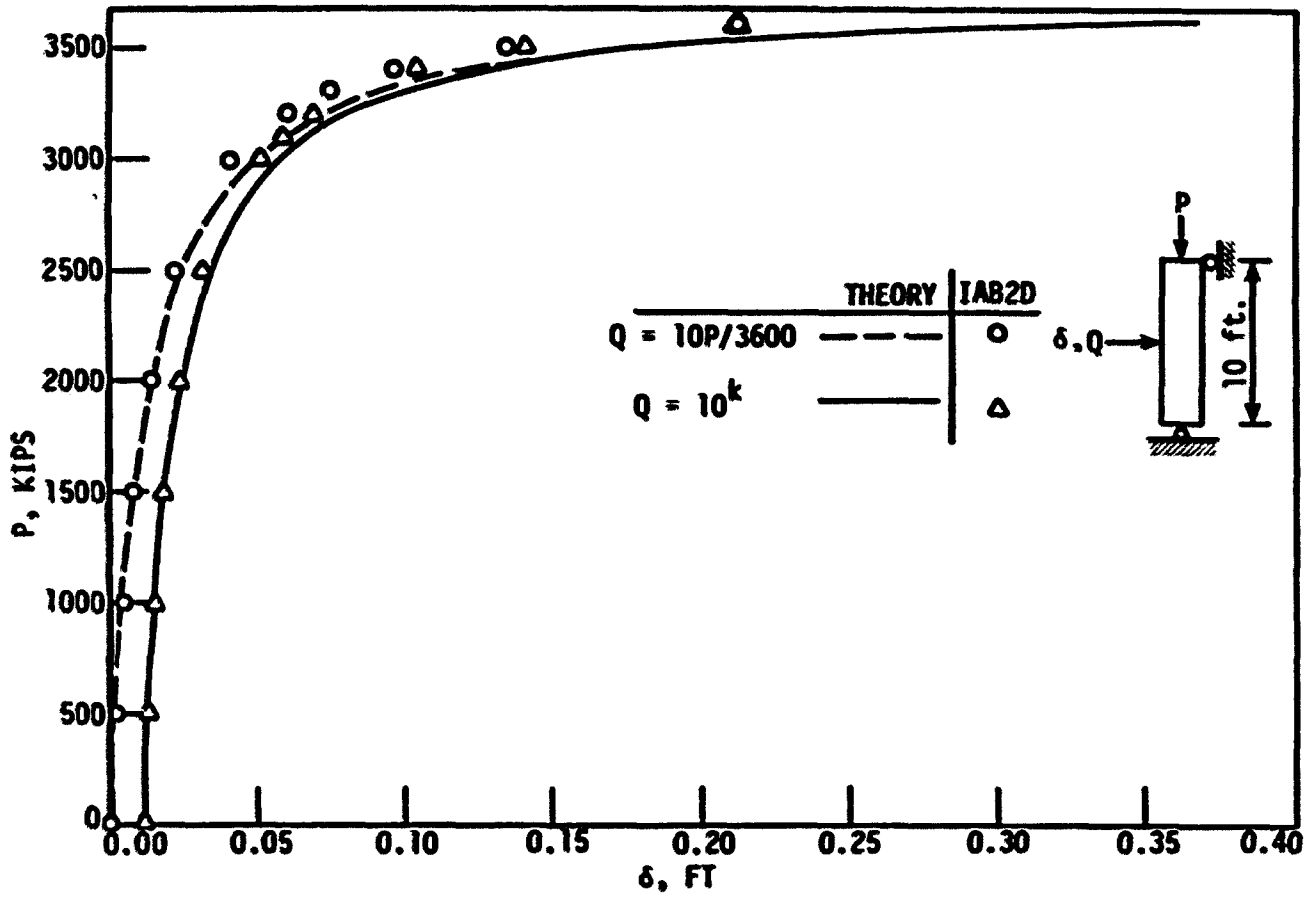

Fig. 20. Load-displacement curves for beam-column problem

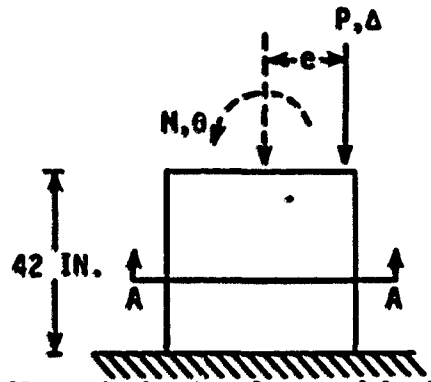

Fig. 21a. A short column subjected to applied load

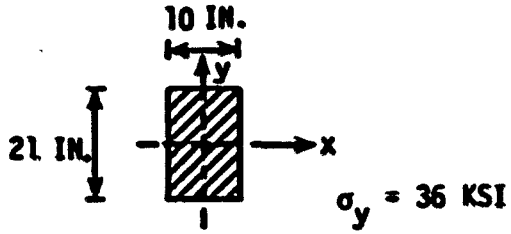

Fig. 21b. Cross section A-A

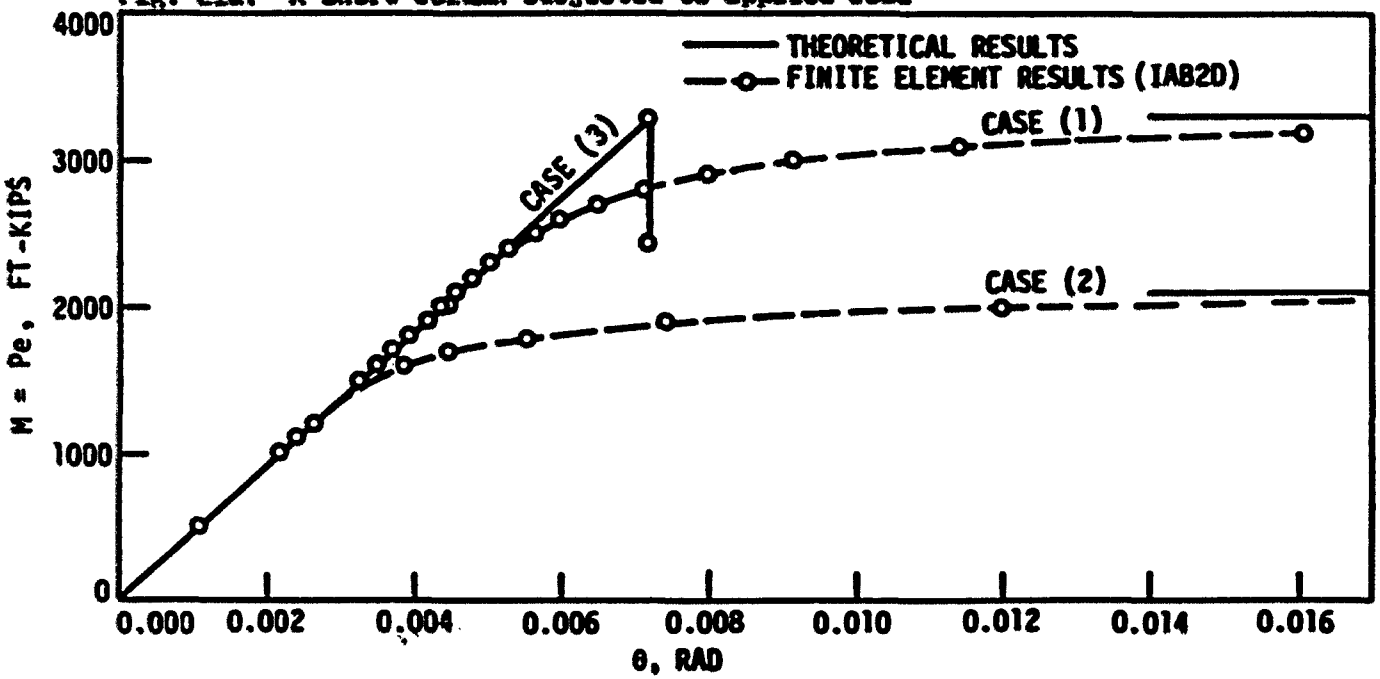

Fig. 21c. N-θ characteristics

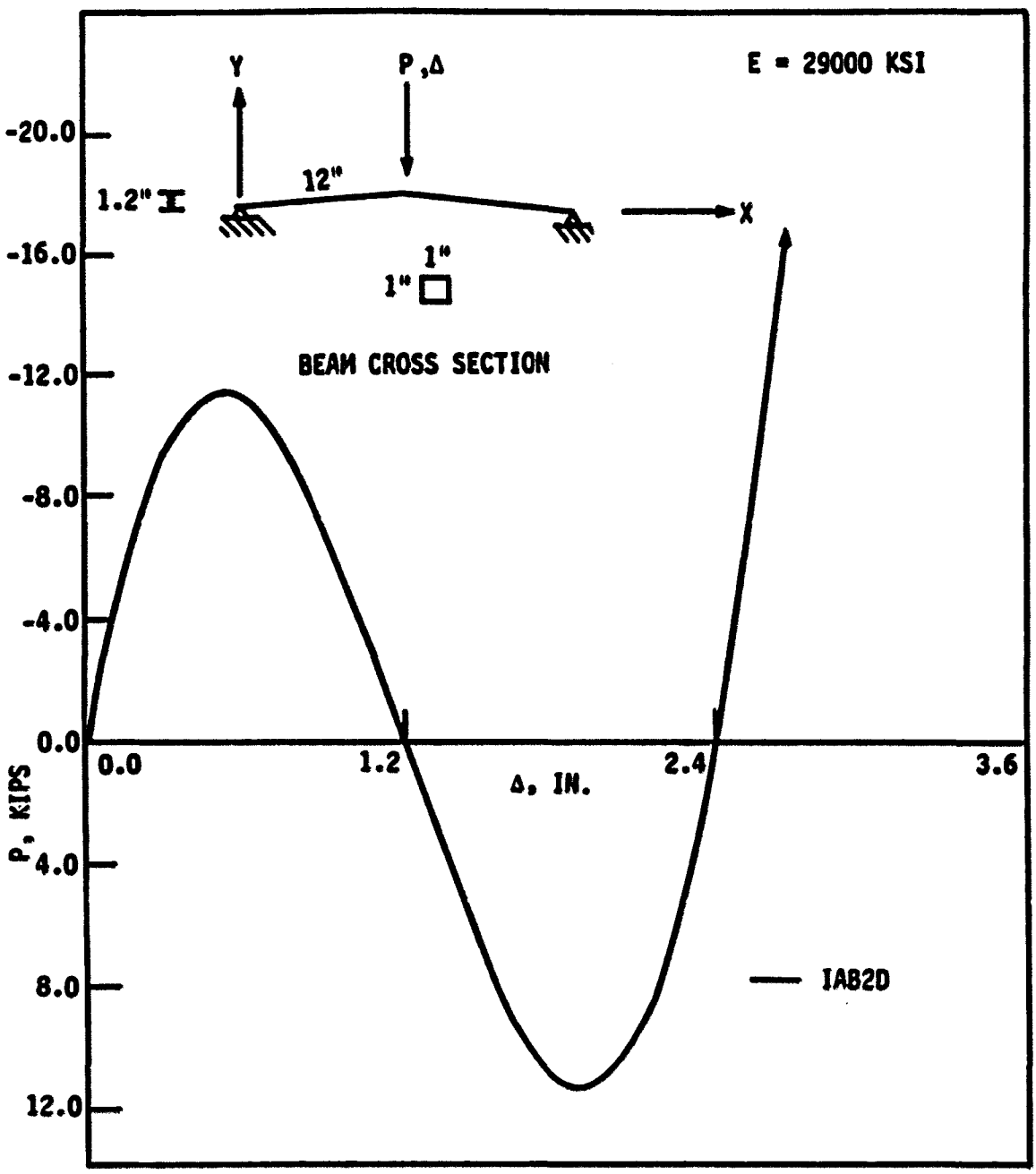

Fig. 22. Load-deflection characteristics of snap-through problem

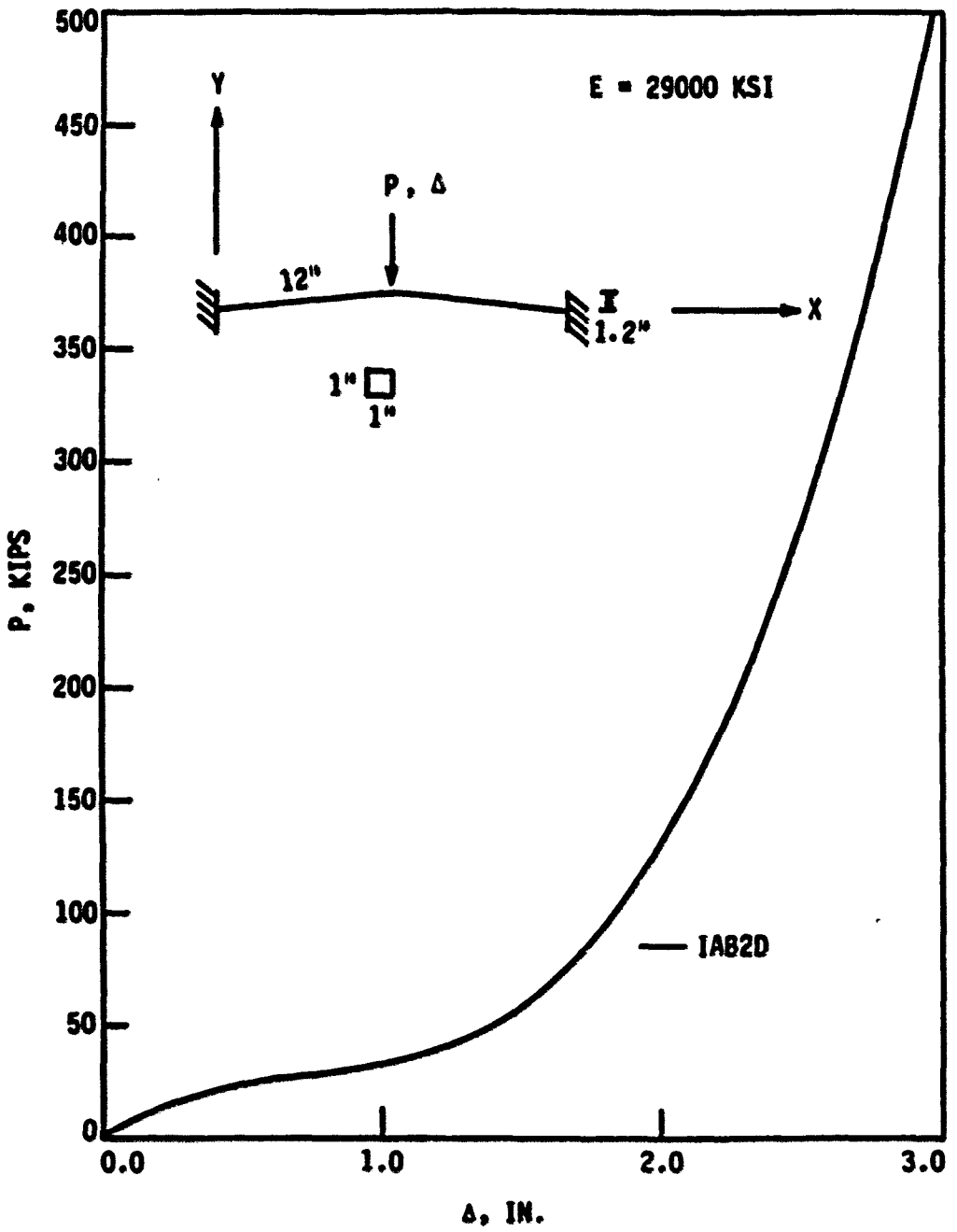

Fig. 23. Load-deflection characteristics of toggle

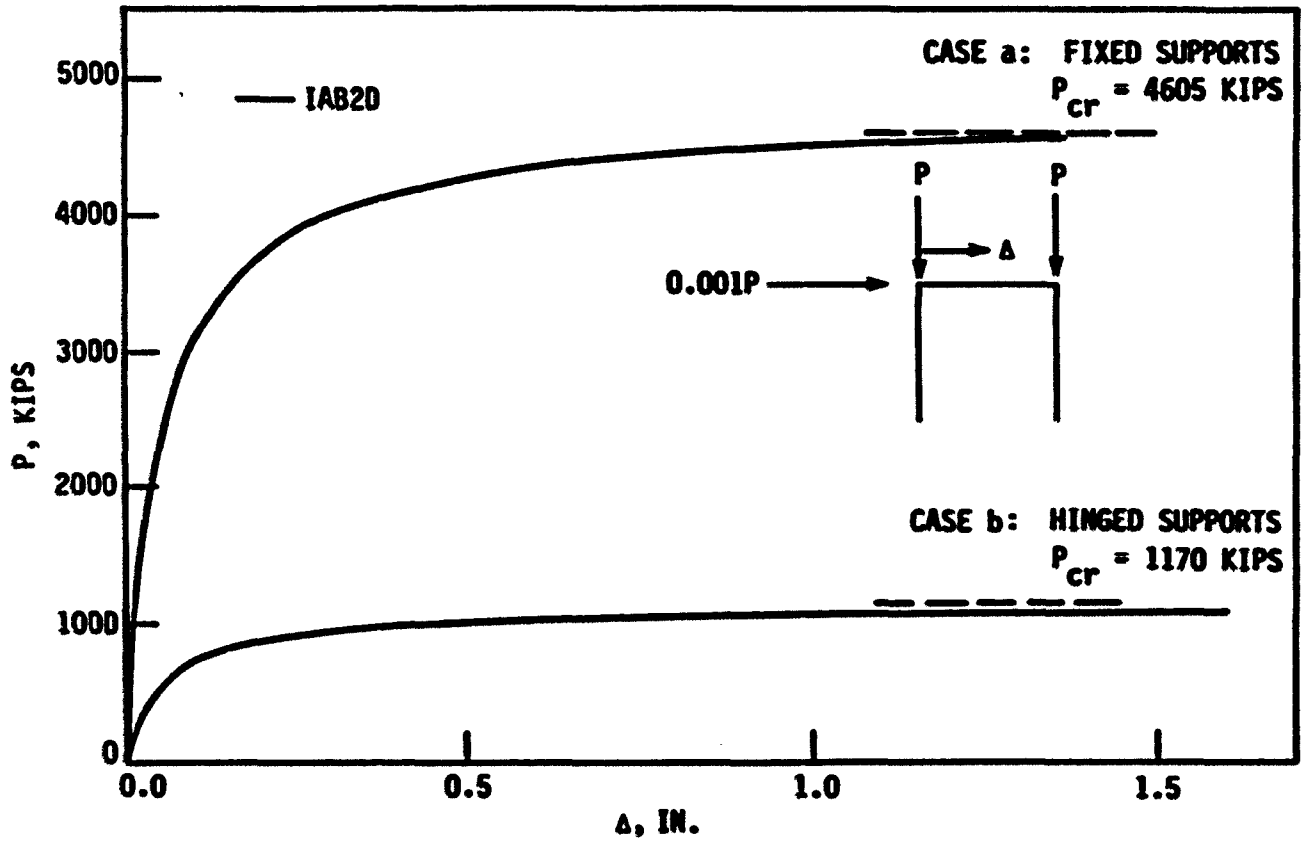

Fig. 24. Load-deflection characteristics of two-dimensional portal frame with fixed base and hinged base

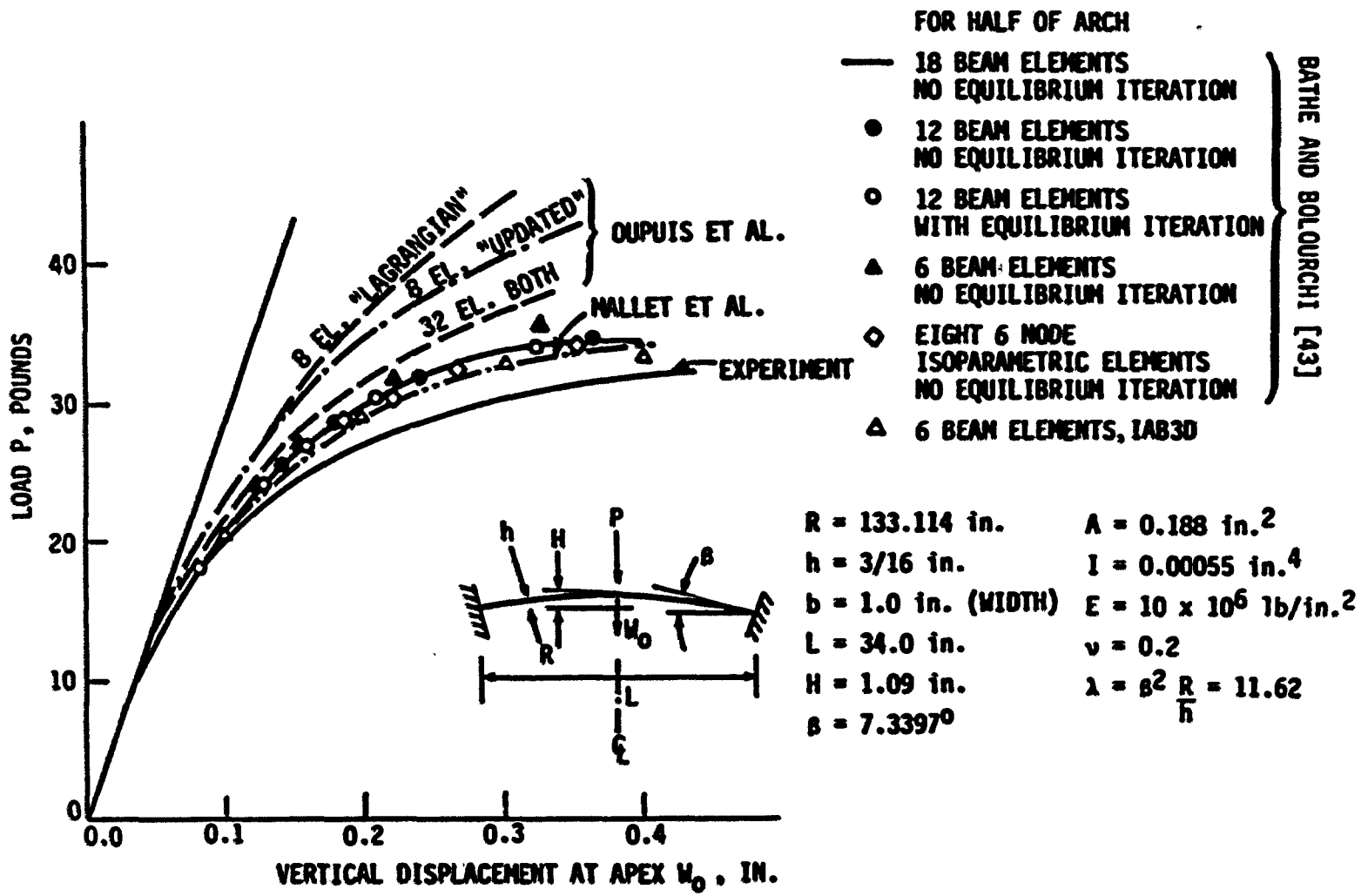

Fig. 25. Large deflection analysis of shallow arch under concentrated load

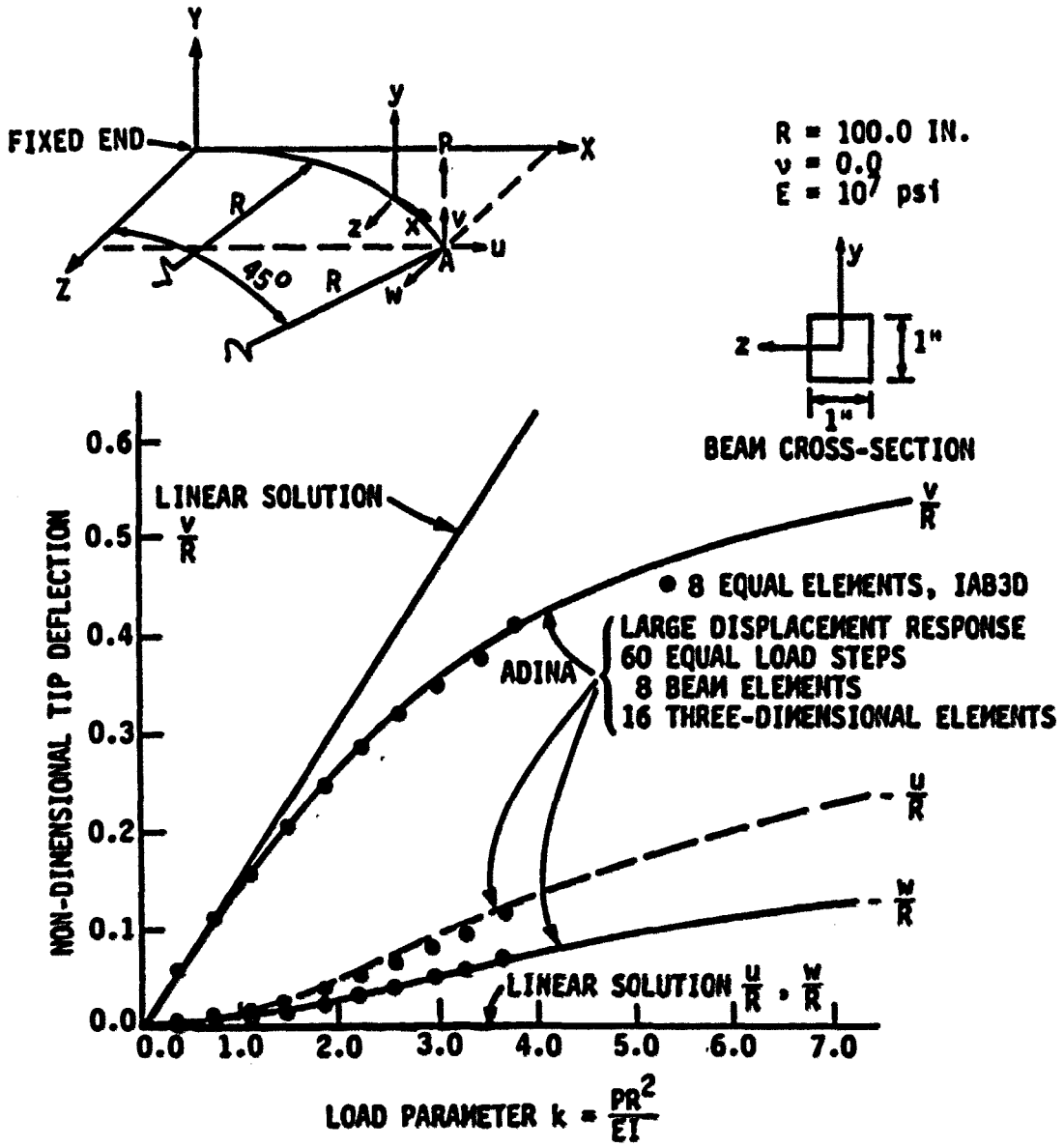

Fig. 26. Three-dimensional large deflection analysis of a 45° circular bend

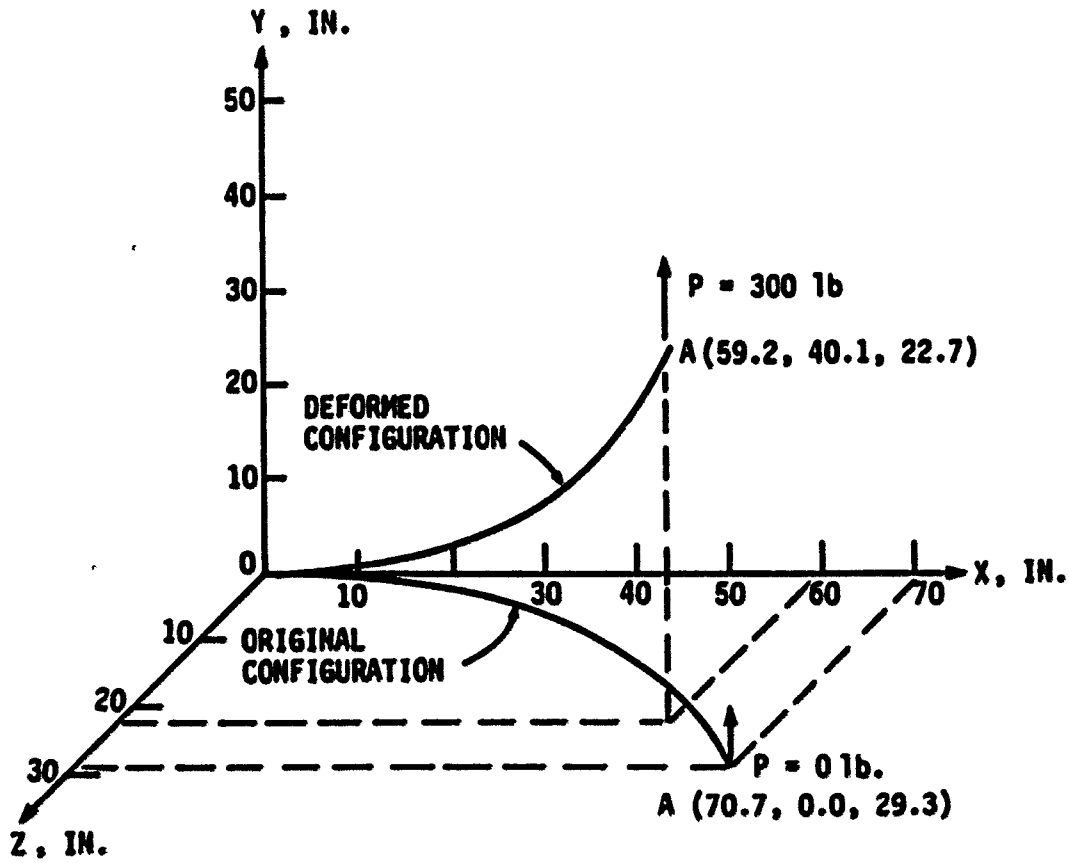

Fig. 27. Deformed configuration of a 45° circular bend

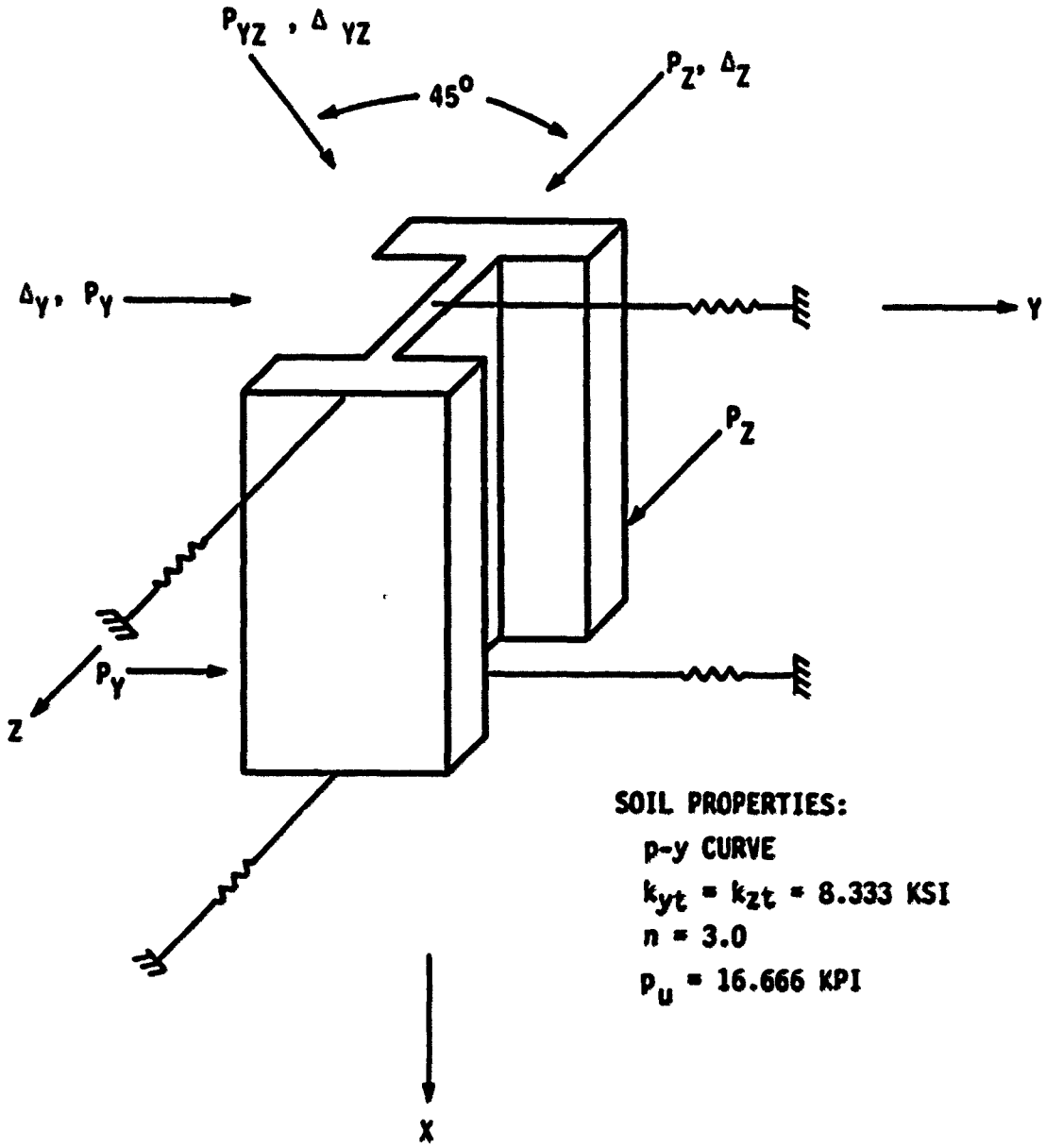

Fig. 28. HP14x73 pile used to check soil response

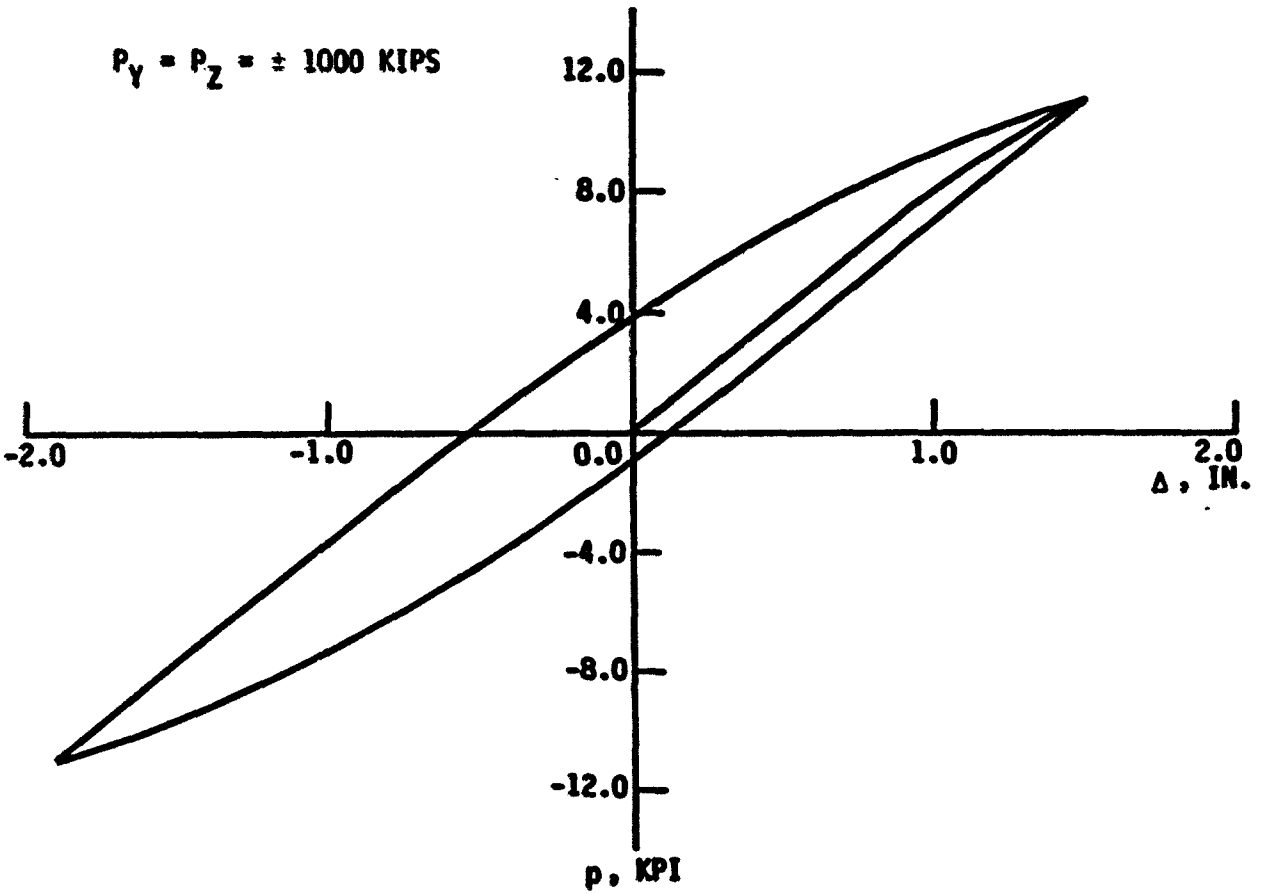

Fig. 29. Soil response for cyclic loads in Y, Z directions

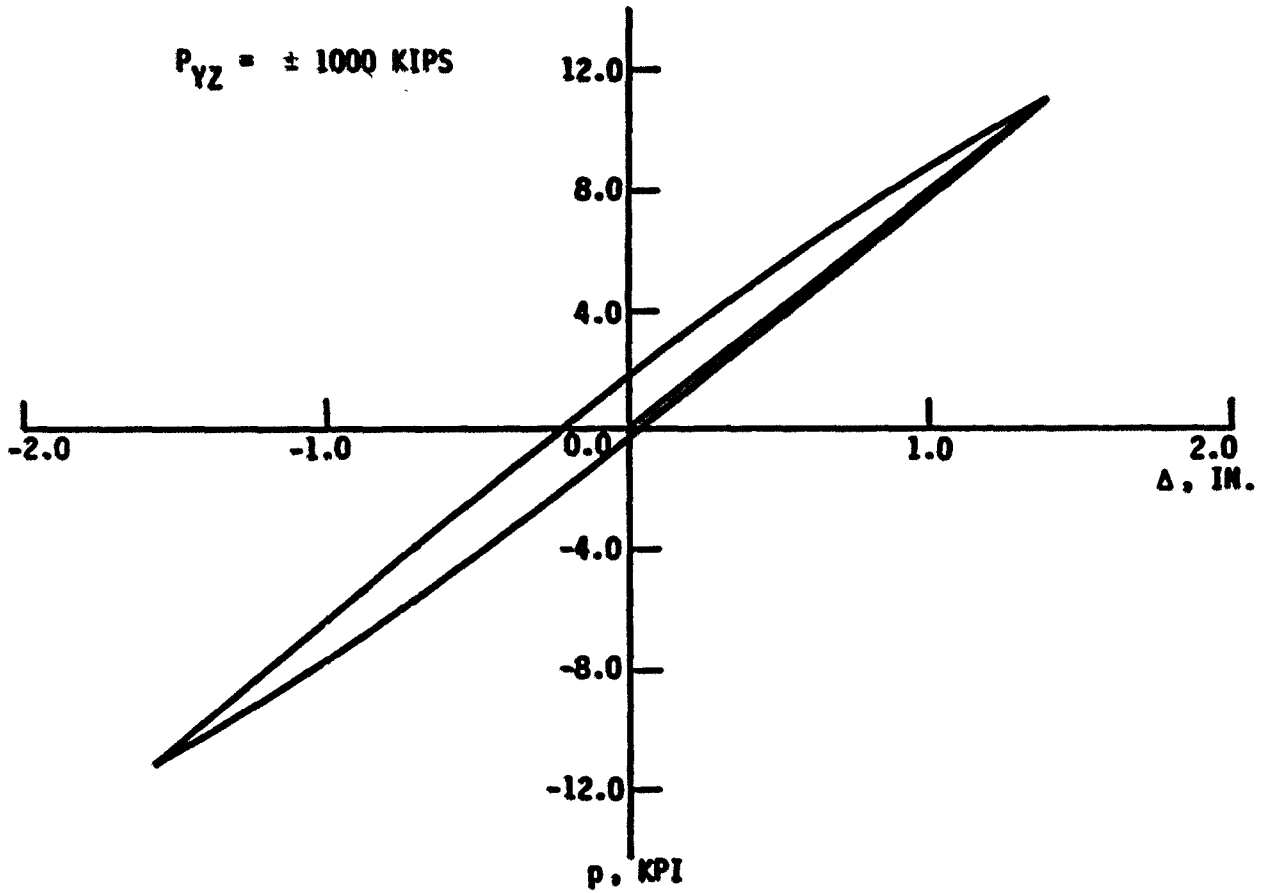

Fig. 30. Soil response for cyclic loads in YZ direction

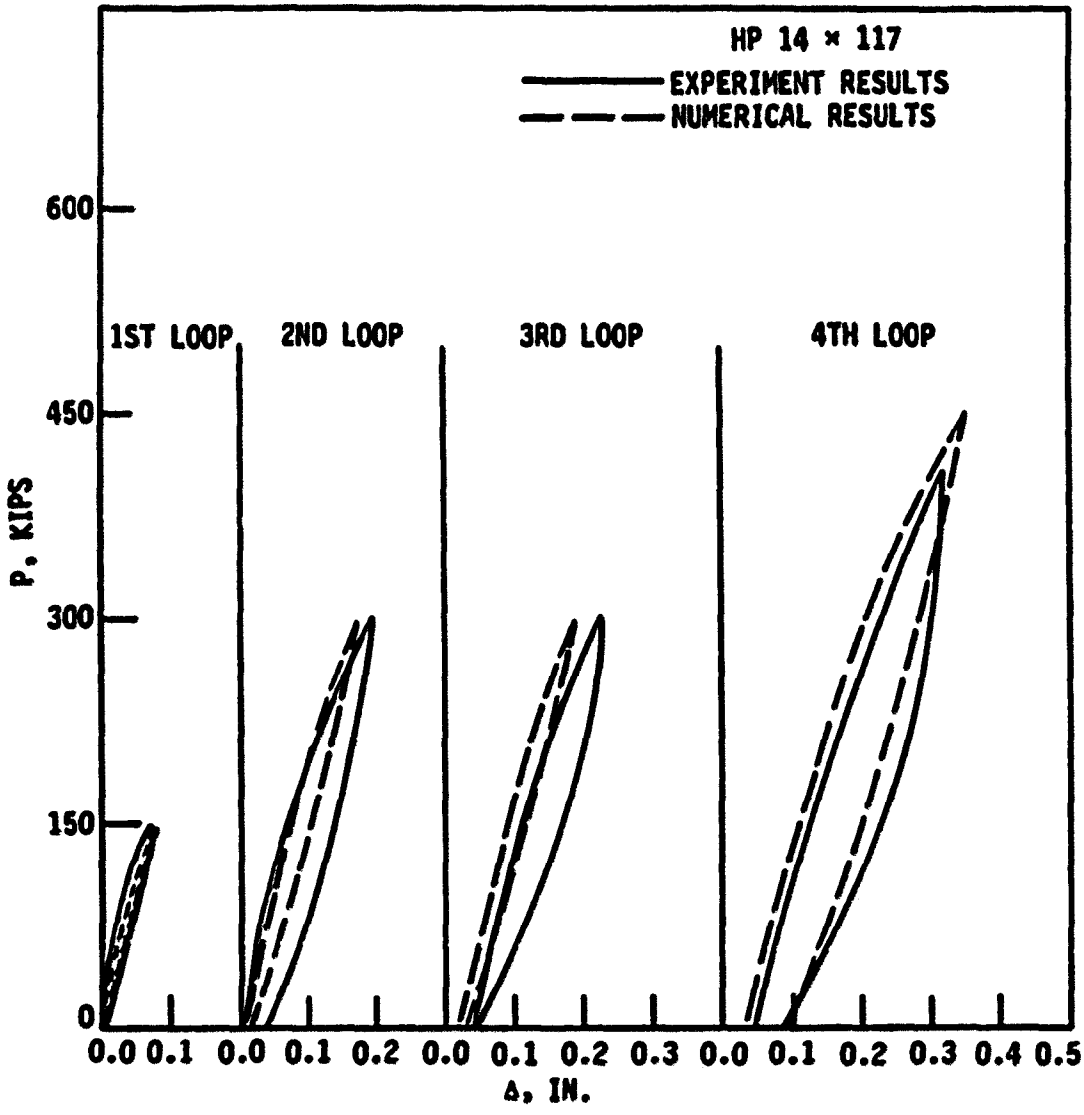

Fig. 31. Load-settlement curve for HP14x117 test pile

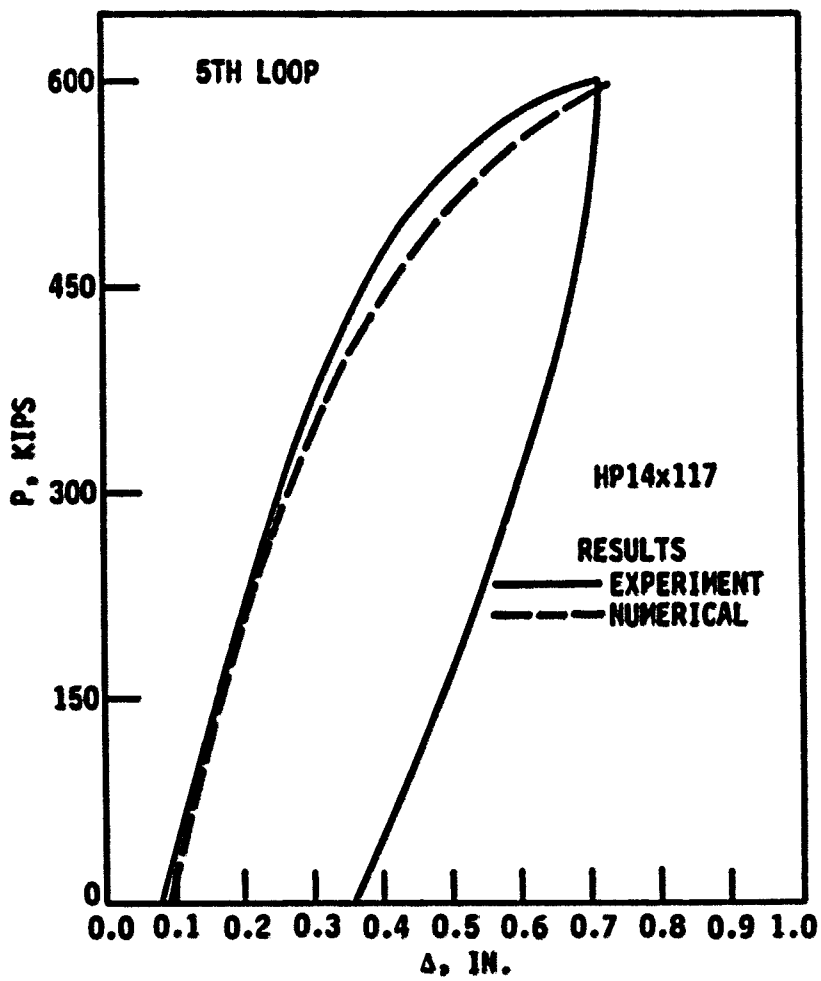

Fig. 31. (continued)

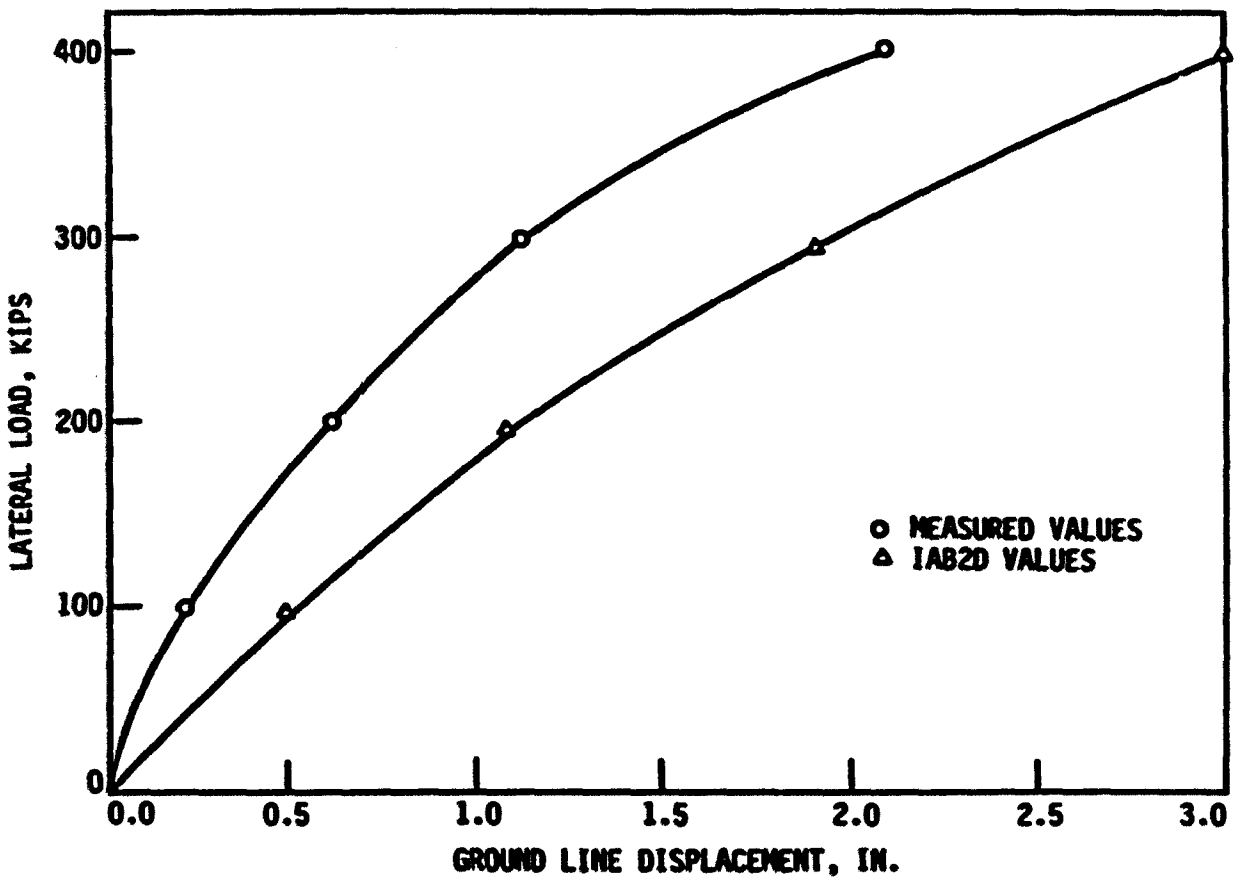

Fig. 32. Load-displacement curves, pier 1

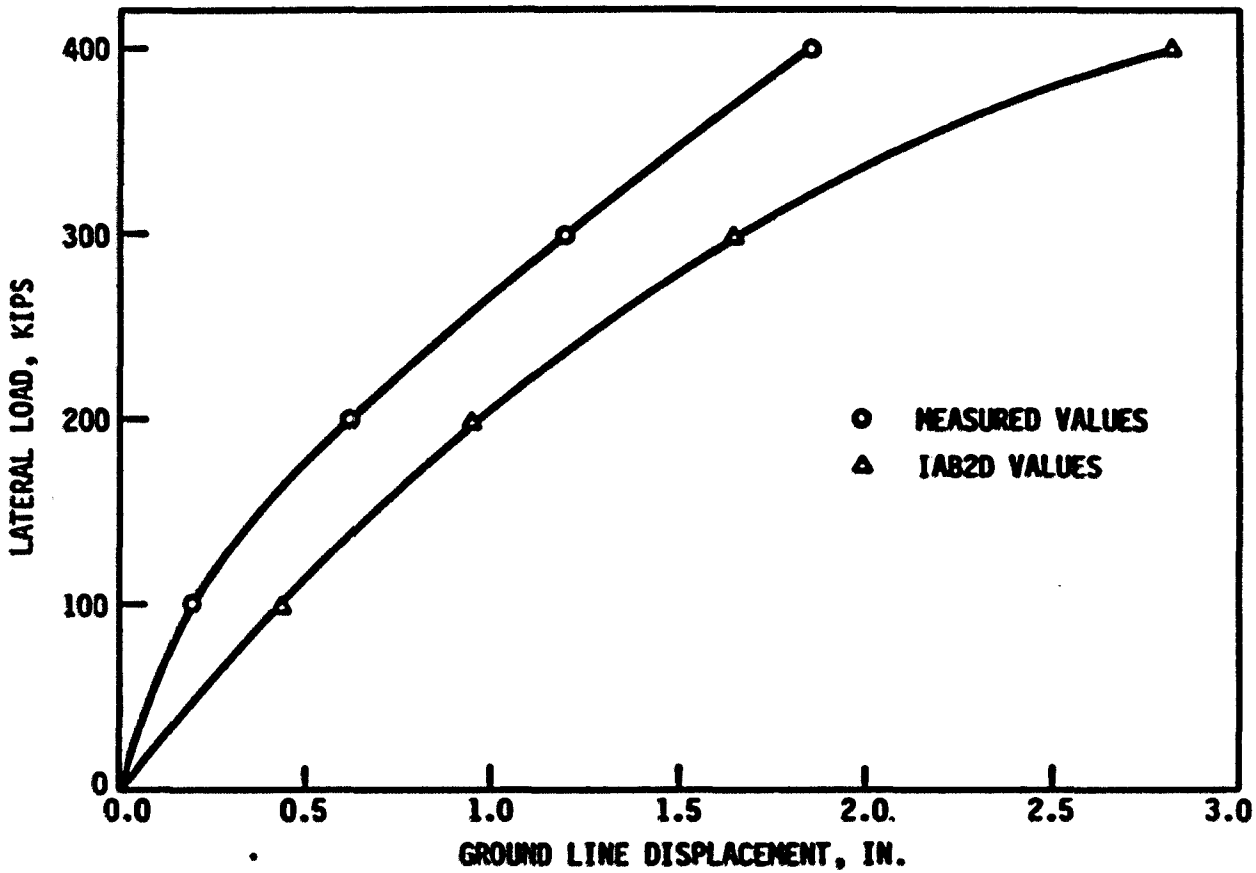

Fig. 33. Load-displacement curves, pier 2

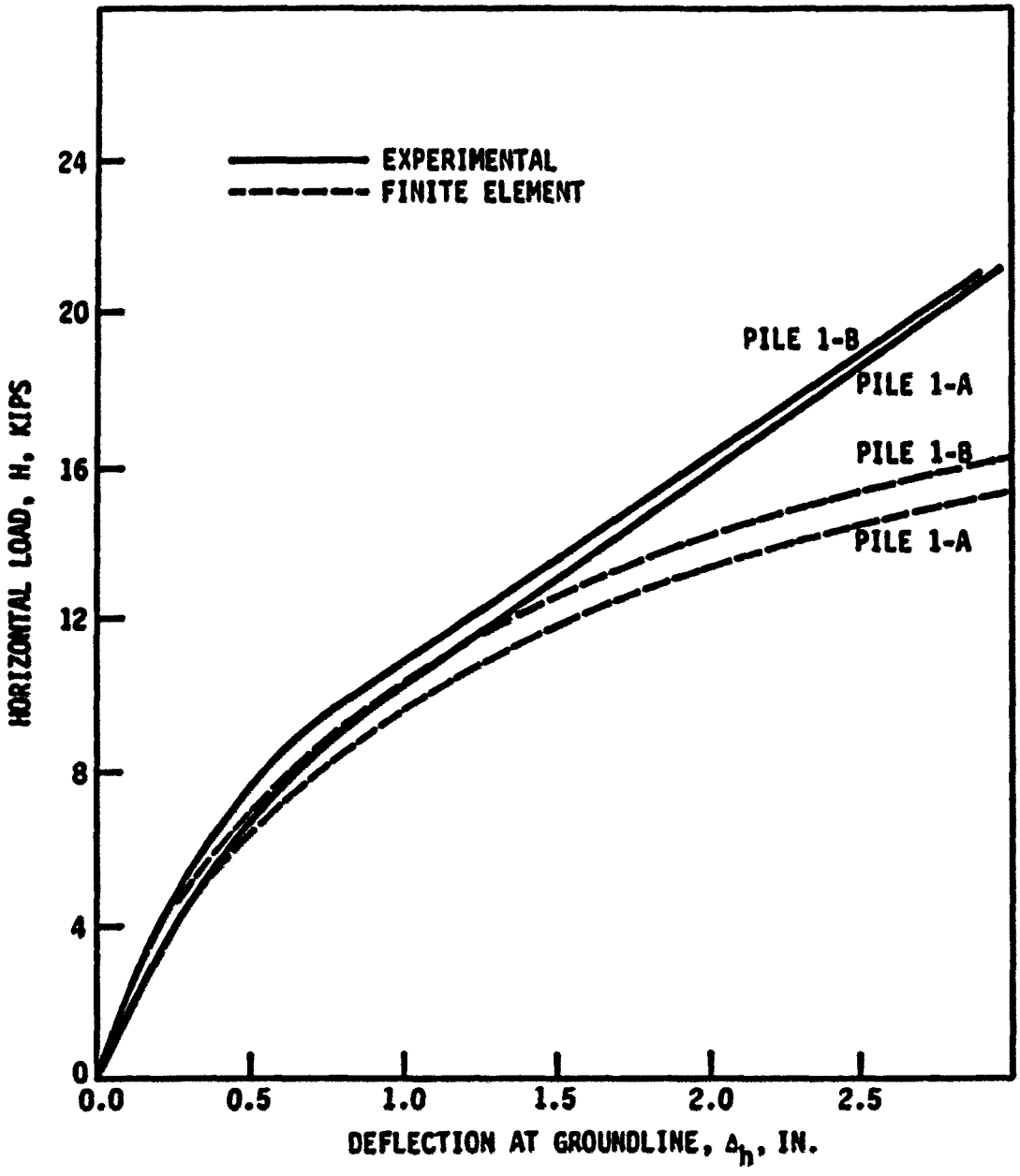

Fig. 34. Load-deflection curve for piles 1-A and 1-B

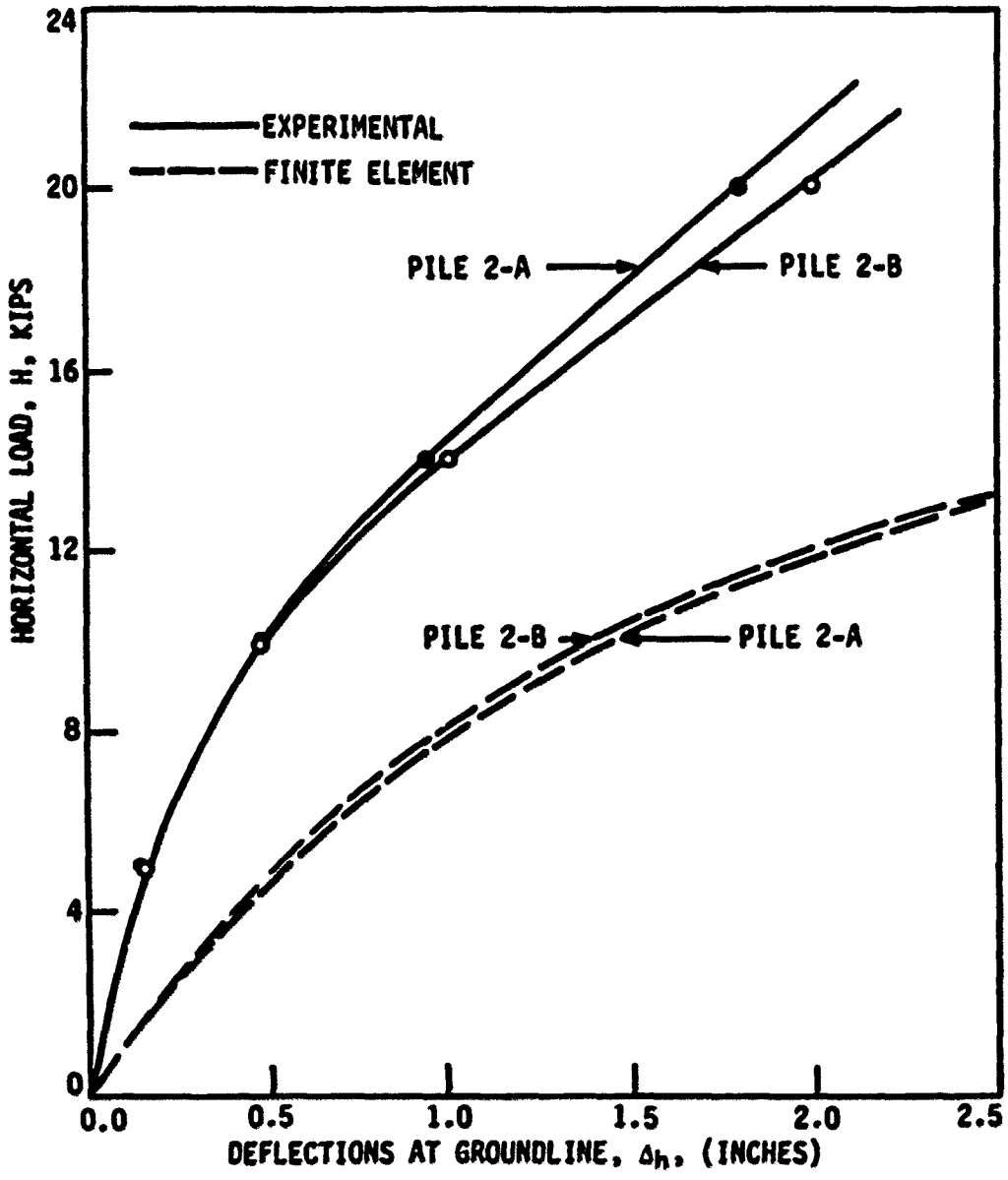

Fig. 35. Load-deflection curve for piles 2-A and 2-B

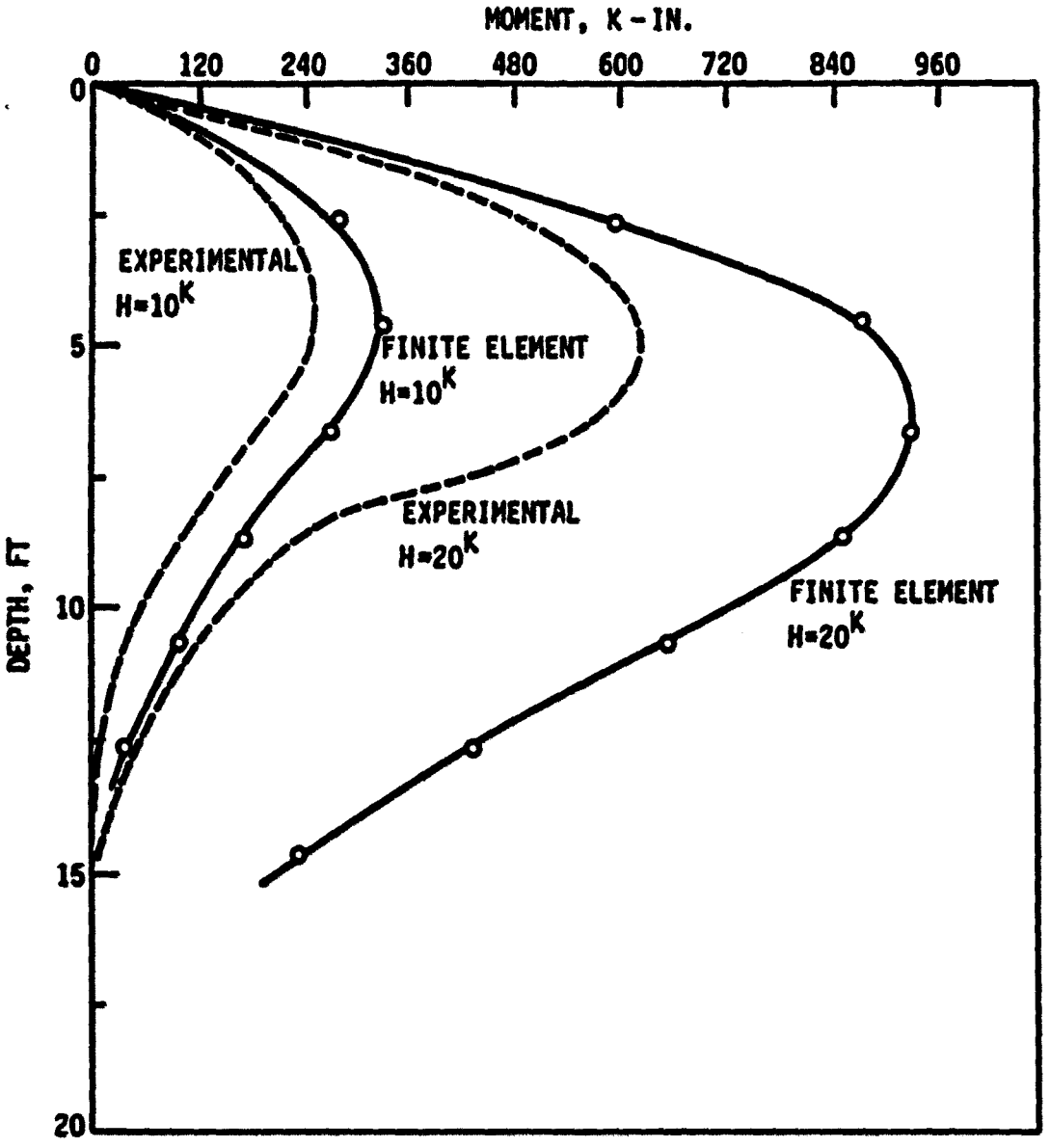

Fig. 36. Moment versus depth diagram for pile 1-A

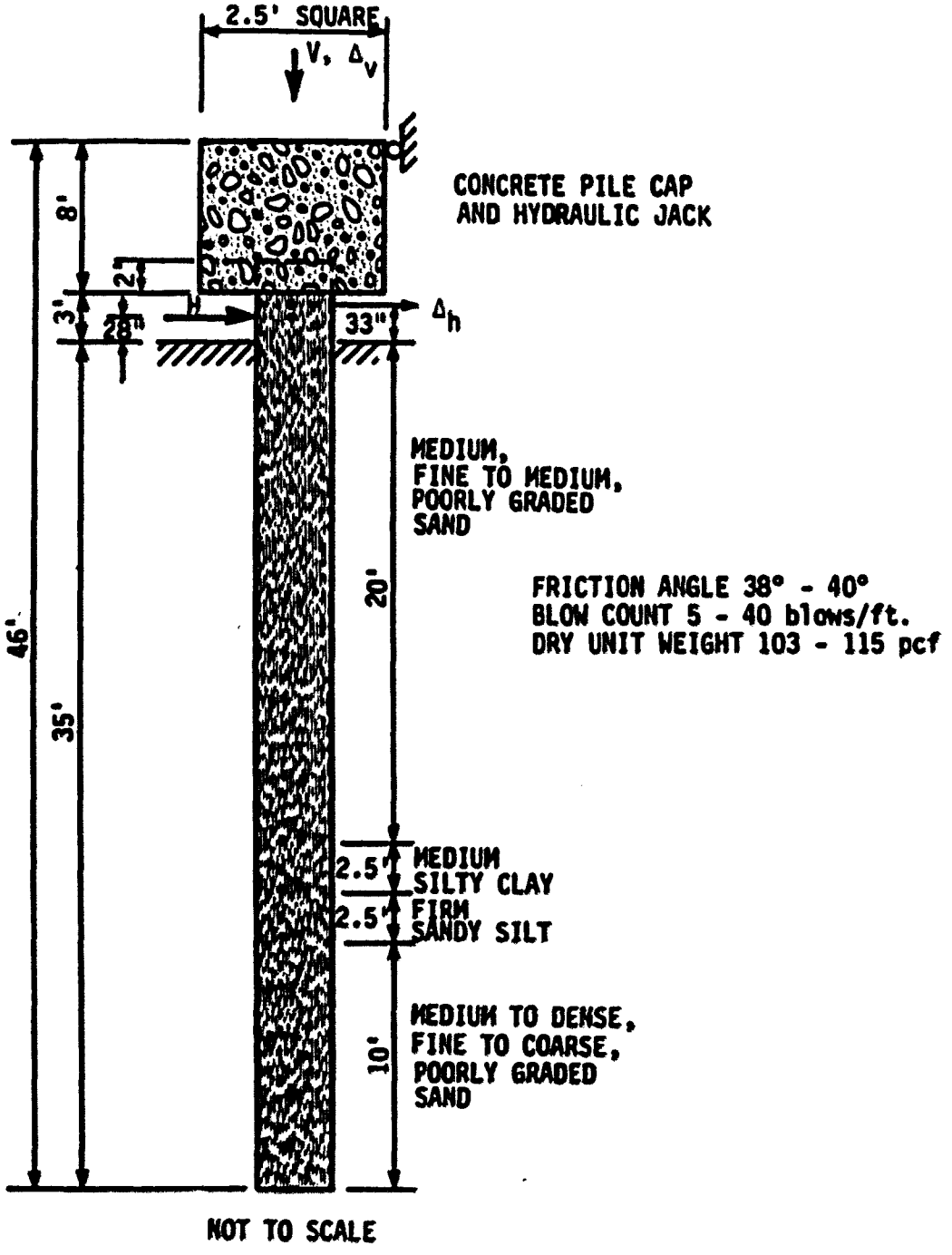

Fig. 37. Schematic diagram of the pile and generalized soil pro[illegible]

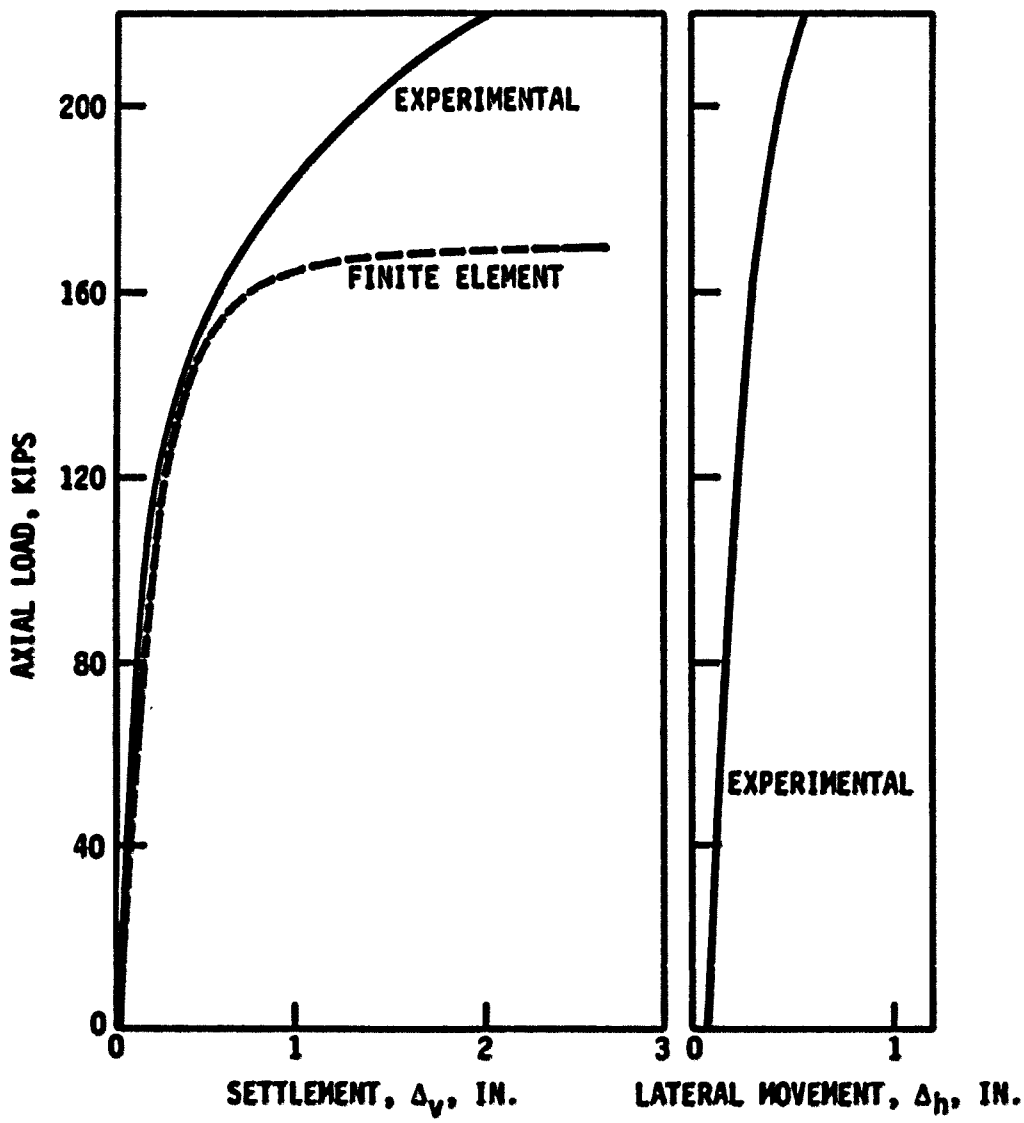

Fig. 38. Load versus settlement for the axial load test

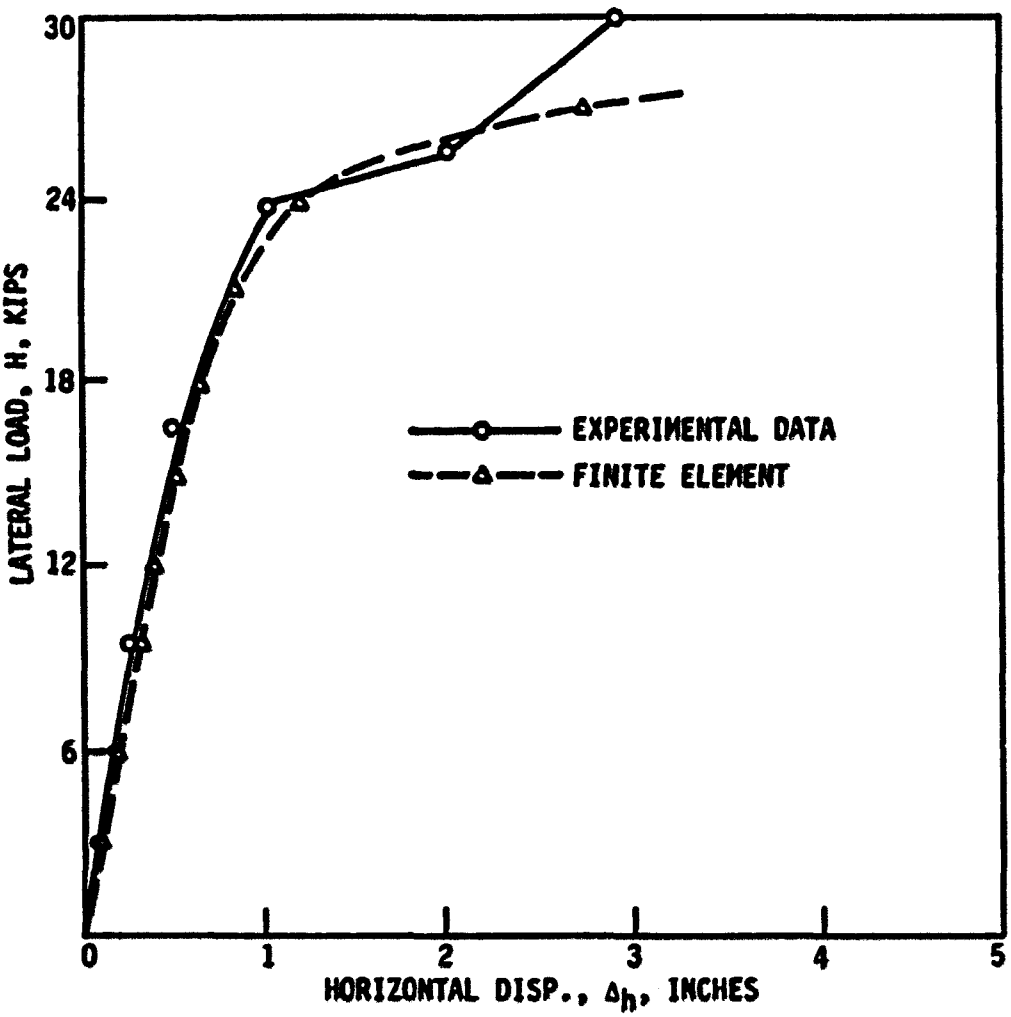

Fig. 39. Lateral load versus displacement for the combined load test (with a 60-kip axial load)

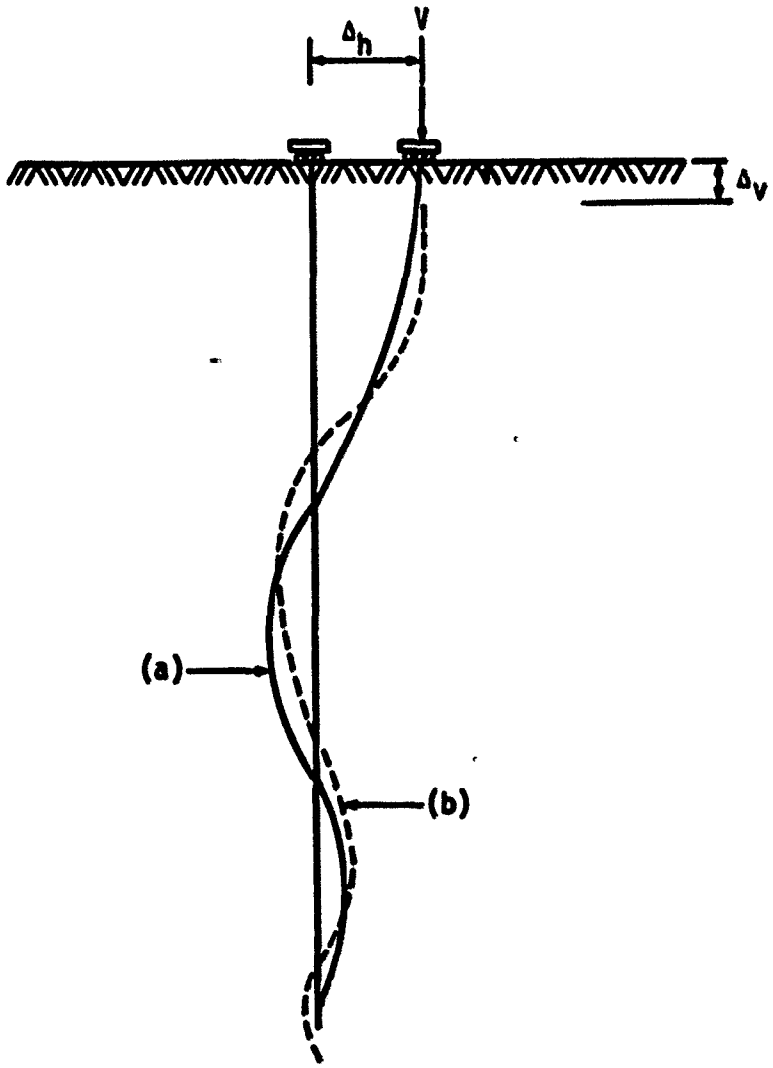

Fig. 40. Pile deflected shapes (a) after a specified displacement Δ_h (solid line), (b) applied vertical load V in case (a) (dashed line)

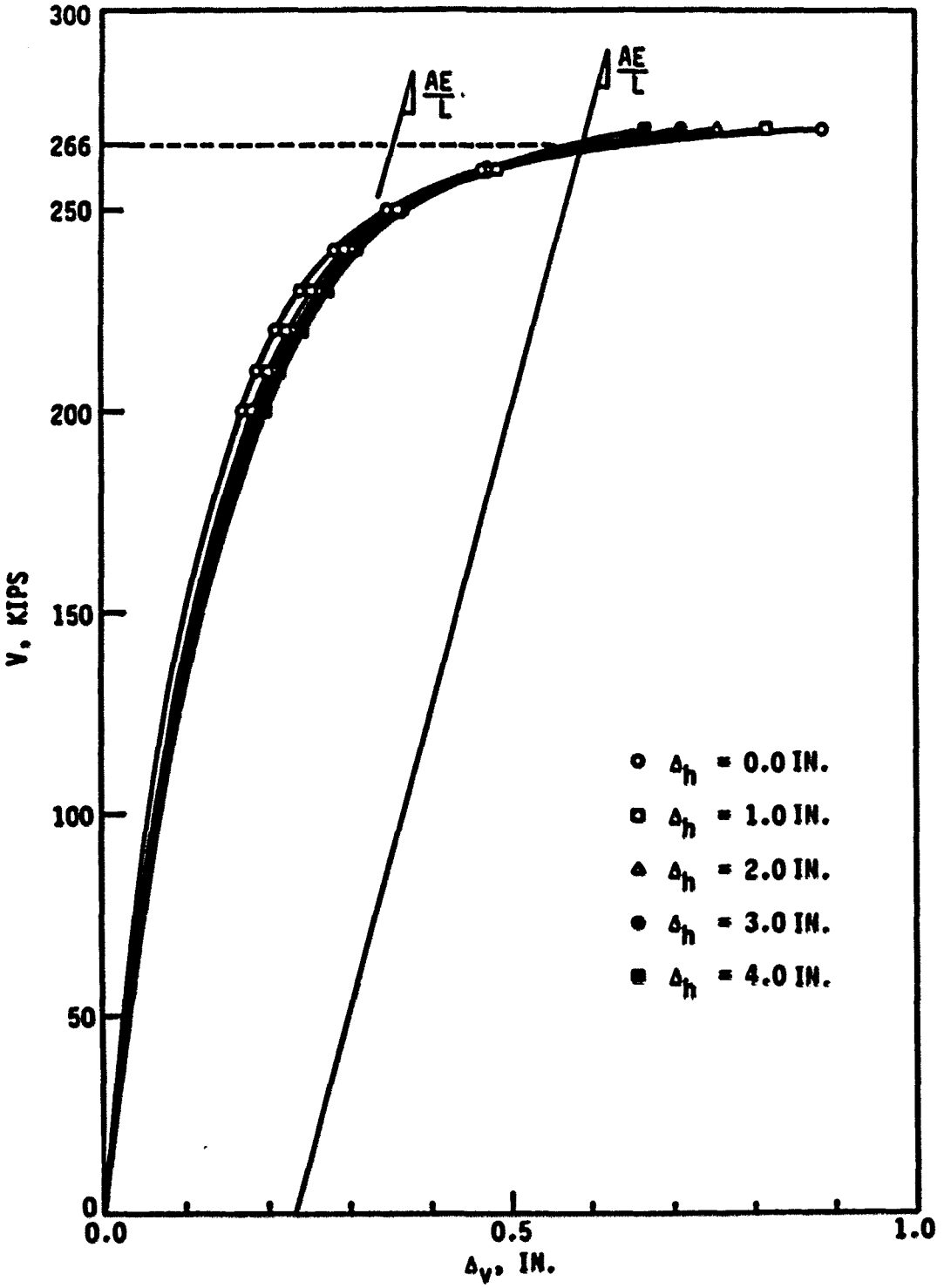

Fig. 41. Vertical load-settlement curves with specified lateral displacements, Δ_h (0, 1, 2, 3, 4 in.) for very stiff cla. (friction pile)

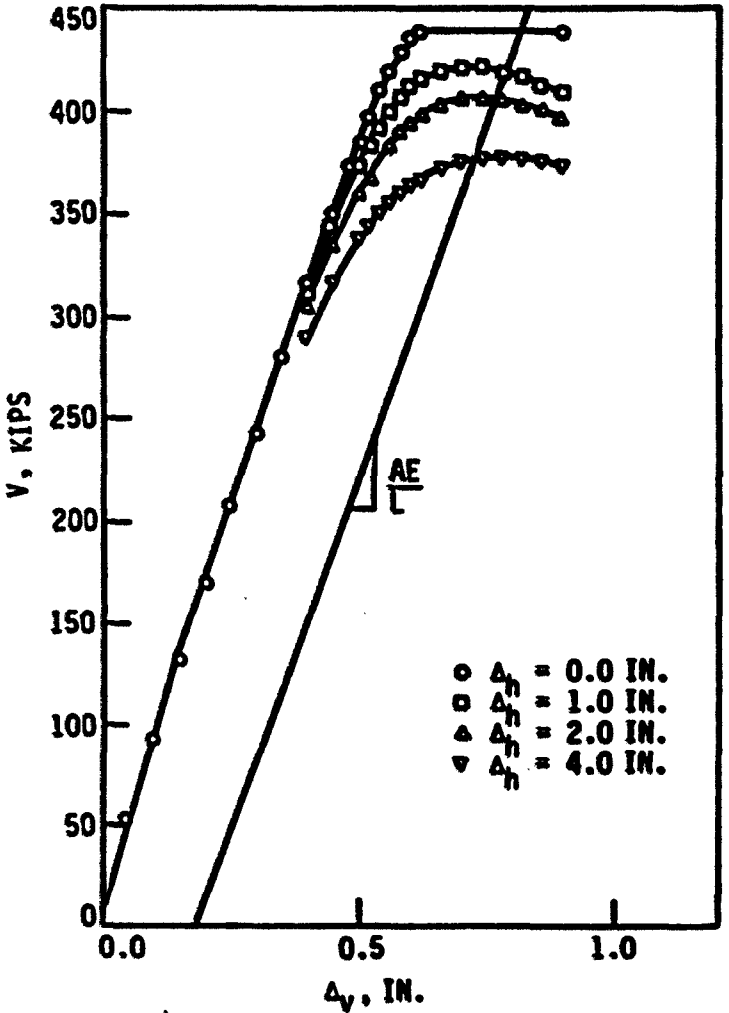

Fig. 42. Vertical load-settlement curves with specified displacements, Δ_h (0, 1, 2, 3, 4 in.) for soft clay (end-bearing pile)

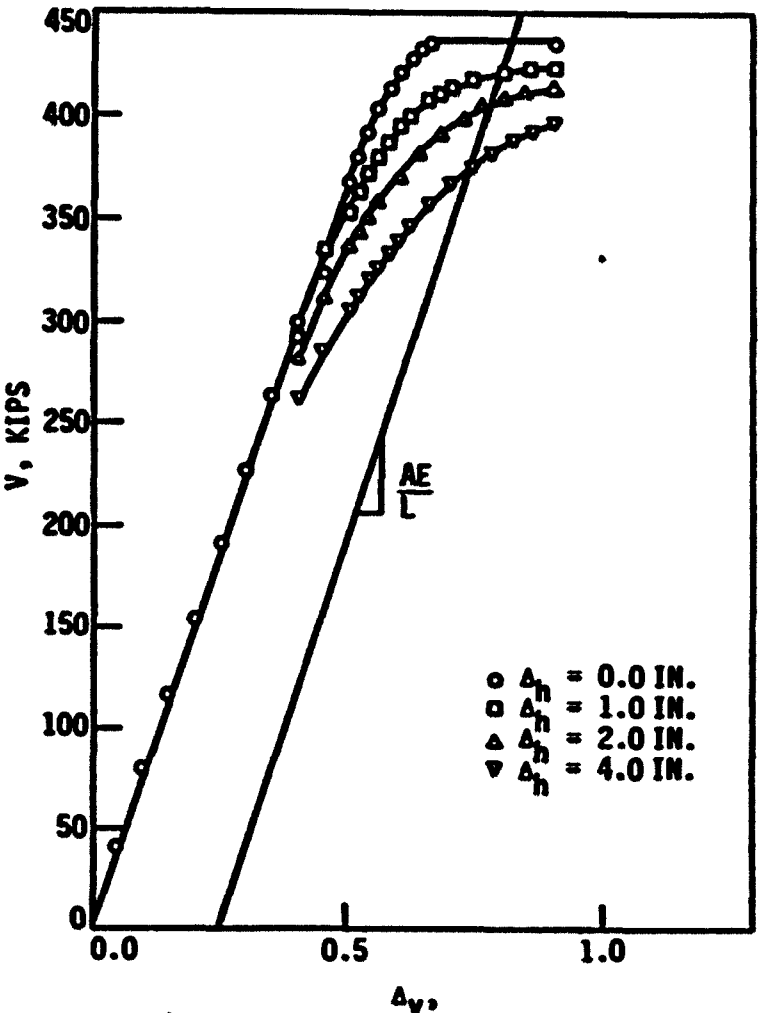

Fig. 43. Vertical load-settlement curves with specified displacements, Δ_h (0, 1, 2, 3, 4 in.) for loose sand (end-bearing pile)

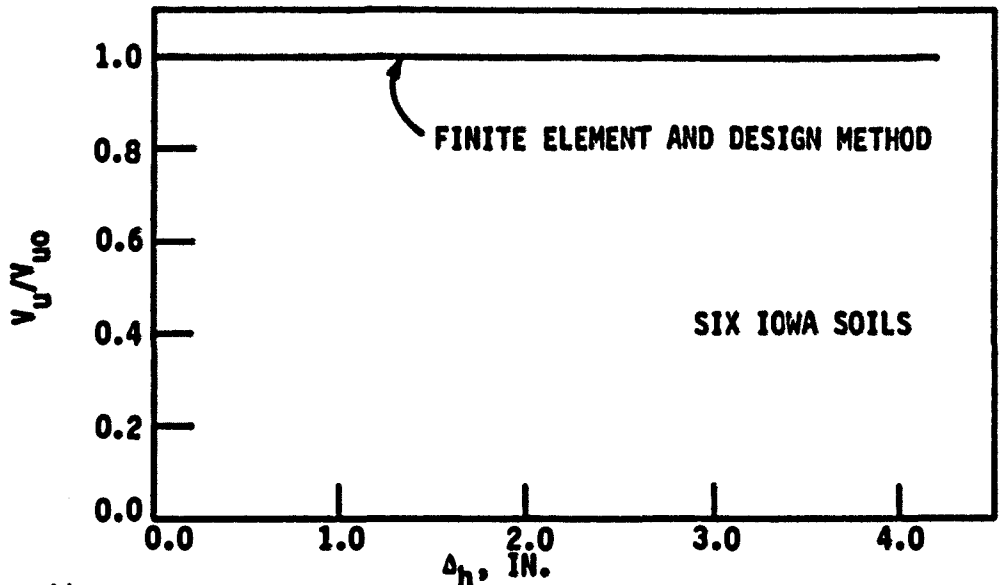

Fig. 44. Nondimensional forms of ultimate vertical load ratio versus specified lateral displacements Δ_h, in Iowa soils (friction pile)

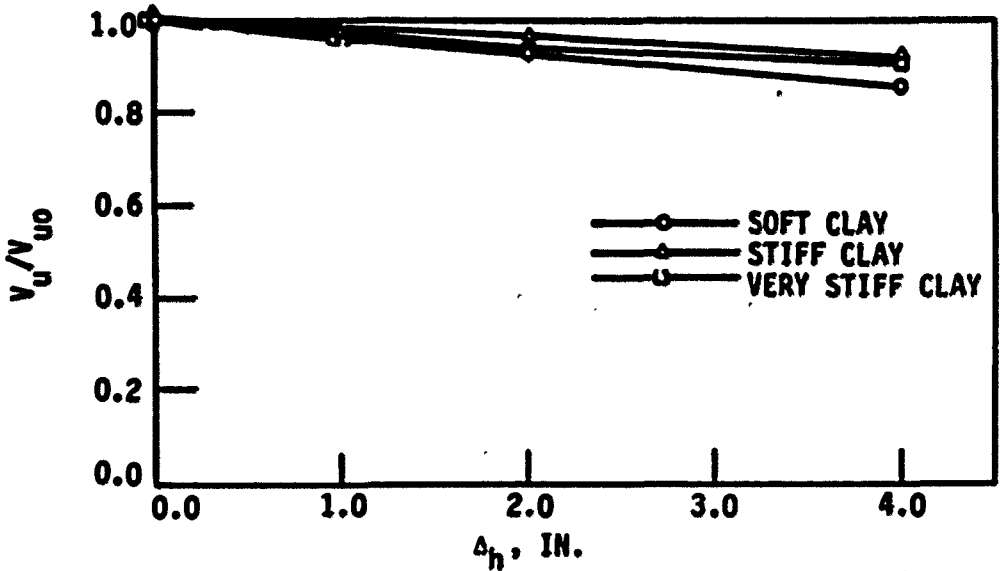

Fig. 45a. Nondimensional forms of ultimate vertical load ratio versus specified lateral displacements Δ_h, in Iowa soils (end-bearing pile)

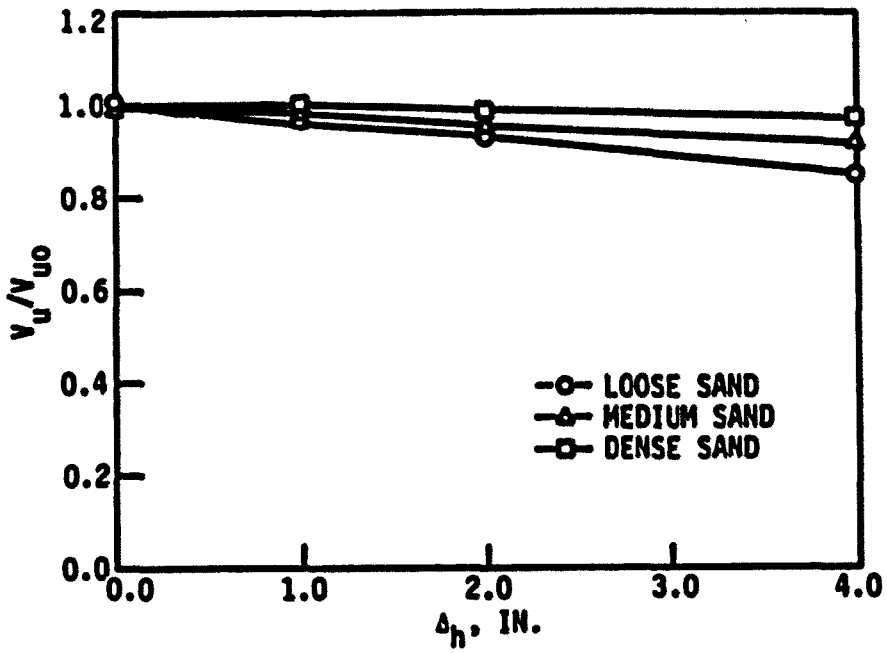

Fig. 45b. Nondimensional forms of ultimate vertical load ratio versus specified lateral displacements Δ_h, in Iowa soils (end-bearing pile)

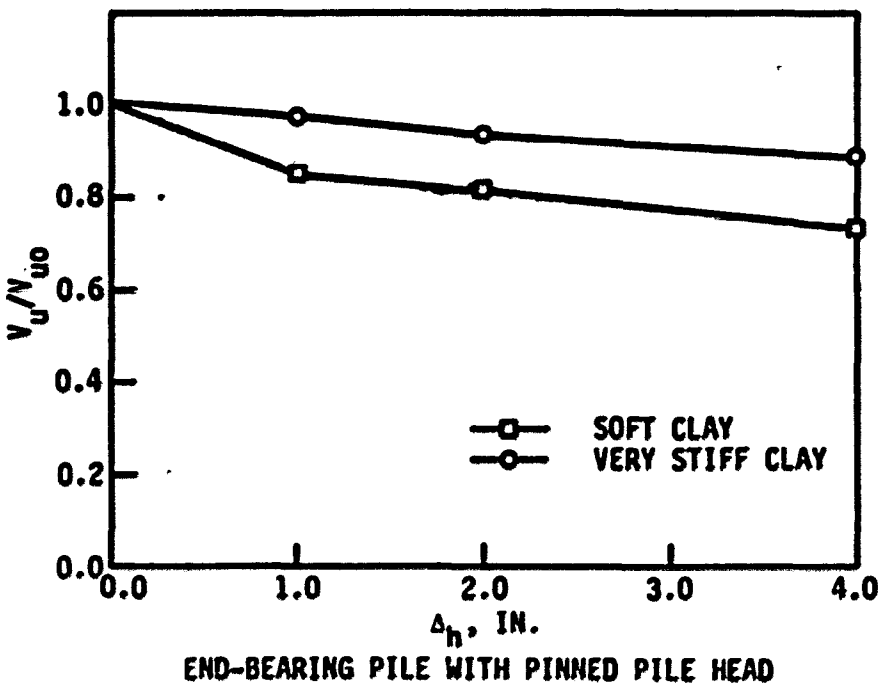

Fig. 46. Nondimensional forms of ultimate vertical load ratio

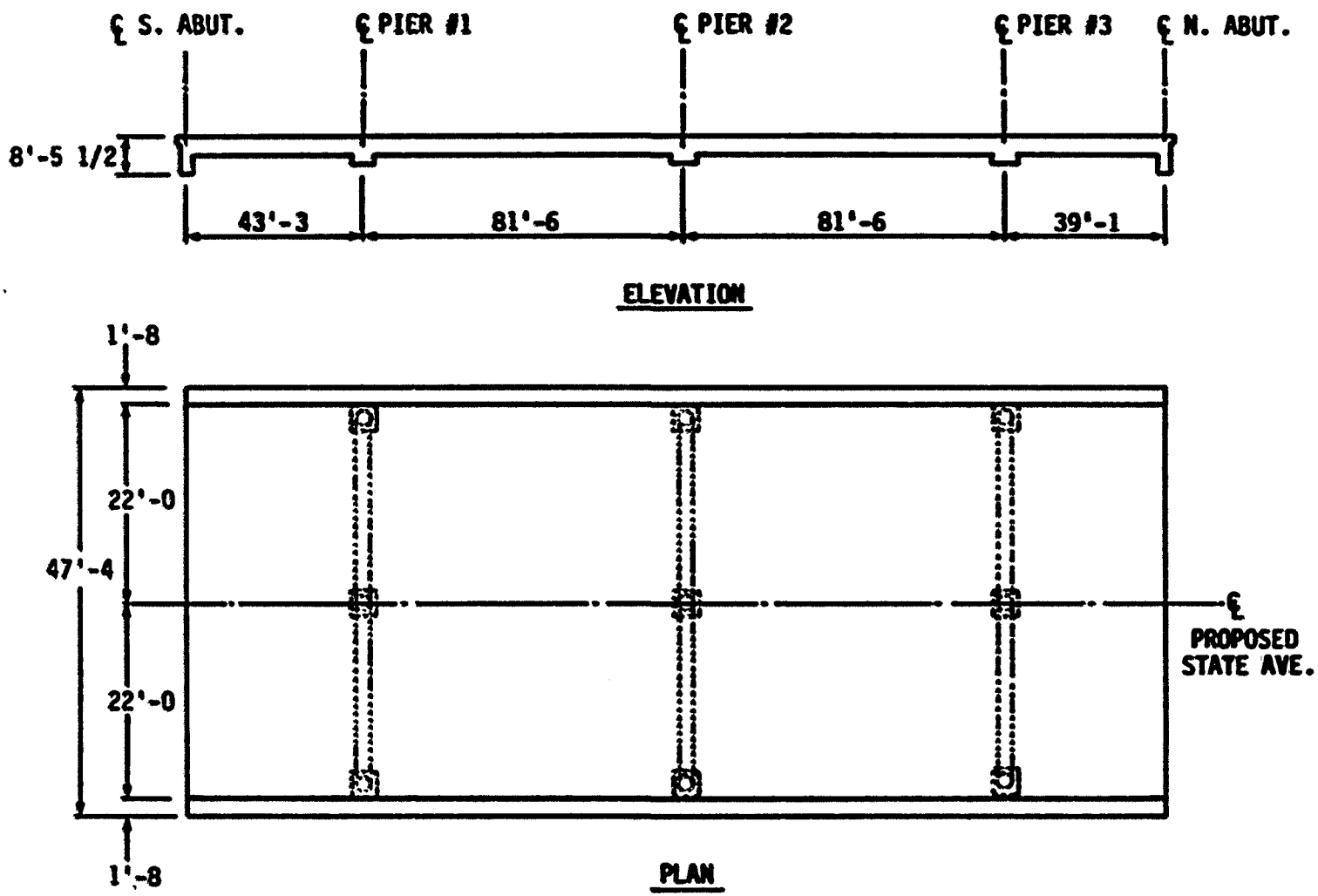

Fig. 47. Plan and elevation of bridge

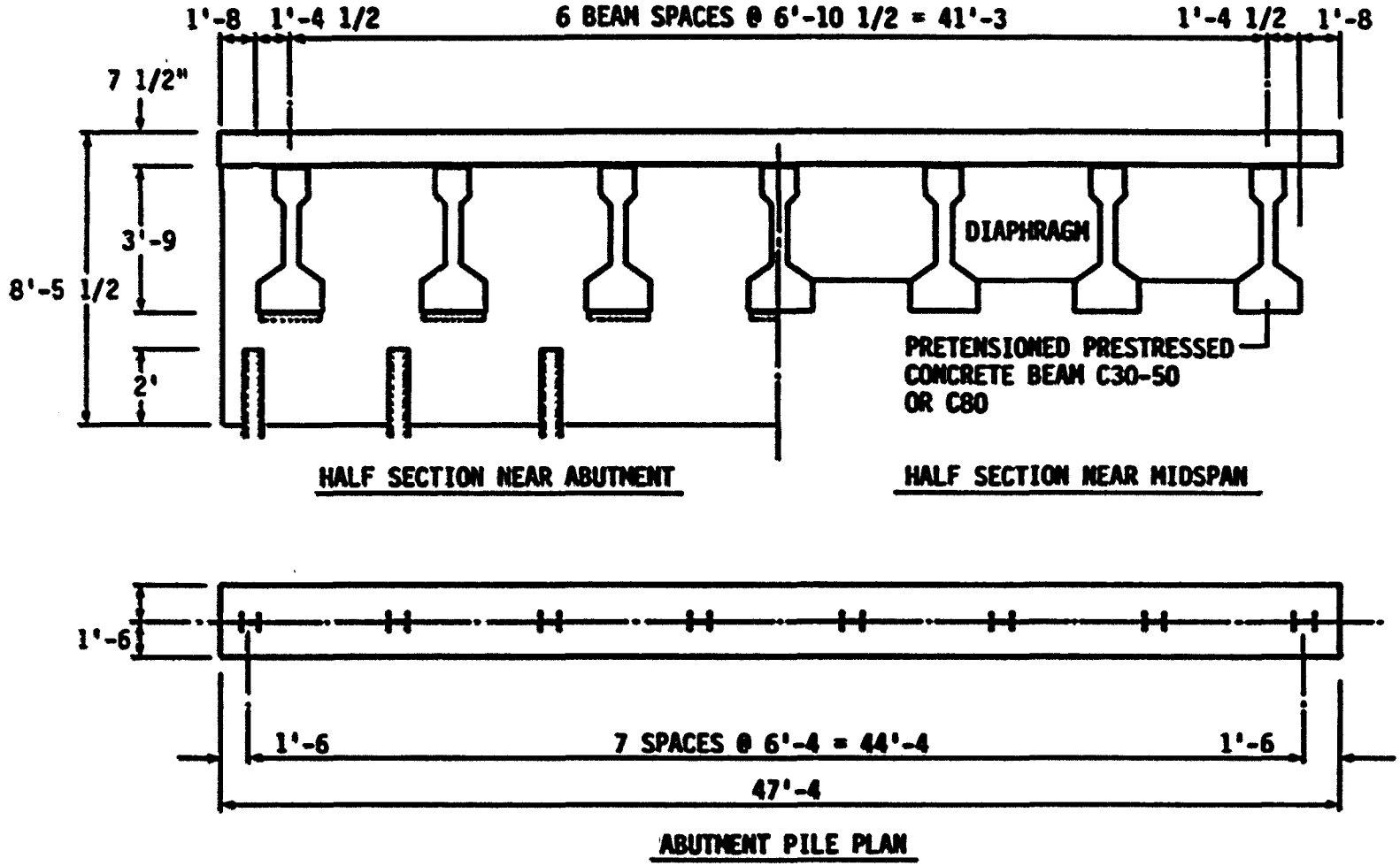

Fig. 48. Transverse section through deck

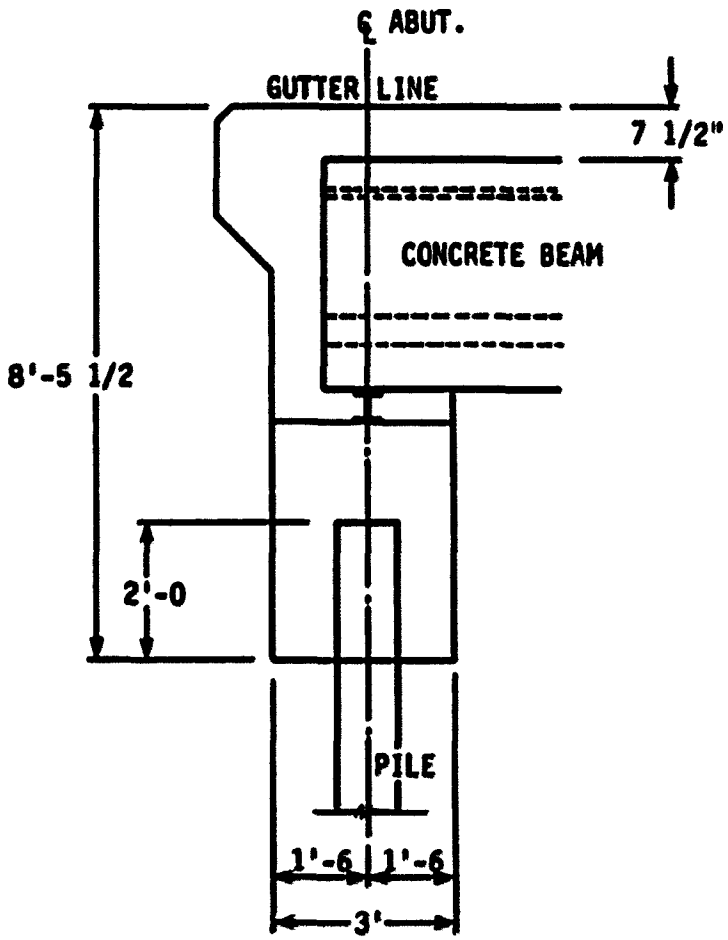

Fig. 49. Section through abutment

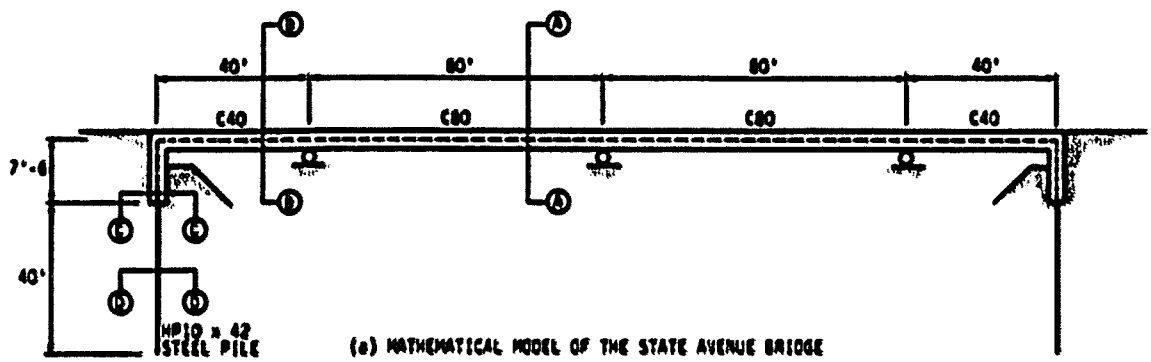

(a) MATHEMATICAL MODEL OF THE STATE AVENUE BRIDGE

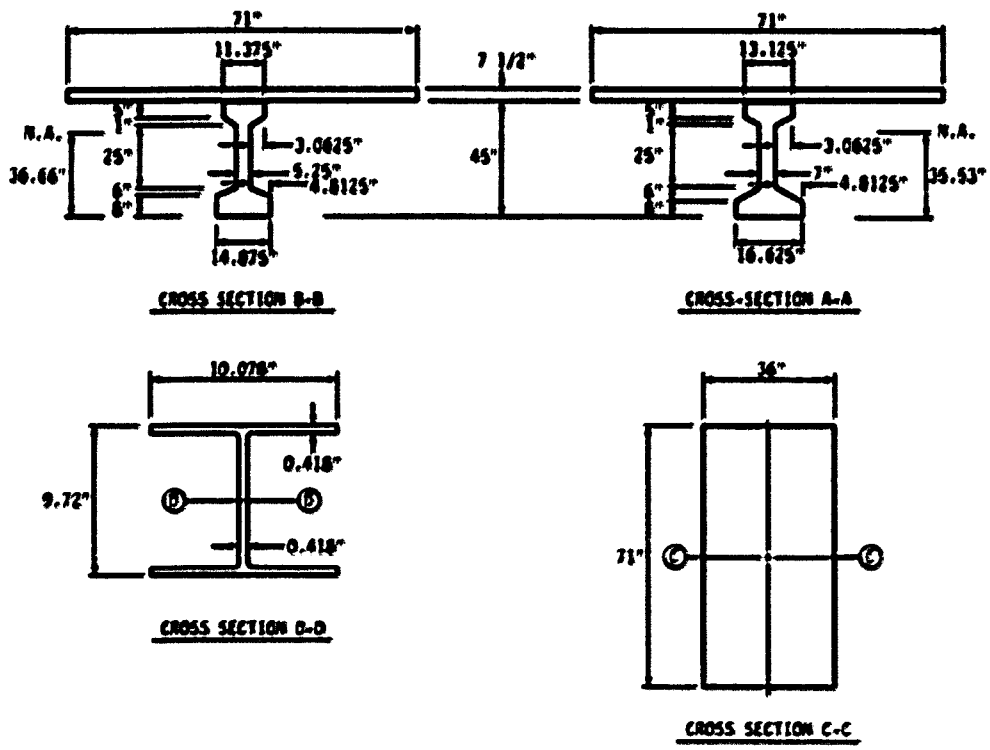

(b) EQUIVALENT CROSS-SECTIONAL PROPERTIES

Fig. 50. Mathematical model of the State Avenue bridge and equivalent cross-sectional properties

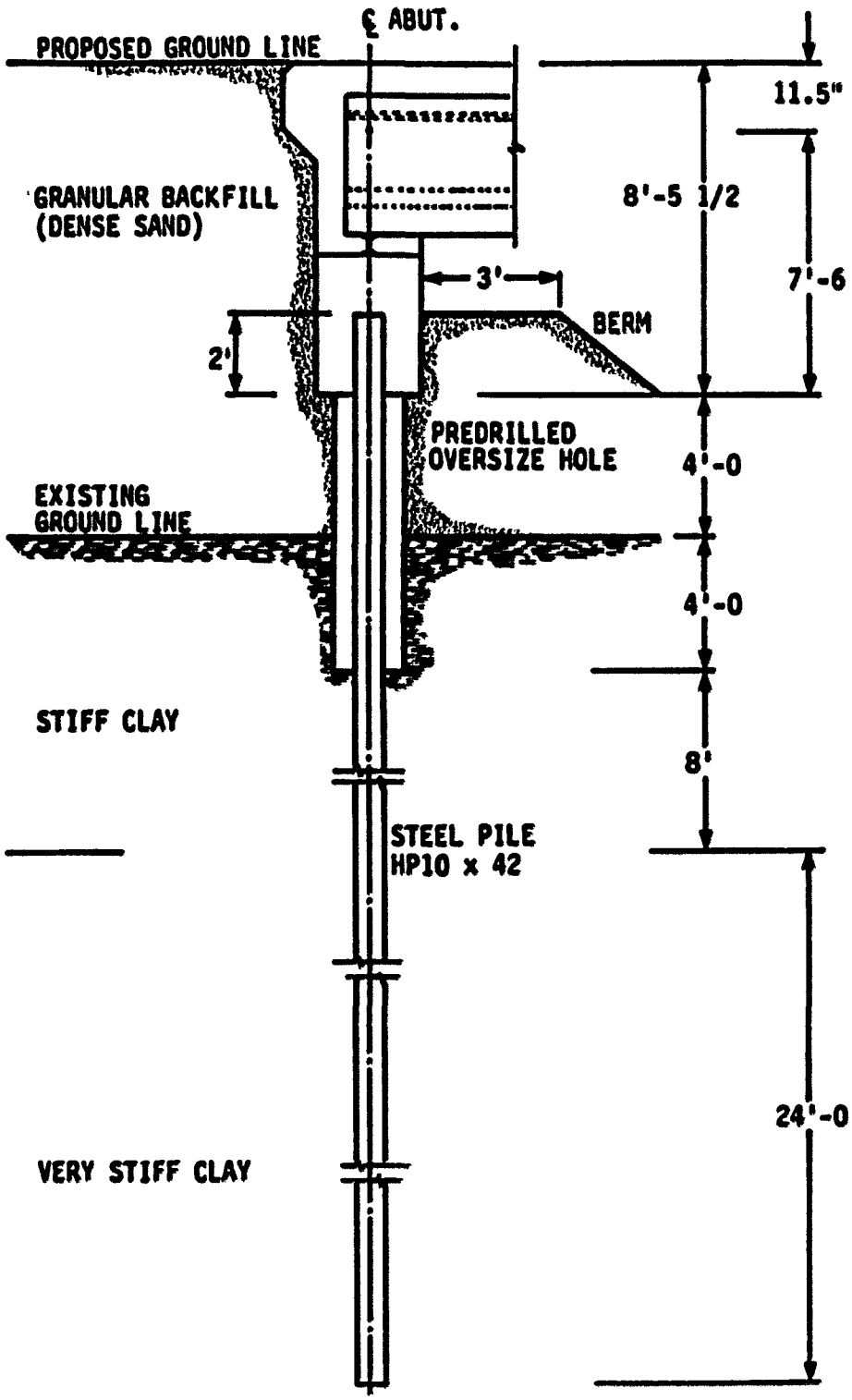

Fig. 51. Section through abutment and soil profile

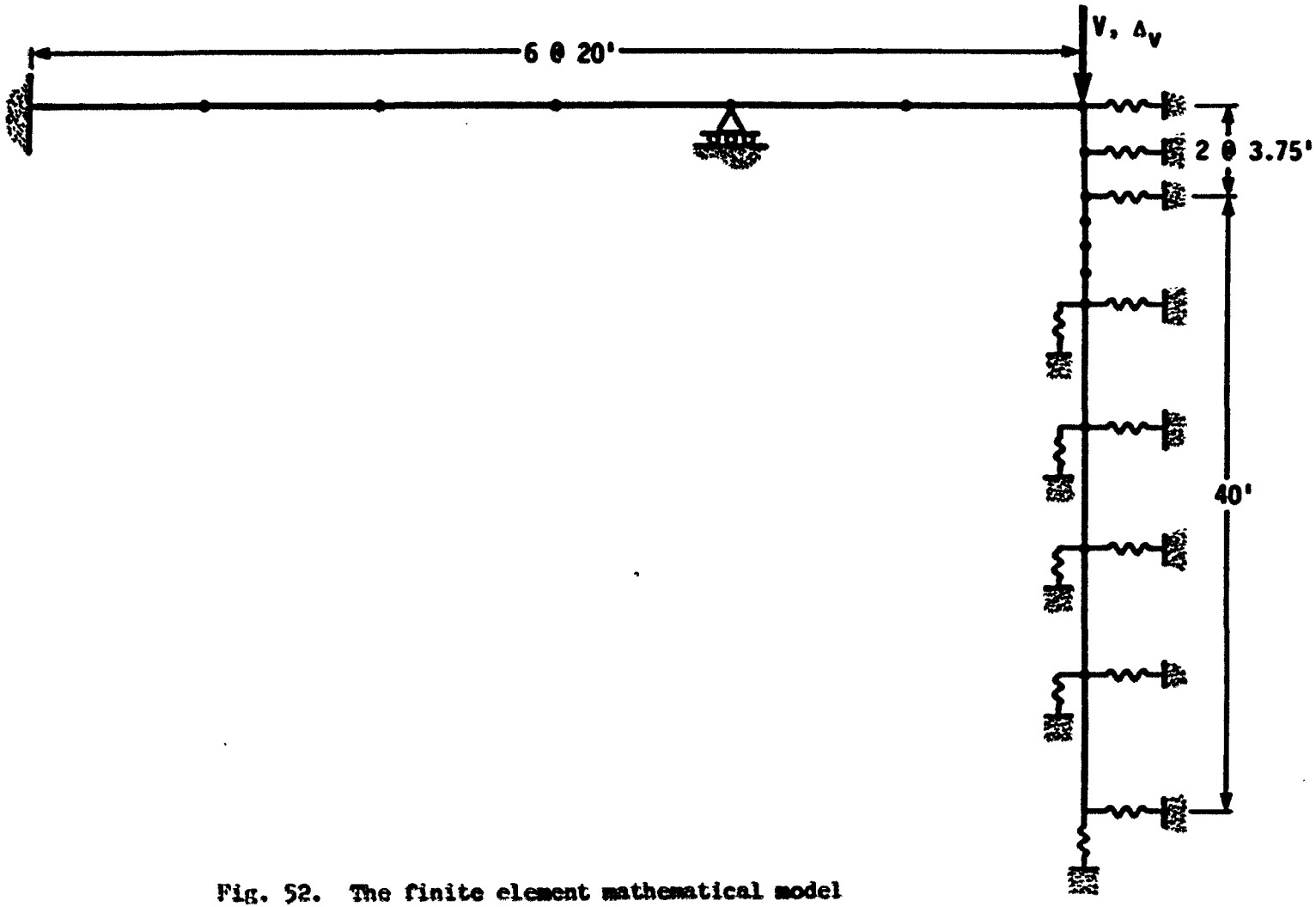

Fig. 52. The finite element mathematical model

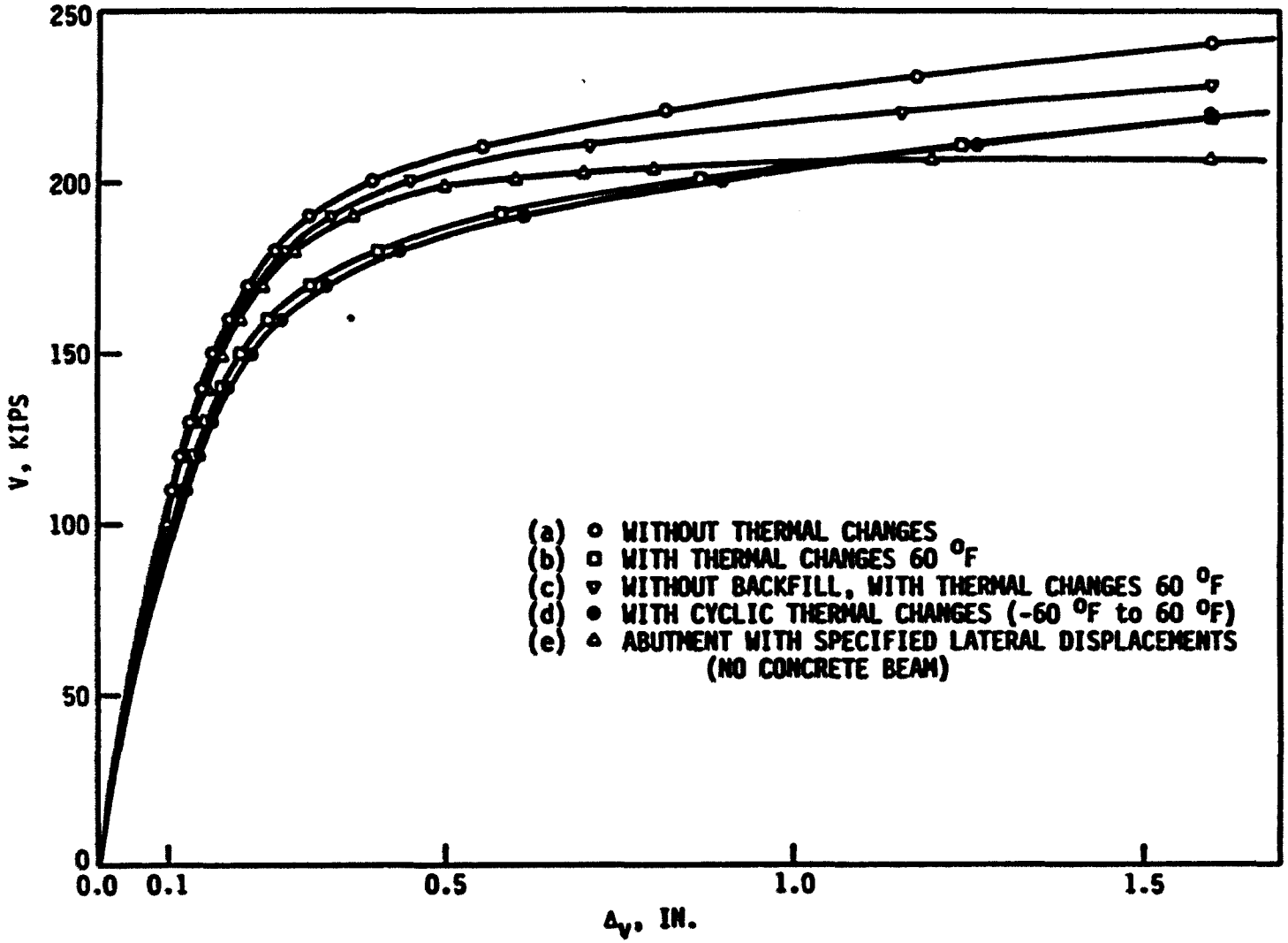

Fig. 53. Vertical load-settlement curves for nonskewed bridge

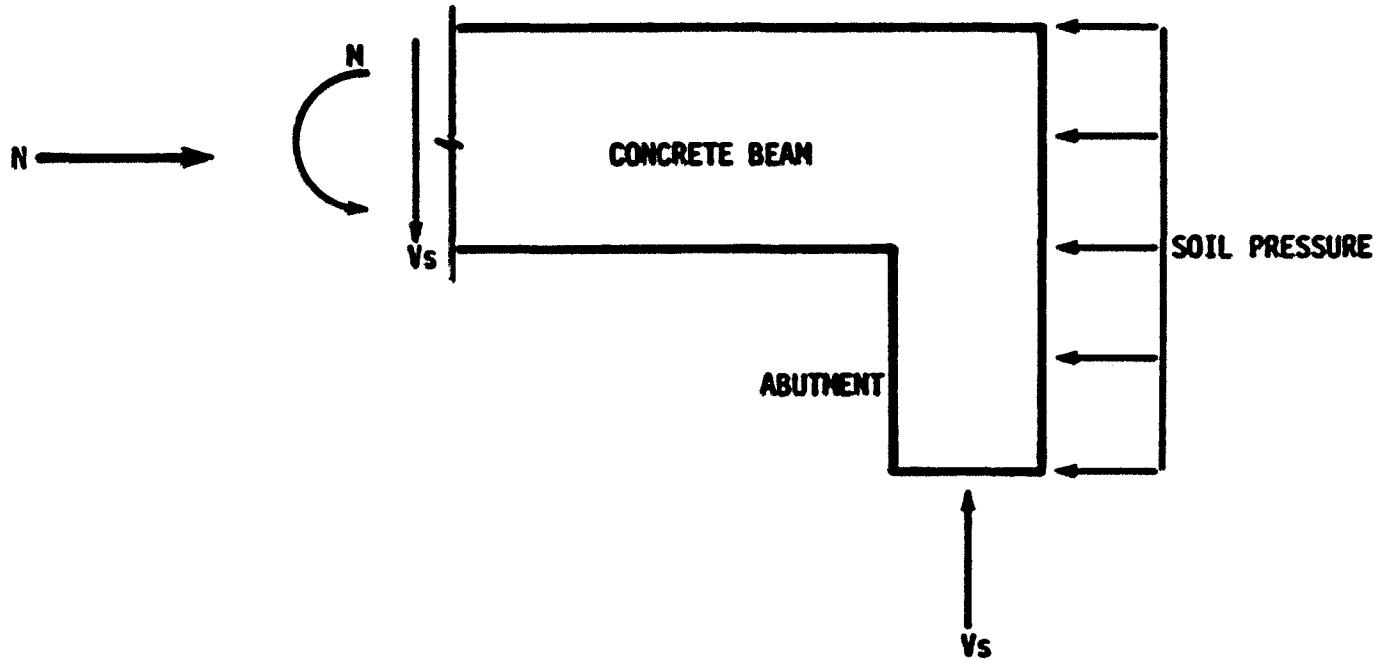

Fig. 54. Free body diagram of the concrete beam and abutment

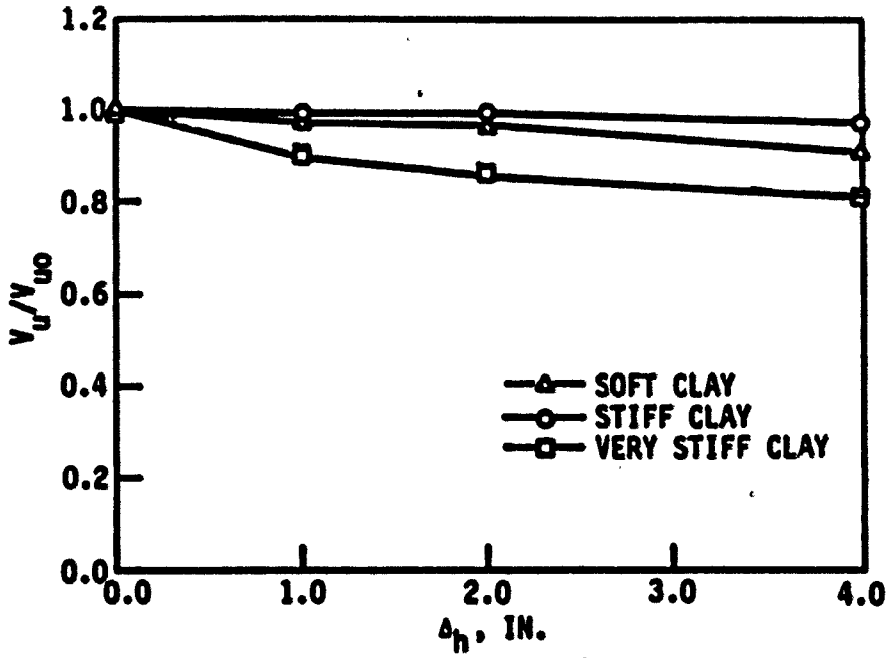

Fig. 55a. Ultimate vertical load ratio (end-bearing piles about strong axis)

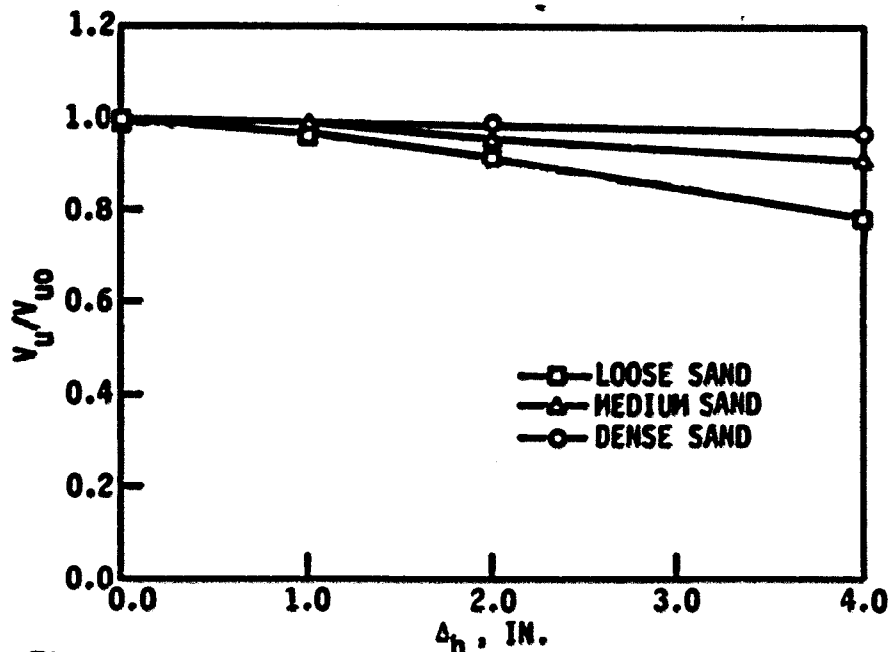

Fig. 55b. Ultimate vertical load ratio (end-bearing piles about strong axis)

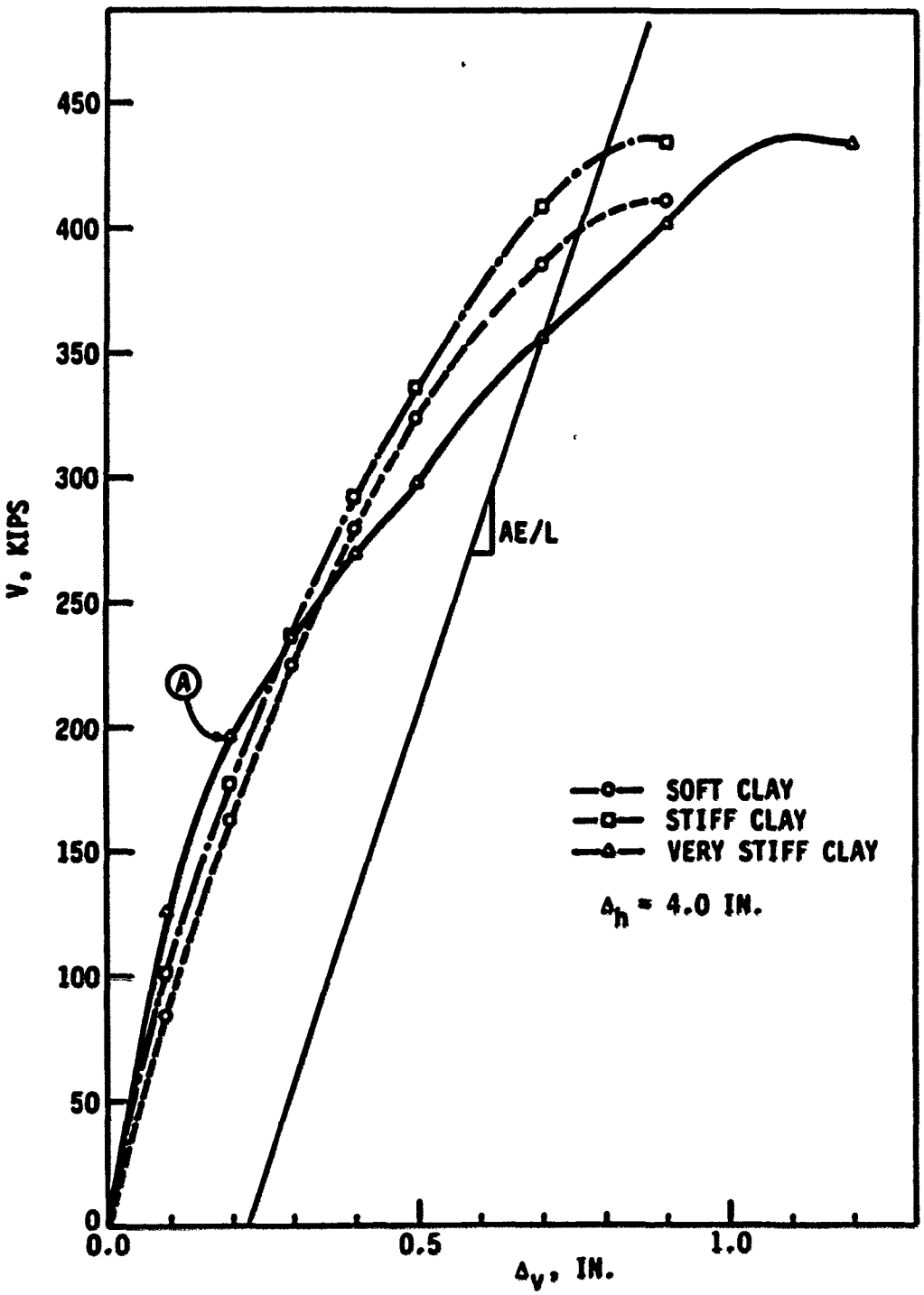

Fig. 56. Load-settlement curve for soft clay, stiff clay, and very stiff clay (end-bearing piles with fixed pile heads bending about strong axis)

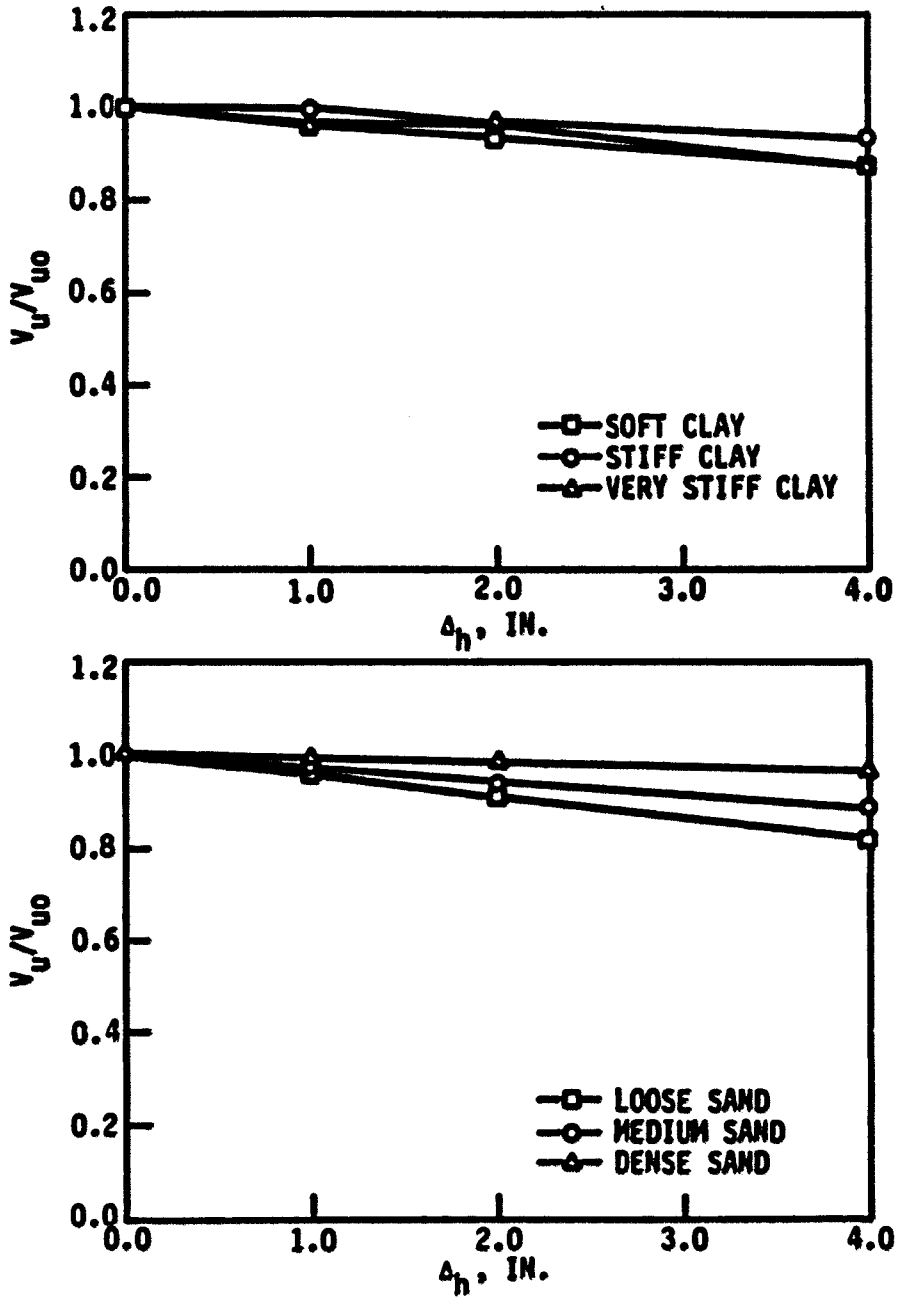

Fig. 57. Ultimate vertical load ratio (end-bearing piles about 45° axis) in Iowa soils

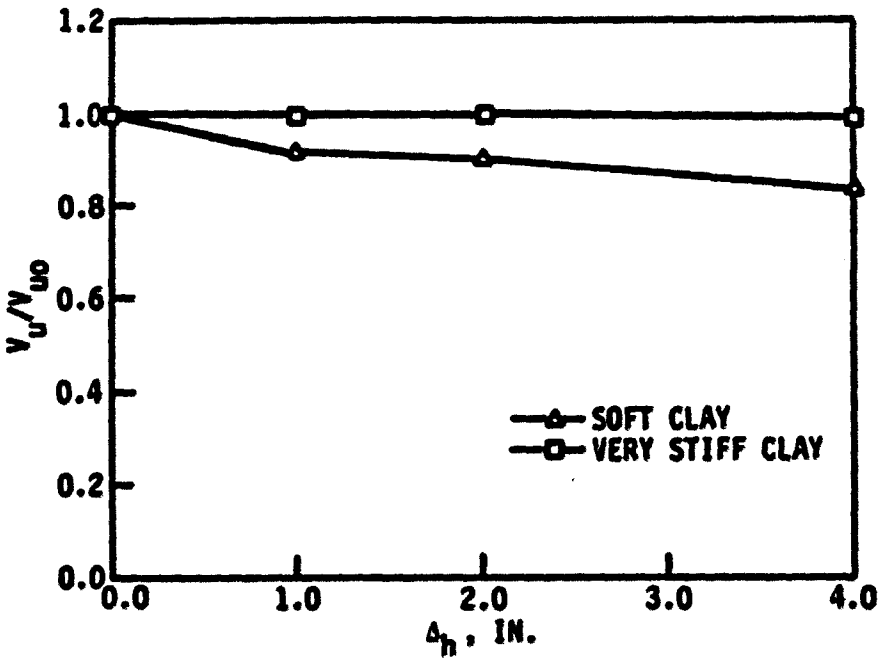

Fig. 58. Ultimate vertical load ratio (end-bearing piles with pinned pile heads bending about the strong axis)

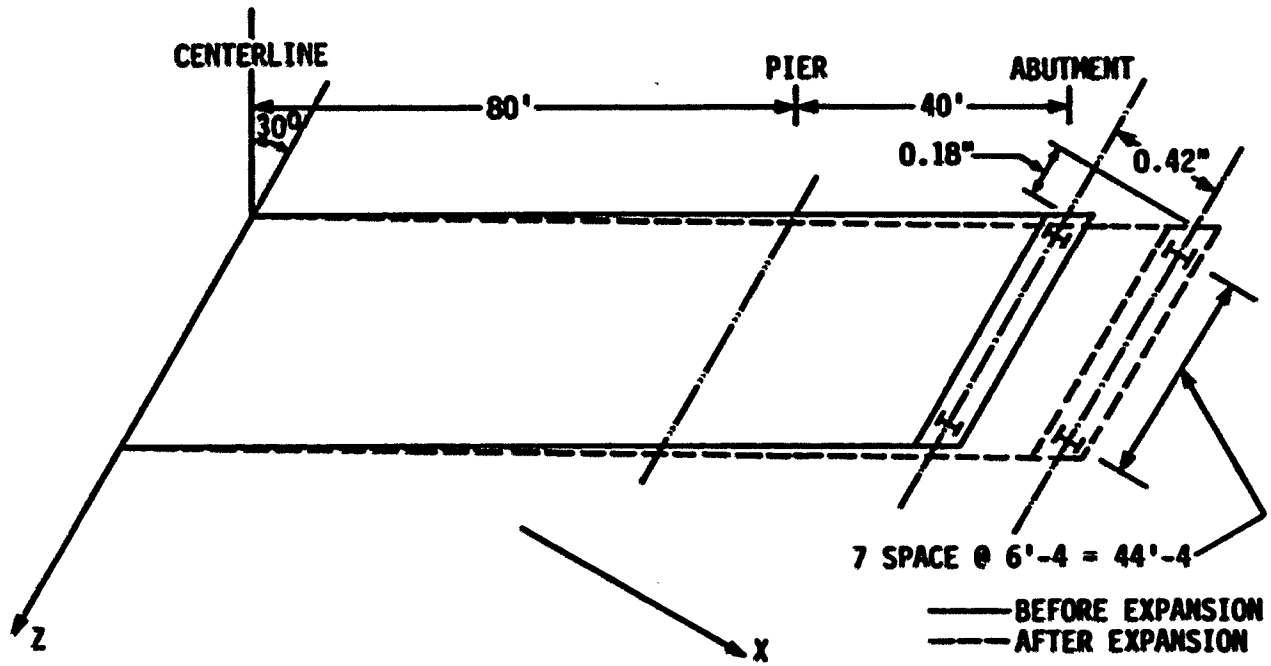

Fig. 59. Plan view of skewed bridge and its global coordinates, before and after thermal expansion (see Fig. 48 for bridge cross section)

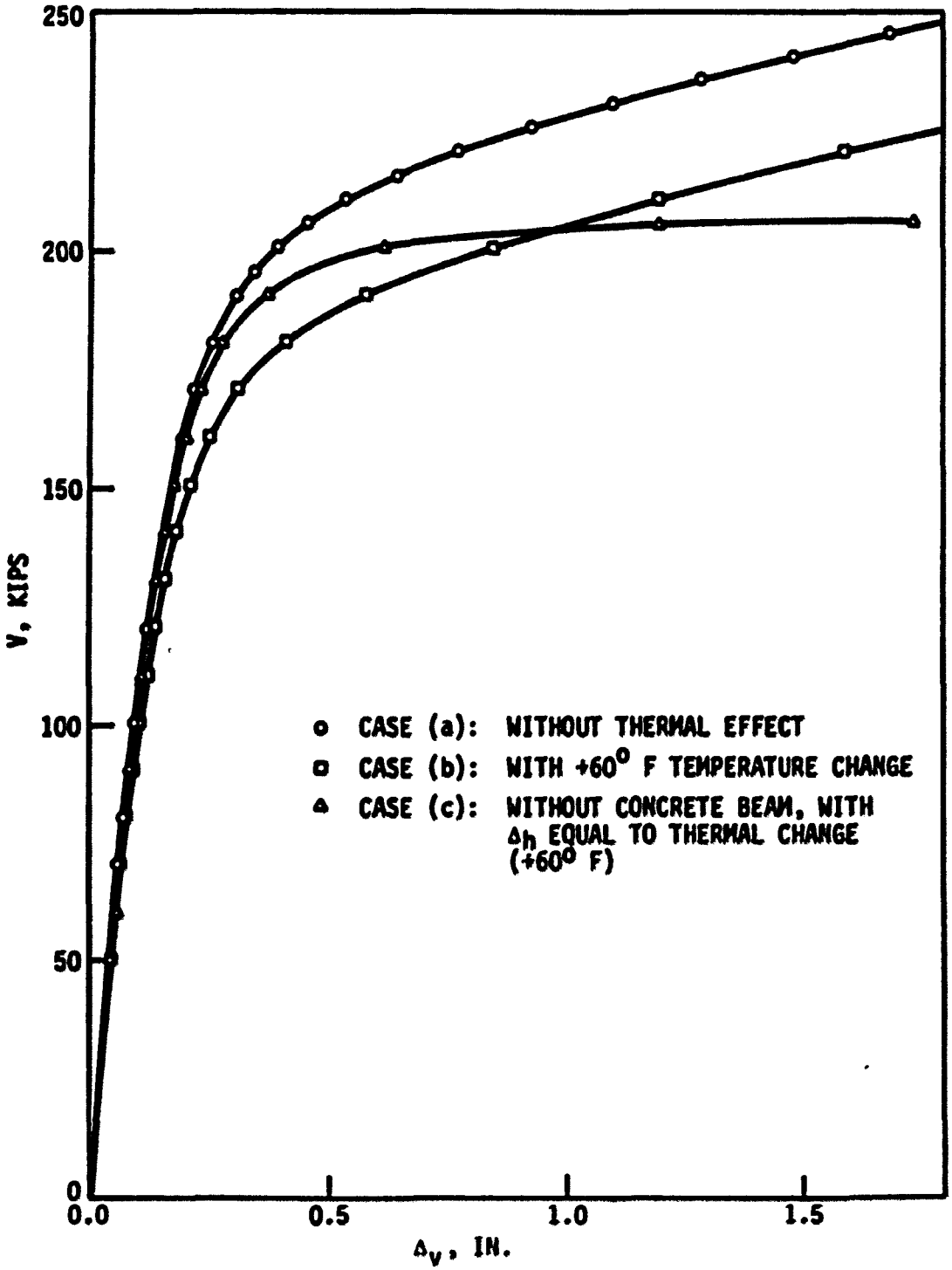

Fig. 60. Load-settlement curve for all pile orientations

9. REFERENCES

1. Lee, H. W. and Sarsam, M. B. Analysis of Integral Abutment Bridges. Final Report, State Study No. 614(70). South Dakota Department of Highways, Pierre, South Dakota, 1973.

2. Emanuel, J. H., et al. An Investigation of Design Criteria for Stresses Induced by Semi-Integral End Bents. Final Report. Department of Civil Engineering, University of Missouri, Rolla, 1972.

3. "Integral, No-Joint Structures and Required Provisions for Movements." Federal Highway Administration, U.S. Department of Transportation, Bulletin T5140.13, January, 1980.

4. Wolde-Tinsae, A. M., Greimann, L. F., and Johnson, B. "Performance of Integral Bridge Abutments." Journal of the International Association for Bridge and Structural Engineering, IABSE PERIODICA 1/1983, February, 1983.

5. Yang, P. S., Wolde-Tinsae, A. M., and Greimann, L. F. Nonlinear Finite Element Study of Piles in Integral Abutment Bridges. Iowa Department of Transportation Project HR-227, ERI Project 1501, ISU-ERI-Ames 83068, September, 1982.

6. Wolde-Tinsae, A. M., Greimann, L. F., and Yang, P. S. Nonlinear Pile Behavior in Integral Abutment Bridges. Iowa DOT Project HR-227. ERI Project 1501, ISU-ERI-Ames 82123, February, 1982.

7. McNulty, J. F. "Thrust Loading on Piles." Journal of the Soil Mechanics and Foundations Division, ASCE, 82, SM2 (April 1956), 1-25.

8. Davisson, M. T. and Gill, H. L. "Laterally Loaded Piles in a Layered Soil System." Journal of the Soil Mechanics and Foundations Division, ASCE, 89, SM3 (May 1963), 63-84.

9. Meyerhof, G. G. "Bearing Capacity and Settlement of Pile Foundations." Journal of the Geotechnical Engineering Division, ASCE, 102, GT3 (March 1976), 195-228.

10. Coyle, H. M. and Reese, L. C. "Load Transfer for Axially Loaded Piles in Clay." Journal of the Soil Mechanics and Foundations Division, ASCE, 92, SM2 (March 2966), 1-26.

11. Reese, L. C. and Matlock, H. "Non-Dimensional Solutions for Laterally Loaded Piles with Soil Modules Assumed Proportional to Depth." Proceedings, 8th Texas Conference on Soil Mechanics and Foundations Engineering, 1956.

12. Davisson, M. T. "Behavior of Flexible Vertical Piles Subjected to Moment, Shear and Axial Load." Ph.D. Dissertation. University of Illinois, Urbana, Illinois, 1960.

13. Poulus, H. G., and Davis, E. H. Pile Foundation Analysis and Design. New York: John Wiley and Sons, Inc., 1980.

14. Valsangkar, A. J., et al. "Generalized Solutions of Axially and Laterally Loaded Piles in Elasto-Plastic Soil." Soils and Foundations, 13, No. 4 (1973), 1-14.

15. Banerjee, P. K. and Davis, T. G. "The Behavior of Axially and Laterally Loaded Single Piles Embedded in Nonhomogeneous Soils." Geotechnique, 28, No. 2 (1978), 309-326.

16. Butterfield, R. and Banerjee, P. K. "Analysis of Axially Loaded Piles and Pile Groups." Geotechnique, 21, No. 1 (1971), 43-60.

17. Mahdav, M. R., Rao, N. S. V. K., and Madhavan, K. "Laterally Loaded Pile in Elasto-Plastic Soil." Soils and Foundations, 11, No. 2 (1971), 1-15.

18. Kubo, J. "Experimental Study of the Behavior of Laterally Loaded Piles." Proceedings, 6th International Conference on Soil Mechanics and Foundations Engineering, 2 (1965), 275-279.

19. Welch, R. C. and Reese, L. C. Lateral Load Behavior of Drilled Shafts. Research Report 89-10. Center for Highway Research, The University of Texas at Austin, May 1972.

20. Matlock, H. "Correlations for Design of Laterally Loaded Piles in Soft Clay." Proceedings, 2nd Offshore Technology Conference, Houston, Texas, 1970.

21. Reese, L. C. and Welch, R. C. "Lateral Loading of Deep Foundations in Stiff Clay." Journal of the Geotechnical Engineering Division, ASCE, 101, GT7 (July 1975), 633-649.

22. Reese, L. C., Cox, W. R., and Koop, F. D. "Analysis of Laterally Loaded Piles in Sand." Proceedings, 6th Offshore Technology Conference, Houston, Texas, 1974.

23. Seed, H. B. and Reese, L. C. "The Action of Soft Clay Along Friction Piles." Transactions, ASCE, 122 (1957), 731-756.

24. D'Appolonia, E. and Romualdi, J. P. "Load Transfer in End-Bearing Steel H Piles." Journal of the Soil Mechanics and Foundations Division, ASCE, 95, SM1 (January 1969), 189-207.

25. Mattes, N. S. and Poulos, H. G. "Settlement of Single Compressible Pile." Journal of the Soil Mechanics and Foundations Division, ASCE, 95, SM1 (January 2969), 189-207.

26. Banerjee, P. K. and Davis, T. G. "Analysis of Pile Groups Embedded in Gibson Soil." Proceedings, 9th International Conference on Soil Mechanics and Foundations Engineering, 1, 1977, 381-386.

27. Poulos, H. G. "Behavior of Laterally Loaded Piles: I - Single Piles." Journal of the Soil Mechanics and Foundations Division, ASCE, 97, SM5 (May 1971), 711-731.

28. Poulos, H. G. "Behavior of Laterally Loaded Piles: III - Socketed Piles." Journal of the Soil Mechanics and Foundations Division, ASCE, 98, SM4 (April 1972), 341-360.

29. Vijayvergiya, V. N. "Load-Movement Characteristics of Piles." Proceedings, Ports '77 Conference, ASCE, Long Beach, California, March, 1971.

30. Greimann, L. F., Yang, P.-S., Edmunds, S. K., and Wolde-Tinsae, A. M. Design of Piles for Integral Abutment Bridges. Iowa Department of Transportation Project HR-252, ERI Project 1619, ISU-ERI-Ames 84286, August, 1984.

31. Alizadeh, M. and Davisson, M. T. "Lateral Load Tests on Piles - Arkansas River Project." Journal of the Soil Mechanics and Foundations Division, ASCE, 96, SM5 (September 1970), 1583-1604.

32. Bhushan, K., Haley, S. C., and Fong, E. T. "Lateral Load Tests on Drilled Piers in Stiff Clays." Journal of the Geotechnical Engineering Division, ASCE, 105, GT8 (August 1979), 969-985.

33. Reese, L. C., Touma, F. T., and O'Neill, M. W. "Behavior of Drilled Piers under Axial Loading." Journal of the Geotechnical Engineering Division, ASCE, 102, GT5 (May 1976), 453-510.

34. Mohan, D., Jain, G. S., and Kumar. V. "Load Bearing Capacity of Piles." Geotechnique, 13, No. 1 (1963), 76-86.

35. Jorgenson, J. L. Behavior of Abutment Piles in an Integral Abutment Bridges. Final Report. Engineering Experiment Station, North Dakota State University, Fargo, North Dakota, November, 1981.

36. Desai, C. S. and Wu, T. H. "A General Function for Stress-Strain Curves." in Numerical Methods in Geomechanics, ASCE, 1976.

37. Duncan, J. M. and Chang, C.-Y. "Nonlinear Analysis of Stress and Strain in Soils." Journal of the Soil Mechanics and Foundations Division, ASCE, 96, SM5 (September 1970), 1629-1653.

38. Finn, W. D., Lee, K. W. and Martin, G. R. "An Effective Stress Model for Liquefaction." Journal of the Geotechnical Engineering Division, ASCE, 103, GT6 (June 1977), 517-533.

39. Martin, P. P. "Nonlinear Methods for Dynamics Analysis of Ground Responses." Ph.D. Dissertation. University of California at Berkeley, 1975.

40. Streeter, V. L., Wylie, E. B. and Richart, F. E., Jr. "Soil Motions Computations by Characteristic Methods." Journal of the Geotechnical Engineering Division, ASCE, 100, GT3 (March 1974), 247-263.

41. Pyke, R. "Nonlinear Soil Models for Irregular Cyclic Loadings." Journal of the Geotechnical Engineering Division, ASCE, 105, GT6 (June 1977), 715-726.

42. Ha, H. B. and O'Neill, M. W. Field Study of Pile Group Action. Final Report. Federal Highway Administration Project DOT-FH-11-9626, FCP-34H2-032, March 1981.

43. Bathe, K. J. and Bolourchi, S. "Large Displacement Analysis of Three-Dimensional Beam Structures." International Journal for Numerical Methods in Engineering, 14 (1979), 961-986.

44. Argyris, J. H., Dunne, P. C., and Scharpf, D. W. "On Large Displacement-Small Strain Analysis of Structures with Rotational Degree of Freedom." Computer Methods in Applied Mechanics and Engineering, 14 (1978), 401-451.

45. Besseling, J. F. "Nonlinear Analysis of Structures by the Finite Element Method as a Supplement to a Linear Analysis." Computer Methods in Applied Mechanics and Engineering, 3 (1974), 173-184.

46. Oden, J. T. and Neighbors, A. "Network-Topological Formulation of Analyses of Geometrically and Materially Nonlinear Space Frame." Space Structures. New York: John Wiley & Sons, Inc., 1967.

47. Johnson, D. and Brotton, D. M. "A Finite Deflection Analysis for Space Structures." Space Structures. New York: John Wiley & Sons, Inc., 1967.

48. Belytschko, T. and Hsieh, B. J. "Nonlinear Transient Finite Element Analysis with Convected Co-ordinates." International Journal of Numerical Methods in Engineering, 7 (1973), 255-271.

49. Belytschko, T., Schwer, L., and Klein, M. J. "Large Displacement, Transient Analysis of Space Frames." International Journal of Numerical Methods in Engineering, 11 (1977), 65-84.

50. Orean, C. "Tangent Stiffness in Plane Frames." Journal of the Structural Division, ASCE, 99, ST6 (June 1973), 973-985.

51. Orean, C. "Tangent Stiffness in Space Frames." Journal of the Structural Division, ASCE, 99, ST6 (June 1973), 987-1001.

52. Rajasekaran, S. and Murray, D. W. "Finite Element Solution of Inelastic Beam Equations." Journal of the Structural Division, ASCE, 99, ST6 (June 1973), 1025-1041.

53. Bavant, Z. P. and Nimeri, M. E. "Large-Deflection Spatial Buckling of Thin-Walled Beams and Frames." Journal of the Engineering Mechanics Division, ASCE, 99, EM6 (December 1973), 1259-1281.

54. Murray, D. W. and Wilson, E. L. "Finite Element Large Deflection Analysis of Plates." Journal of the Engineering Mechanics Division, ASCE, 95, EM1 (February 1969), 143-165.

55. Yen, J. T., Clough, R. W., and Yamamoto, Y. Advances in Computational Methods in Structural Mechanics and Design. Huntsville, Alabama: UAH (The University of Alabama in Huntsville) Press, 1972.

56. Gallagher, R. H., Yamada, Y., and Oden, J. T. Recent Advances in Matrix Methods of Structural Analysis and Design. Huntsville, Alabama: UAH Press, 1969.

57. Wunderlich, W., Stein, E., and Bathe, K. J. Nonlinear Finite Element Analysis in Structural Mechanics. New York: Springer-Verlag, 1981.

58. Belytschko, T., Osias, J. R., and Marcel, P. V. Finite Element Analysis of Transient Nonlinear Structural Behavior. New York: The American Society of Mechanical Engineers, 1975.

59. Cook, R. D. Concepts and Applications of Finite Element Analysis. 2nd edition. New York: John Wiley & Sons, Inc., 1981.

60. Zienkiewicz, O. C. The Finite Element Method. 3rd edition. New York: McGraw-Hill Book Co., 1977.

61. Przemieniecki, J. S. Theory of Matrix Structural Analysis. New York: McGraw-Hill Book Co., 1968.

62. Beaufait, F. W., Rowan, W. H., Jr., Hoadley, P. G., and Hackett, R. M. Computer Methods of Structural Analysis. 3rd edition. Nashville, Tennessee: Department of Civil Engineering, Vanderbilt University, 1975.

63. Kohnke, P. C. Engineering Analysis System Theoretical Manual. Houston: Swanson Analysis System, Inc., 1984.

64. Argyris, J. H., Hilpert, O., Malejannakis, G. A., and Scharpf, D. W. "On the Geometrical Stiffness of a Beam in Space." Computer Methods in Applied Mechanics and Engineering, 20 (1979), 105-131.

65. Desai, C. S. and Abel, J. F. Introduction to the Finite Element Method. New York: Van Nostrand Reinhold Co., 1972.

66. Parker, F. Jr. and Reese, L. C. Experimental and Analytical Behavior of Single Piles in Sand Under Lateral and Axial Loading. Research Report 117-2. Center of Highway Research, The University of Texas at Austin, November 1970.

67. Desai, C. S. and Christian, J. T. Numerical Methods in Geotechnical Engineering. New York: McGraw-Hill Book Co., 1977.

68. Heténgi, M. Beam on Elastic Foundation. Ann Arbor, Michigan: The University of Michican Press, 1946.

69. Timoshenko, S. P. and Gere, J. M. Theory of Elasticity Stability. 2nd edition. New York: McGraw-Hill Book Co., 1961.

70. Beedle, L. S. Plastic Design of Steel Frame. 2nd edition. New York: John Wiley & Sons, Inc., 1961.

71. Commentary on Plastic Design in Steel. Manual of Engineering Practice, No. 41. New York: ASCE, 1961.

72. Neal, B. G. The Plastic Methods of Structural Analysis. 2nd edition. New York: John Wiley & Sons, Inc., 1963.

73. Williams, F. W. "An Approach to the Nonlinear Behavior of the Members of a Rigid Jointed Plane Framework with Finite Deflections." Quarterly Journal of Mechanics and Applied Mathematics, 17 (1964), 451-469.

74. Chajes, A. Principles of Structural Stability Theory. Englewood Cliffs: Prentice-Hall, Inc., 1974.

75. Mallet, R. H. and Berke, L. Automated Method for the Large Deflection and Instability Analysis of Three-Dimensional Truss and Frame Assemblies. AFFDL-TR-66-102, December, 1966.

76. Dupuis, G. A., Hibbitt, H. D., McNamara, S. F., and Marcel, P. V. "Nonlinear Material and Geometric Behavior of Shell Structure." Computer and Structure, 1 (1971), 223-239.

77. Gjelsvik, A. and Bodner, S. R. "The Energy Criterion and Snap Buckling of Arches." Journal of the Engineering Mechanics Division, ASCE, 88, EM5 (May 1962), 87-134.

78. Bathe, K. J. ADINA - A Finite Element Program for Automatic Dynamic Incremental Nonlinear Analysis. Report 82442-1. Accoustics and Vibration Laboratory, Mechanical Engineering Department, Massachusetts Institute of Technology, 1977.

79. Edmunds, S. K. "Design of Piles for Integral Abutment Bridges." Master's Thesis. Iowa State University, Ames, Iowa, 1984.

80. D'Appolonia, E. and Romualdi, J. D. "Load Transfer in End-Bearing Steel H-Pile." Journal of the Soil Mechanics and Foundations Division, ASCE, 89, SM2 (March 1963), 1-25.

81. Bhushan, K., Haley, S. C. and Fong, P. T. "Lateral Load Tests on Drilled Piers in Stiff Clays." Journal of the Geotechnical Engineering Division, ASCE, 105, GT8 (August 1979), 969-985.

82. [illegible], M. "[illegible] on Instrumented Timber Piles." Performance of Deep Foundations, ASTM STP444. Philadelphia, PA: American Society for Testing and Materials, 1969, pp. 379-[illegible].

83. Bodig, J. B. and Jayne, R. A. Mechanics of Wood and Wood Composites. New York: Van Nostrand Reinhold Co., 1982.

84. Stevens, J. B., Holloway, D. M., Moriwaki, Y., and Demsky, E. C. "Pile Group Response to Axial and Lateral Loading." Symposium on Deep Foundations, Ed. by F. Fuller. New York: ASCE, 1979, pp. 356-419.

85. Peck, R. B., Hanson, W. E., and Thornburn, T. H. Foundation Engineering. New York: John Wiley & Sons, Inc., 1974.

10. ACKNOWLEDGEMENTS

The author wishes to express his deep appreciation to Dr. Lowell Greimann for his supervision, patience and support throughout the research and writing of this thesis. In addition, the author wishes to express his appreciation to Dr. A. M. Wolde-Tinsae for his invaluable support of this research. The author would also like to thank Steve K. Edmunds and Bruce Johnson for their considerable assistance throughout this research, and Dr. Wayne Klaiber, Dr. Fred Graham, Dr. William Riley, and Dr. Mardith Thomas for serving on my graduate committee.

This research would not have been possible without generous support from the Engineering Research Institute of Iowa State University and Iowa Department of Transportation. Their financial support of the author and for the extensive computing costs involved in this research is gratefully acknowledged.

Last but not least, the author expresses his deep sense of gratitude to his parents and his wife, who made the author's higher education possible.

11. APPENDIX A: QUESTIONNAIRE FOR BRIDGES WITH INTEGRAL ABUTMENTS AND SUMMARY OF RESPONSES

Part 1. Questionnaire for Bridges with Integral Abutments

1. Do you use bridge designs with integral abutments and without expansion devices, similar to the following sketch? yes_____ no_____
   Primary (one) reason why, or why not:_____
   If the answer is no, skip the remainder of the questionnaire and please return.

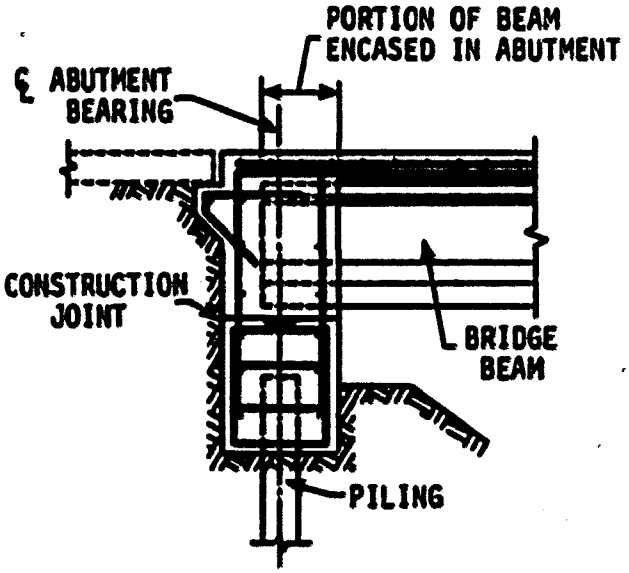

2. With what type of bridges do you use integral abutments?
   steel_____ prestressed concrete_____ poured-in-place concrete_____

3. What are your maximum length limits (in feet)?

	0°	0° - 15°	15° - 30°	30°< skew
steel				
prstressed concrete				
poured-in-place concrete				

4. What limits, if any, do you place on the piles? (bearing vs. friction, soil type etc.)
   steel pile _____
   timber pile _____
   concrete pile _____

5. What type of structural assumption is made for the end of the girder?
   pinned (moment equal zero) _____
   fixed (rotation equal zero) _____
   partially restrained _____ {restrained by pile _____ / restrained by soil on abut. _____}
   other assumptions _____

6. What type of structural assumption is made for the top of the pile?

   pinned (moment equal zero) ___ Is the joint detailed as a pin?
   fixed (rotation equal zero) ___ ____
   partially restrained ___ {restrained by girder ___ / restrained by soil on abut. ___}
   other assumptions _____

7. What loads do you include when calculating pile stress?

   thermal ___ temperature range _____
   shrinkage ___
   soil pressure on abutment face ___

8. How is bending accounted for in the pile?

   Neglect or assume bending stresses do not affect pile performance ___
   Assume location of pile inflection point and analyze pile as bending member ___
   Reduce bending by prebored hole ___
   Other _____

9. What type of backfill material do you specify on the backside of the abutment?

   _____
   _____
   _____

10. Does the approach pavement rest directly on the abutment?

    yes ___ no ___

11. Briefly evaluate the performance of integral abutment bridges in your state. (Compare to bridges with expansion devices.)

Construction
relative cost more ___ same ___ less ___
special problems _____
_____

Maintenance
relative costs more ___ same ___ less ___
special problems _____
_____

Please return to: Lowell Greimann
420 Town Engineering
Iowa State University
Ames, Iowa 50011

Part 2. Summary of Responses to Questions 1, 2, 3, 5, 6, and 7.

		Steel			Concrete			Pre
			Length			Length		
State	Reason	Use	≤30"	>30"	Use	≤30"	>30"	Use
AL	Cost	Y	300	---	Y	---	115	Y
AZ	Maint	Y	253	N	Y	330	N	Y
CA	Cost	Y	---	---	Y	320	320	Y
CO	Cost	Y	200	---	Y	400	---	Y
CT	---	Y	200	---	N	---	---	N
GA	El. Jt	Y	300	---	Y	300	---	Y
IA	Cost	N	---	---	Y	265	---	Y
ID	Cost	Y	200	N	Y	400	N	Y
IN	Cost	N	---	---	Y	---	100	N
KS	El. Jt	Y	300	300	Y	350	350	Y
KY	Cost	N	N	N	Y	300	N	Y
MO	El. Jt	Y	400	---	Y	400	400	Y
MT	Cost	Y	300	N	Y	100	N	Y
ND	Maint	Y	350	---	Y	350	---	Y
NE	El. Jt	Y	300	---	N	300	---	Y
NM	El. Jt	Y	---	---	Y	---	---	Y
NY	Cost	Y	305	---	---	---	---	---
OH	Cost	Y	300	300	Y	300	300	Y
OK	---	Y	200	N	Y	200	N	Y
OR	El. Jt	Y	N	N	Y	350	300	Y
SD	Cost	Y	320	---	Y	450	---	Y

Use	Prestressed Length ≤30'	Prestressed Length >30'	Girder End Fixity	Pile Top Fixity	Pile Loads Thermal	Pile Loads Shrinkage	Pile Loads Soil Pressure
Y	416	10[illegible]	Pin	Pin	Y	N	Y
Y	404	N	Pin	Pin	Y	Y	Y
Y	230	230	Pin	P. Res	N	N	N
Y	400	---	Pin	Pin	N	N	Y
N	---	---	Pin	Fix	Y	N	N
Y	300	---	Pin	---	N	N	N
Y	265	---	Pin	Fix	Y	N	N
Y	400	N	Pin	Pin	N	N	N
N	---	---	---	---	N	N	N
Y	300	300	Pin	Pin	Y	Y	N
Y	300	N	Fix	Fix	Y	N	Y
Y	500	500	Pin	Pin	N	N	N
Y	300	N	Pin	Pin	N	N	Y
Y	450	---	Pin	Fix	N	N	N
Y	N	---	Pin	Pin	Y	N	N
Y	---	---	P. Res.	P. Res.	Y	Y	Y
---	---	---	Pin	---	Y	N	N
Y	300	300	Pin	Pin	N	N	N
Y	200	N	P. Res.	P. Res.	N	N	N
Y	350	300	Pin	Pin	N	N	N
Y	450	---	Pin	Fix	N	N	N

Part 2. (Continued)

		Steel			Concrete			Prest	
			Length			Length			
State	Reason	Use	≤30*	>30*	Use	≤30*	>30*	Use	≤
TN	El. Jt	Y	400	400	Y	800	800	Y	8
UT	El. Jt	Y	300	250	N	---	---	Y	3
VA	Simp.	Y	242	---	N	---	---	Y	4
VT	Cost	Y	150	100	N	N	N	N	N
WA	Cost	N	---	---	Y	350	---	N	-
WS	Cost	Y	200	200	Y	300	N	Y	3
WY	Simp.	Y	300	300	Y	500	500	Y	5
R15	El. Jt	N	N	N	Y	270	160	Y	3

Y Yes
N No
--- No Response
* Bridge skew in degrees

Use	Prestressed Length ≤30*	Prestressed Length >30*	Girder End Fixity	Pile Top Fixity	Thermal	Pile Loads Shrinkage	Pile Loads Soil Pressure
Y	800	800	Pin	Pin	N	N	N
Y	300	250	Pin	Pin	N	N	N
Y	454	---	Pin	Pin	N	N	Y
N	N	N	P. Res.	P. Res.	Y	N	N
N	---	---	Pin	Pin	N	N	N
Y	300	300	P. Res.	Fix	N	N	N
Y	500	500	Pin	Pin	N	N	N
Y	300	240	P. Res.	Pin	N	N	N

Part 2. Summary of Responses to Questions 8, 9, 10, and 11.

State	Neglect	Pile Bending	Prebore	Backfill	Approach Pvmt. on Abutment
		Infl. Pt.			
AL	Y	Y	N	Gran.	N
AZ	Y	N	N	Cohes.	Y
CA	Y	N	N	Perv.	Y
CO	Y	N	Y	Gran.	Y
CT	Y	N	N	Perv.	Y
GA	Y	N	N	Rd. Fill	Y
IA	N	N	Y	Gran.	Y
ID	Y	N	N	Rd. Fill	Y
IN	Y	N	N	Gran.	Y
KS	Y	N	N	Rd. Fill	Y
KY	N	Y	Y	Gran.	N
MO	Y	N	N	Rd. Fill	Y
MT	Y	N	N	Gran.	Y
ND	Y	N	N	Gran.	Y
NE	Y	N	N	Rd. Fill	Y
NM	N	Y	N	Rd. Fill	Y-N
NY	Y	N	N	Gran.	Y
OH	Y	N	N	Gran.	Y
OK	Y	N	N	---	Y
OR	Y	N	N	Gran.	Y
SD	N	N	Y	Gran.	Y

Approach Pvmt. on Abutment	Construction Cost			Maintenance Cost		
	More	Same	Less	More	Same	Less
N	N	N	Y	N	N	Y
Y	N	N	Y	N	N	Y
Y	N	N	Y	N	N	Y
Y	N	N	Y	N	N	Y
Y	N	N	Y	N	N	Y
Y	N	N	Y	N	N	Y
Y	N	N	Y	N	N	Y
Y	N	N	Y	N	N	Y
Y	N	N	Y	N	N	Y
Y	N	N	Y	N	N	Y
N	N	N	Y	N	N	Y
Y	N	N	Y	N	N	Y
Y	N	N	Y	N	N	Y
Y	N	N	Y	N	N	Y
Y	N	Y	N	N	N	Y
Y-N	N	N	N	N	N	N
Y	N	N	Y	N	N	Y
Y	N	N	Y	N	N	Y
Y	N	N	Y	N	N	Y
Y	N	N	Y	N	N	Y
Y	N	N	Y	N	N	Y

Part 2. (Continued)

State	Neglect	Pile Bending Infl. Pt.	Prebore	Backfill	Approach Pvmt. on Abutment
TN	Y	N	N	Gran.	Y
UT	Y	N	N	Gran.	Y
VA	Y	N	N	Gran.	N
VT	Y	N	N	---	N
WA	N	N	N	Gran.	Y
WS	Y	N	N	Gran.	N
WY	Y	N	N	Gran.	Y
R15	Y	N	N	Perv.	Y

Y Yes
N No
--- No Response

Approach Pvmt. on Abutment	Construction Cost			Maintenance Cost		
	More	Same	Less	More	Same	Less
Y	N	N	Y	N	N	Y
Y	N	N	Y	N	N	Y
N	N	N	N	N	N	N
N	N	N	Y	N	N	Y
Y	N	N	Y	N	N	Y
N	N	N	Y	N	N	Y
Y	N	N	Y	N	N	Y
Y	N	N	Y	N	Y	N

Part 3. Summary of responses to Question 4.

State	Steel	Timber	Concrete
AL	*	*	*
AZ	9 ksi in Brg., <9 ksi in Fric.	Not used	In friction only
CA	Assume 5 kips Lat. Resis./pile	Same as steel	13 k. Lat. R./pile
CO	*	Not used	Not used
CT	Use in bearing	---	---
GA	Use in weak axis	Not used	Not used
IA	Use in weak axis, Fric. only	Use of Br. Length < 150'	Not used
ID	*	Not used	Not used
IN	Use H-pile or shell	---	---
KS	Mostly used in bearing	Mostly used in bearing	Mostly used in Brg.
KY	Used in Brg. or friction	---	Used in friction
NO	10' minimum length	Not used	Used in friction
NT	9 ksi in bearing	Used in friction	Not used
ND	*	*	*
NE	Used in weak axis	---	---
NM	Use steel only	Not used	Not used

Part 3. (Continued).

State	Steel	Timber	Concrete
NY	*	Not used	*
OH	*	Not used	*
OK	Use in bearing	Not used	Not used
OR	*	Not used	*
SD	*	*	*
TN	*	Not used	*
UT	Use in single row	Use in single row	Use in single row
VA	Upper portion allowed to flex	---	---
VT	15' minimum length	Not used	Not used
WA	Use in bearing or friction	Use in Brg. or Fric.	Use in Brg. or Fric.
WS	Use in bearing or friction	Use in friction	Use in Brg. or Fric.
WY	Use in bearing or friction	Not used	Not used
R15	Use in weak axis	Not used	Not used

*No limitations

--- No response

12. APPENDIX B: QUESTIONNAIRE FOR SKEWED BRIDGES WITH INTEGRAL ABUTMENTS AND SUMMARY OF RESPONSES

Part 1. Questionnaire for Skewed Bridges with Integral Abutments.

1. If you design skewed bridges with integral abutments, which of the kinds of pile orientations shown below do you use in the integral abutments? If neither, please sketch the type of pile orientation you use.

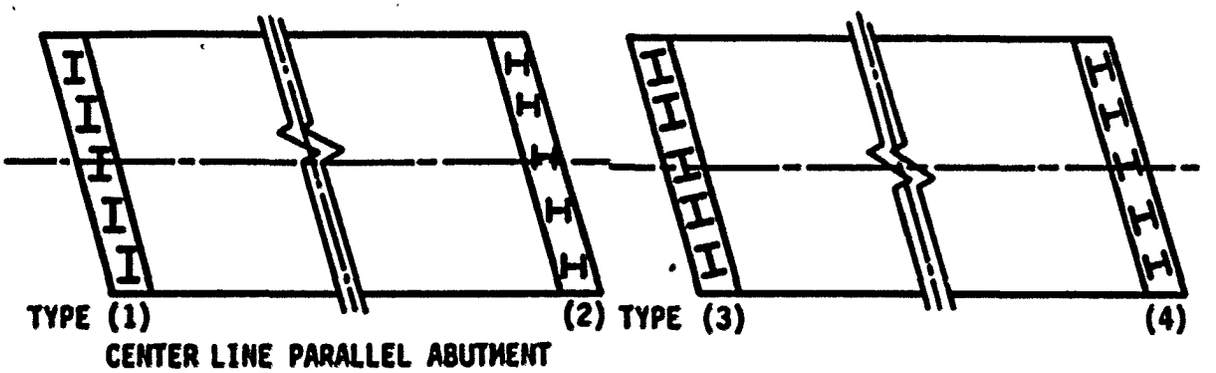

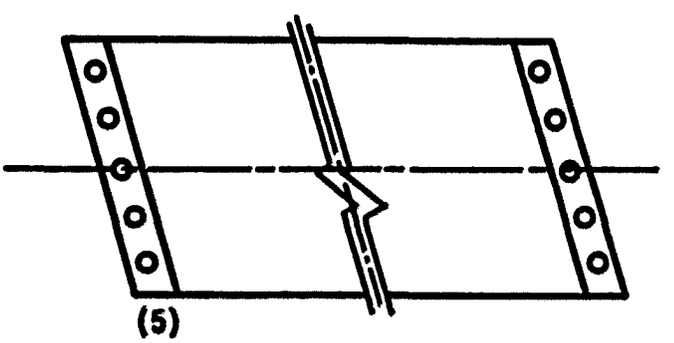

2. If you use either orientation, what structural assumptions are made for (1) the top of the pile, (2) thermal expansion or contraction (one direction or both directions) and (3) diagonal thermal expansion or contraction?

3. When you design skewed bridges with integral abutments, how do you treat the approach slab, backfill, and pile cap?

4. Any additional comments on skewed bridges with integral abutments?

Part 2. Summary of responses by the different states.

State	Pile Orientation					Structural Assumption				
	1(a)	1(b)	2(a)	2(b)	3	Pile Head	Thermal Exp. & Cont.			Ap
							Long.	Trans.	Diag.	
AK			--		---		---	---	---	---
AZ	N	N	N	Y	N	Roller	Y (due to roller)	Restrained by abutment cap	N	Is t ment and fort supe
CA	N	N	N	Y	N	Hinge	N	N	N	
CO	Y	Y	Y	Y	N	---	---	---	---	Bridg 200' slab
CT	N	N	N	N	N	N	N	N	N	N
GA	Y	N	N	N	N	Free translation; free rotation; roller	Y	Y	N	Expan betwe slab
IA	N	N	Y	N	N	Fixed	Y	N	N	
ID	N	N	Y	Y	N	Fixed	Y	Y	---	1) Ex is sp rigid proac 2) No ment flexi

Design Consideration				Comment
Cont.	Approach Slab	Backfill	Pile Cap	
Diag.				
---	---	---	---	---
ined ment N	Is tied to abutment with dowels and moves back & forth with the superstructure	N	N	---
N	---	---	---	Battered piles are used to resist the active earth pressure
---	Bridge length > 200' use approach slab	N	N	1) Steel bridge $\leq$250'; concrete bridge $\leq$350' 2) No problem in skew 3) Use pre-drilled oversize hole
N	N	N	N	---
N	Expansion joint between the approach slab & bridge slab	---	---	---
N	Neglect	Neglect	Neglect	Conservative design
---	1) Expansion joint is specified between rigid pavement & approach slab. 2) No special treatment is specified for flexible pavement	Use free draining granular material as backfill	Rigid pile cap	A skewed three span steel girder bridge with integral abutment was built. Rotational forces from the lateral earth pressure on the end wall caused a failure in the pier anchor bolts on the exterior girder

Part 2. (Continued)

State	Pile Orientation					Structural Assumption				
	1(a)	1(b)	2(a)	2(b)	3	Pile Head	Thermal Exp. & Cont.			App
							Long.	Trans.	Diag.	
IN	N	N	N	Y	N	Hinge	N	N	N	20' ap integr ed to
KS	N	N	Y	Y	N	Hinge	Y	Y	N	Uses s at bac ment r approx of wea
KY	Y	N	N	N	N	Partially restrained	Y	N	---	No spe with f ment
MO	N	N	N	Y	N	Fixed	N	N	N	
MT	N	N	N	Y	N	N	N	N	N	Not fi ment

Cont. Diag.	Design Consideration: Approach Slab	Backfill	Pile Cap	Comment
N	20' approach slab integrally attached to bridges	Use select granular fill	Pile is cast in pile cap 1 ft.	150' maximum
N	Uses slab support at backwall and pavement rests on slab w/ approx. 30' from end of wearing surface	Backfill compaction has settlement just off end of bridge	Pile caps are not used	Cast-in-plate bridges w/ the end of steel beams into abutment concrete, reinforcing to make them essentially integral
---	No special treatment with flexible pavement	Special granular backfill specified	---	Bridge length 300', max skews $\leq 30°$, pile prebored for distance of 8' before bottom of pile cap
N	---	---	Use shear key on bottom of pile cap to prevent lateral movement of pile cap on extreme skews ($\pm 40°$)	Piles designed for direct load only: <500' for prestressed bridges, <400' for steel bridges
N	Not fixed to abutment	Granular material as backfill	N	$\leq 30°$ skews

Part 2. (Continued)

State	Pile Orientation					Structural Assumption				
	1(a)	1(b)	2(a)	2(b)	3	Pile Head	Thermal Exp. & Cont.			Ap
							Long.	Trans.	Diag.	
ND	N	N	N	Y	N	Fixed	Y	Y	N	Assum slab t
NE	Y	N	N	N	N	---	Y	N	N	Same bridg abutm
NM	N	N	Y	N	N	Fixed	Y	N	N	Used not us
NY	N	N	Y	N	N	---	N	N	N	Const is pr appro bridg
OH	N	N	Y	N	N	---	N	N	N	Tie t slab t
OK	N	N	N	N	N	---	---	---	---	
OR	N	N	N	Y	N	Hinge	---	---	---	Approa tied t

ion		Design Consideration			Comment
Exp. & Cont.		Approach Slab	Backfill	Pile Cap	
Trans.	Diag.				
Y	N	Assume approach slab has no effect	Select granular material	Abutment wall is pile cap & is reinforced to resist bending below super structure	Hold skew to a max of 30°
N	N	Same as square bridges bridges with integral abutments	"	"	15° skew for integral abutment
N	N	Used on some bridges not used on others	Do not use specified backfill anymore	---	Have built bridges with 15° skew; skew angle neglected
N	N	Construction joint is provided between approach slab & bridge slab	Granular fill behind backwall & wing walls	N	1) Neglect stress caused by rotation; designed to take vertical load only 2) In skewed bridges, neglect some twisting induced in piles when structure deflects. Use pre-drilled oversize hole
N	N	Tie the approach slab to abutment	Same as non integral abutments for usual short bridge	Pile is cast in pile cap 2 ft.	Oil country pipe lines are not used in integral abutments, because they are stiffer than H-piles about weak axis
---	---	---	---	---	Integral abutments only with zero skews
---	---	Approach slab was tied to pile cap	---	Pile is cast in pile cap 1 ft.	---

Part 2. (Continued)

State	Pile Orientation					Structural Assumption				
	1(a)	1(b)	2(a)	2(b)	3	Pile Head	Thermal Exp. & Cont.			Appr
							Long.	Trans.	Diag.	
SD	Y	N	Y	N	N	Fixed	Y	N	N	Tied w/ prevent of shou
TN	N	N	N	Y	N	---	Y	N	N	A const between backwal slab
UT	N	N	N	N	Y	Hinge	---	---	---	Expansi tween a & bridg
VA	N	N	Y	N	N	Fixed	N	N	N	No appr
VT	N	N	N	Y	N	Fixed	Y	N	N	The app anchore ment
WA	Y	N	N	Y	Y	Hinge	Y	N	N	Approac tached with al expansi

Design Consideration					Comment
p. & Cont.		Approach Slab	Backfill	Pile Cap	
ans.	Diag.				
N	N	Tied w/bridge to prevent erosion of shoulder	---	N	---
N	N	A construction joint between the abutment backwall & approach slab	N	N	---
---	---	Expansion joint between approach slab & bridge slab	96% of optimum	N	1) Steel piles used primarily thru granular material over bed rock 2) No problem in thermal movements
N	N	No approach slab	Used 1'-6" of porous backfill w/ 6" dia. pipe underdrain	Uniform width & parallel to bridge skew	Max. skew 10°; relatively small movement at each abutment (±3/8")
N	N	The approach slab is anchored to the abutment	No special treatment	Rigid pile cap	≤30° skew
N	N	Approach slab is attached to abutment with allowance for expansion	Backfill earth pressure is applied normal to abutment	Pile cap is designed as cross beam on simple supports	Calculate moments of inertia along roadway center

Part 2. (Continued)

State	Pile Orientation					Structural Assumption				
	1(a)	1(b)	2(a)	2(b)	3	Pile Head	Thermal Exp. & Cont.			App
							Long.	Trans.	Diag.	
WS	N	N	N	Y	Y	---	N	N	N	Design load c
WY	N	N	N	Y	N	Plastic Hinge	Y	Y	N	
R15	N	N	Y	N	N	Hinge	N	N	N	

Design Consideration					Comment
). & Cont.		Approach Slab	Backfill	Pile Cap	
ns.	Diag.				
N	N	Designed for vertical load only	---	Designed as reinforced continuous beam over piling	Piles designed for vertical loads ≤30° for slabs; ≤15° for prestressed or or steel girders
Y	N	Neglect	Neglect	Assumed to be a mass attached to end of girder	Max length ≤300'
N	N	---	---	Pile was cast in pile cap 1 ft.	---

13. APPENDIX C: IAB3D AND IAB2D PROGRAM INPUT

13.1. IAB3D Program Input

The program uses a fixed input format, so all data must be input exactly according to the format specified for each card, and the card groups must appear in sequence according to their number. An outline of the data is given in Table 14. This part gives the order in which the data appears and when it can be omitted. Prior to constructing his own data sets, the user is advised to peruse the data sets for some sample problems.

Table 14. Input data structure overflow

Card Group	Description	When Needed
1	Title	Always
2	Pile data sets	Always
3	Soil data sets	When soil spring elements appear
4	Nodal data sets	Always

The details of the data sets for each data group are as follows. The data card for each card group is given by CARD a.b in which a represents the card group and b represents the card number.

CARD 1.1 (20A4)

Cols.	FORTRAN Name	Description
1-80	TITLE	Any 80 alphanumeric characters to identify the problem: these characters

will be printed as a heading to the output.

CARD 2.1 (2I4)

Cols.	FORTRAN Name	Description
1-4	NMP	Number of nodes in the structure
5-8	NM	Number of elements in the structure

CARD 2.2 (2F9.3)

Cols.	FORTRAN Name	Description
1-9	PIL	Pile length
10-18	AREAP	Pile tip area

CARD 2.3 (I4, I6, 3F12.5)

Cols.	FORTRAN Name	Description
1-4	IM	Nodal number
5-10	KODE	One or more degrees of freedoms at node IM are specified. There are six integers to define the translations and rotations in the X, Y, and Z directions, respectively. 0 indicates no constraints on that degree of freedom. 1 indicates that the displacement or rotation component is specified
11-22	XC	X - coordinate of node IM
23-34	YC	Y - coordinate of node IM
35-46	ZC	Z - coordinate of node IM

CARD 2.4 (I3, 3F12.5)

Cols.	FORTRAN Name	Description
1-3	IM	Element number
4-15	XK	X - coordinate of K node
16-27	YK	Y - coordinate of K node
28-39	ZK	Z - coordinate of K node

CARD 2.5 (6I3, 3I8.3)

Cols.	FORTRAN Name	Description
1-3	IM	Element number
4-6	NODI	Node I on element IM
7-9	NODJ	Node J on element IM
10-12	MAT	Member type on element IM 0 indicates no spring elements attached 1 indicates lateral and vertical spring elements attached 2 indicates lateral, vertical, and point spring elements attached
13-16	IAX	Member cross-sectional shape on element IM 1 indicates rectangular cross section 2 indicates wide flange cross section (y-axis along the web) 3 indicates wide flange cross section (z-axis along the web)

		4 indicates arbitrary shape not covered by any of the above
17-20	ITEMP	Temperature changes on element IM 0 indicates no temperature changes 1 indicates temperature changes
21-28	SW	Section width
29-36	SD	Section depth
37-44	DC	Distance from the bottom of the cross section to the centroid

CARDS 2.5.1-2.5.6 depend on the cross section shapes. IAX = 1 uses CARD 2.5.1, IAX = 2 uses CARD 2.5.2, IAX = 3 uses CARD 2.5.3, and IAX = 4 uses CARDS 2.5.4, 2.5.5, and 2.5.6.

CARD 2.5.1 to 2.5.4 (4F8.3, 4I3)

Cols.	FORTRAN Name	Description
1-8	FT	Flange thickness or 0.0
9-16	WT	Web thickness or 0.0
17-24	WD	Section depth
25-32	FW	Section width, flange width, or 0.0
33-36	N1	The number of divisions along the width for IAX = 1
	N3	The number of divisions along the flange thickness for IAX = 2
	N7	The number of divisions along the flange thickness for IAX = 3

	N11	The total number of divisions of the arbitrary cross section
37-39	N2	The number of divisions along the depth for IAX = 1
	N4	The number of divisions along the flange width for IAX = 2
	N8	The number of divisions along the flange width for IAX = 3
40-42	N5, N9	The number of divisions along the web depth for IAX = 2 and 3, respectively
	N6, N10	The number of divisions along the web thickness for IAX = 2 and 3, respectively

CARD 2.5.5 (2F8.3, F9.3, 2F15.5)

Cols.	FORTRAN Name	Description
1-8	ZG	Distance from centroid of the subelement to centroid of the cross section along the z-direction for IAX = 4
9-16	YG	Distance from centroid of the subelement to centroid of the cross section along the y-direction for IAX = 4
17-25	AG	Area of the subelement for IAX = 4
26-40	XGY	Moment of inertia of the subelement with respect to y-axis for IAX = 4
41-55	XGZ	Moment of inertia of the subelement with respect to z-axis for IAX = 4

CARD 2.5.6 (F15.5)

Cols.	FORTRAN Name	Description
1-15	XIN	Torsional constant for IAX = 4

CARD 2.6 (E12.3, F5.2, E12.3, E12.3, E12.3)

Cols.	FORTRAN Name	Description
1-12	E	Initial modulus of elasticity of the beam-column element
13-17	CN	Shape parameter
18-29	FY	Yield stress
30-41	AFH	Coefficient of thermal expansion
42-53	GMOD	Shear modulus

CARD 3.1 (F15.5, F10.5, F15.5)

Cols.	FORTRAN Name	Description
1-15	SSI	Initial lateral stiffness in y-direction for MAT $\neq$ 0
16-25	CH	Shape parameter
26-40	PH	Ultimate lateral soil resistance in y-direction

CARD 3.2 (F15.5, F10.5, F15.5)

Cols.	FORTRAN Name	Description
1-15	SSJ	Initial lateral stiffness in z-direction for MAT $\neq$ 0
16-25	CL	shape parameter

26-40	PL	Ultimate lateral soil resistance in z-direction

CARD 3.3 (F15.5, F10.5, F15.5)

Cols.	FORTRAN Name	Description
1-15	SKI	Initial vertical stiffness for MAT ≠ 0
16-25	CV	shape parameter
26-40	PV	Maximum shear stress

CARD 3.4 (F15.5, F10.5, F15.5)

Cols.	FORTRAN Name	Description
1-15	SPI	Initial point stiffness
16-25	CP	shape parameter
26-40	PP	Maximum bearing stress

CARD 4.1 (I2)

Cols.	FORTRAN Name	Description
1-2	LDCASE	Load cases LDCASE = 1 represents the initial stage LDCASE = 2 represents the second one and the consecutive stages

CARD 4.2 (I2)

Cols.	FORTRAN Name	Description
1-2	LDOF	The total number of degrees of freedoms

		which prescribed load/displacement were applied for each load case.

CARD 4.3 (F10.5)

Cols.	FORTRAN Name	Description
1-10	DCOV	Use-prescribed tolerance

CARD 4.4 (2I4)

Cols.	FORTRAN Name	Description
1-4	JICR	The number of increments for each load case
5-8	JTER	The maximum number of iterations for each increment

CARD 4.5 (I3)

Cols.	FORTRAN Name	Description
1-3	IDOF	The degree of freedom of the node which the prescribed load/displacement was applied for each load case

CARD 4.6 (F9.3)

Cols.	FORTRAN Name	Description
1-9	T	The prescribed load/displacement was applied at the degree of freedom for each load case

CARD 4.7 (2F9.2)

Cols.	FORTRAN Name	Description
1-9	TEMP	The temperature changes at the top of the element for each load case if ITEMP ≠ 0
10-18	TEMP	The temperature changes at the bottom of the element for each load case of ITEMP ≠ 0

13.2. Sample Problems for IAB3D Computer Program

Sample problem 1: The large displacement response of a cantilevered 45° bend beam subjected to a concentrated end load, as shown in Fig. 26. The input data cards are given in Table 15. Eight equal straight beam-column elements are used.

Sample problem 2: The soil problem presented here is used to check the soil material nonlinearity and cyclic behavior of the lateral springs in the direction of 45° with respect to Y and Z directions. The input data cards are given in Table 16.

Table 15. Input cards for sample problem 1-a 45° cantilevered bend beam

```
12345678901234567890123456789012345678901234567890123456789012345678901234567890123  CARD
                                                                                       NO.

YANG3D EXAMPLE                                                                         1.1
   9   8                                                                               2.1
    0.000     0.000                                                                    2.2
   1111111      0.00000       0.00000       0.00000                                   2.3
   2000000      9.80171       0.00000       0.48153                                   2.3
   3000000     19.50903       0.00000       1.92147                                   2.3
   4000000     29.02847       0.00000       4.30597                                   2.3
   5000000     38.26834       0.00000       7.61205                                   2.3
   6000000     47.13967       0.00000      11.80787                                   2.3
   7000000     55.55702       0.00000      16.85304                                   2.3
   8000000     63.43933       0.00000      22.69895                                   2.3
   9000000     70.71068       0.00000      29.28932                                   2.3
  1      4.90086      5.00000      0.24077                                           2.4
  2     14.65537     10.00000      1.20150                                           2.4
  3     24.26875     15.00000      3.11372                                           2.4
  4     33.64841     20.00000      5.95901                                           2.4
  5     42.70741     25.00000      9.70996                                           2.4
  6     51.34835     30.00000     14.33046                                           2.4
  7     59.49818     35.00000     19.77600                                           2.4
  8     67.07501     40.00000     25.99414                                           2.4
  1  1  2  0  1  0    1.000    1.000    0.500                                        2.5
   0.000    0.000    1.000    1.000  8  8                                           2.5.1
  2  2  3  0  1  0    1.000    1.000    0.500                                        2.5
   0.000    0.000    1.000    1.000  8  8                                           2.5.1
  3  3  4  0  1  0    1.000    1.000    0.500                                        2.5
   0.000    0.000    1.000    1.000  8  8                                           2.5.1
  4  4  5  0  1  0    1.000    1.000    0.500                                        2.5
   0.000    0.000    1.000    1.000  8  8                                           2.5.1
  5  5  6  0  1  0    1.000    1.000    0.500                                        2.5
   0.000    0.000    1.000    1.000  8  8                                           2.5.1
  6  6  7  0  1  0    1.000    1.000    0.500                                        2.5
   0.000    0.000    1.000    1.000  8  8                                           2.5.1
  7  7  8  0  1  0    1.000    1.000    0.500                                        2.5
   0.000    0.000    1.000    1.000  8  8                                           2.5.1
  8  8  9  0  1  0    1.000    1.000    0.500                                        2.5
```

Table 15. (Continued)

```
  0.000    0.000    1.000    1.000  8  8                          2.5.1
  1.000E+0415.00    1.200E+08    6.500E-06    5.000E+03           2.6
  1.000E+0415.00    1.200E+08    6.500E-06    5.000E+03           2.6
  1.000E+0415.00    1.200E+08    6.500E-06    5.000E+03           2.6
  1.000E+0415.00    1.200E+08    6.500E-06    5.000E+03           2.6
  1.000E+0415.00    1.200E+08    6.500E-06    5.000E+03           2.6
  1.000E+0415.00    1.200E+08    6.500E-06    5.000E+03           2.6
  1.000E+0415.00    1.200E+08    6.500E-06    5.000E+03           2.6
  1.000E+0415.00    1.200E+08    6.500E-06    5.000E+03           2.6
2                                                                 4.1
1                                                                 4.2
1                                                                 4.2
  0.01                                                            4.3
  1  20                                                           4.4
 45  20                                                           4.4
50                                                                4.5
50                                                                4.5
   0.000                                                          4.6
   0.450                                                          4.6
```

Table 16. Input cards for sample problem 2 - soil problem

```
12345678901234567890123456789012345678901234567890123456789123  CARD
                                                                 NO.

YANG3D EXAMPLE                                                    1.1
   2   1                                                          2.1
  180.000  198.895                                               2.2
   1000100      0.00000      0.00000      0.00000                2.3
   2000100    180.00000      0.00000      0.00000                2.3
  1     90.00000     45.00000      0.00000                       2.4
  1  1  2  2  2  0  14.586  13.636   6.818                        2.5
   0.506   0.506  13.635  14.586  2  7 10  1                     2.5.1
   3.000E+0415.00   3.600E+01   6.500E-06   1.200E+04            2.6
```

Table 16. (Continued)

```
        8.33333   3.00000        16.66667                3.1
        8.33333   3.00000        16.66667                3.2
        9.33333  10.00000         8.33333                3.3
        0.69444  10.00000         0.69444                3.4
4                                                        4.1
4                                                        4.2
4                                                        4.2
4                                                        4.2
4                                                        4.2
  0.01                                                   4.3
   1   20                                                4.4
  10   20                                                4.4
  20   20                                                4.4
  20   20                                                4.4
   2                                                     4.5
   3                                                     4.5
   8                                                     4.5
   9                                                     4.5
   2                                                     4.5
   3                                                     4.5
   8                                                     4.5
   9                                                     4.5
   2                                                     4.5
   3                                                     4.5
   8                                                     4.5
   9                                                     4.5
   2                                                     4.5
   3                                                     4.5
   8                                                     4.5
   9                                                     4.5
    0.000                                                4.6
    0.000                                                4.6
    0.000                                                4.6
    0.000                                                4.6
  707.107                                                4.6
  707.107                                                4.6
  707.107                                                4.6
  707.107                                                4.6
 -707.107                                                4.6
 -707.107                                                4.6
 -707.107                                                4.6
 -707.107                                                4.6
  707.107                                                4.6
  707.107                                                4.6
  707.107                                                4.6
  707.107                                                4.6
```

13.3. IAB2D Program Input

The structure of the input data in IAB2D computer program is similar to the input data cards in IAB3D computer program. However, in this two-dimensional version, free format is used for input since the IAB2D computer progarm was executed in the VAX system. The input data are separated by putting a comma or blank. The following are the line numbers used to identify the sequence of the input data.

LINE 1 (20A4)

FORTRAN Name	Description
TITLE	Any 80 alphanumeric characters to identify the problem: these characters will be printed as a heading to the output

LINE 2

FORTRAN Name	Description
NMP	Number of nodes in the structure
NM	Number of elements in the structure
JTSOIL	Node where the soil starts
IAY	Dummy variable which is not used in the program, however, it can be used as a control key to control output

LINE 3

FORTRAN Name	Description
PIL	Pile length
ARZAP	Pile tip area

LINE 4

FORTRAN Name	Description
I	Nodal number
KODE (I,J)	One or more degrees of freedoms at node I are specified. There are three degrees of freedoms per node to define the translations in X and Y directions and the rotation in the Z direction; respectively, for each load change 0 indicates no constraints on that degree of freedom 1 indicates that the displacement or rotation component is specified
XC	X - coordinate of node I
YC	Y - coordinate of node I

LINE 5

FORTRAN Name	Description
I	Element number
IAX	Member cross-sectional shape on element I

	0 indicates arbitrary cross-sectional shape
	1 indicates wide flange cross section (bending about the strong axis)
	2 indicates wide flange cross section (bending about the weak axis)
	3 indicates rectangular cross section
	4 indicates any shape of the cross section which is symmetry with respect to neutral axis
	5 control key to generate input automatically for IAX = 4
ITEMP	Temperature changes on element I
	0 indicates no temperature changes
	1 indicates temperature changes
NODI	Node I on element I
NODJ	Node J on element I
FT	Flange thickness or 0.0
WT	Web thickness or 0.0
WD	Section depth
FW	Section width, flange width, or 0.0
PER	Perimeter of the cross section
B	Section width
DC	Distance from the bottom of the cross section to the centroid

LINE 5.1

FORTRAN Name	Description
AR	Area of the subelement for IAX=0 on each element
Y	Distance from centroid of the subelement to centroid of the cross section along the y-direction for IAX=0 on each element
XR	Moment inertia of the subelement with respect to y-axis for IAX=0 on each element

LINE 5.2

FORTRAN Name	Description
AR,Y,XR	The same descriptions as listed in LINES 1, except only input the data of the upper half of the cross section (7 subelements) for IAX=4 on the first element. It will generate the data of the lower half of the cross section (7 subelements) and the rest of the elements have the same shapes

LINE 6

FORTRAN Name	Description
E	Initial modulus of elasticity of the beam-column element

CN	Shape parameter
PY	Yield stress
APH	Coefficient of thermal expansion

LINE 7

FORTRAN Name	Description
SSI	If the lateral spring elements are attached, then input initial stiffness. Otherwise input 0.0
CH	If the lateral spring elements are attched, then input shape parameter Otherwise input nonzero value
PH	If the lateral spring elements are attached, then input ultimate soil resistance. Otherwise input nonzero value

LINE 8

FORTRAN Name	Description
SKI,CV,PV	The same descriptions as listed in LINE 7, except only for vertical springs

LINE 9

FORTRAN Name	Description
SPI,CP,PP	The same description as listed in LINE 7 except only for point springs at the last element

LINE 10

FORTRAN Name	Description
LDCHAN	Number of load changes LDCHAN=1 represents the initial stage LDCHAN=2 represents the second and the consecutive stages

LINE 11

FORTRAN Name	Description
LDOF	The total number of degrees of freedoms which prescribed load/displacement were applied for each load change

LINE 12

FORTRAN Name	Description
DCOV	User-prescribed tolerance

LINE 13

FORTRAN Name	Description
JICR	The number of increments for each load change

JTZR	The maximum number of iterations for each increment

LINE 14

FORTRAN Name	Description
IDOF	The degree of freedom at the node which the prescribed load/displacement was applied for each load change

LINE 15

FORTRAN Name	Description
T	The prescribed load/displacement was applied at the degree of freedom for each load change

LINE 16

FORTRAN Name	Description
TEMP	The temperature changes at the top and bottom of the element for each load change of ITEMP $\neq$ 0

LINE 17

FORTRAN Name	Description
INODE	The total number of nodes where the boundary conditions change for LDCHAN > 3

LINE 18

FORTRAN Name	Description
LNODE	Nodes where the boundary conditions change for LDCHAN > 3

LINE 19

FORTRAN Name	Description
KODE	One or more degrees of freedoms at node where the boundary conditions change for LDCHAN > 3

13.4. Sample Problem for IAB2D Computer Program

Sample Problem 3: The State Avenue bridge example is illustrated here to demonstrate the input data for IAB2D computer program. The input data are given in Table 17.

Table 17. Input data for sample problem 3 - State Avenue bridge

```
12345678901234567890123456789012345678901234567890123   LINE NO.
'YANG2D EXAMPLE STATE AVE.'                                1
21,20,7,1                                                  2
480.0,97.96                                                3
1,111,0.0,570.0                                            4
2,000,240.0,570.0                                          4
3,000,480.0,570.0                                          4
4,000,720.0,570.0                                          4
5,010,960.0,570.0                                          4
6,000,1200.0,570.0                                         4
7,000,1440.0,570.0                                         4
8,000,1440.0,525.0                                         4
9,000,1440.0,480.0                                         4
10,000,1440.0,456.0                                        4
11,000,1440.0,432.0                                        4
12,000,1440.0,408.0                                        4
13,000,1440.0,384.0                                        4
14,000,1440.0,336.0                                        4
15,000,1440.0,288.0                                        4
16,000,1440.0,240.0                                        4
17,000,1440.0,192.0                                        4
18,000,1440.0,144.0                                        4
19,000,1440.0,96.0                                         4
20,000,1440.0,48.0                                         4
21,000,1440.0,0.0                                          4
1,0,1,1,2,7.5,7.0,52.5,71.0,247.0,71.0,35.53               5
24.29,1.735,97.49                                          5.1
10.0625,4.02,163.49                                        5.1
32.8125,5.72,1090.66                                       5.1
32.8125,8.22,2234.18                                       5.1
177.5,10.72,20490.46                                       5.1
177.5,13.22,31113.84                                       5.1
177.5,15.72,43955.96                                       5.1
50.26,-3.59,863.67                                         5.1
50.26,-10.765,6040.31                                      5.1
50.26,-17.94,16391.78                                      5.1
28.21875,-23.16,15154.10                                   5.1
42.65625,-26.11,29122.10                                   5.1
66.5,-29.53,58078.06                                       5.1
66.5,-33.53,74852.02                                       5.1
2,0,1,2,3,7.5,7.0,52.5,71.0,247.0,71.0,35.53               5
```

Table 17. (Continued)

24.29,1.735,97.49	5.1
10.0625,4.02,163.49	5.1
32.8125,5.72,1090.66	5.1
32.8125,8.22,2234.18	5.1
177.5,10.72,20490.46	5.1
177.5,13.22,31113.84	5.1
177.5,15.72,43955.96	5.1
50.26,-3.59,863.67	5.1
50.26,-10.765,6040.31	5.1
50.26,-17.94,16391.78	5.1
28.21875,-23.16,15154.10	5.1
42.65625,-26.11,29122.10	5.1
66.5,-29.53,58078.06	5.1
66.5,-33.53,74852.02	5.1
3.0,1.3,4.7.5,7.0,52.5,71.0,247.0,71.0,35.53	5
24.29,1.735,97.49	5.1
10.0625,4.02,163.49	5.1
32.8125,5.72,1090.66	5.1
32.8125,8.22,2234.18	5.1
177.5,10.72,20490.46	5.1
177.5,13.22,31113.84	5.1
177.5,15.72,43955.96	5.1
50.26,-3.59,863.67	5.1
50.26,-10.765,6040.31	5.1
50.26,-17.94,16391.78	5.1
28.21875,-23.16,15154.10	5.1
42.65625,-26.11,29122.10	5.1
66.5,-29.53,58078.06	5.1
66.5,-33.53,74852.02	5.1
4.0,1.4,5,7.5,7.0,52.5,71.0,247.0,71.0,35.53	5
24.29,1.735,97.49	5.1
10.0625,4.02,163.49	5.1
32.8125,5.72,1090.66	5.1
32.8125,8.22,2234.18	5.1
177.5,10.72,20490.46	5.1
177.5,13.22,31113.84	5.1
177.5,15.72,43955.96	5.1
50.26,-3.59,863.67	5.1
50.26,-10.765,6040.31	5.1
50.26,-17.94,16391.78	5.1
28.21875,-23.16,15154.10	5.1
42.65625,-26.11,29122.10	5.1
66.5,-29.53,58078.06	5.1
66.5,-33.53,74852.02	5.1
5.0,1.5,6,7.5,5.25,52.5,71.0,247.0,71.0,36.66	5
12.285,1.17,22.42	5.1
8.3125,2.90,70.64	5.1
28.4375,4.59,613.94	5.1

Table 17. (Continued)

```
28.4375,7.09,1444.31                                                    5.1
177.5,9.59,16416.79                                                     5.1
177.5,12.09,26037.29                                                    5.1
177.5,14.59,37876.54                                                    5.1
39.6375,-3.78,754.64                                                    5.1
39.6375,-11.33,5276.51                                                  5.1
39.6375,-18.88,14317.25                                                 5.1
22.96875,-24.32,13598.62                                                5.1
37.40625,-27.26,27817.42                                                5.1
59.5,-30.66,56011.45                                                    5.1
59.5,-34.66,71557.61                                                    5.1
6,0,1,5,7,7.5,5.25,52.5,71.0,247.0,71.0,36.66                           6
12.285,1.17,22.42                                                       5.1
8.3125,2.90,70.64                                                       5.1
28.4375,4.59,613.94                                                     5.1
28.4375,7.09,1444.31                                                    5.1
177.5,9.59,16416.79                                                     5.1
177.5,12.09,26037.29                                                    5.1
177.5,14.59,37876.54                                                    5.1
39.6375,-3.78,754.64                                                    5.1
39.6375,-11.33,5276.51                                                  5.1
39.6375,-18.88,14317.25                                                 5.1
22.96875,-24.32,13598.62                                                5.1
37.40625,-27.26,27817.42                                                5.1
59.5,-30.66,56011.45                                                    5.1
59.5,-34.66,71557.61                                                    5.1
7,3,0,7,8,0,0,0,0,36.0,71.0,214.0,71.0,18.0                             5
8,3,0,8,9,0,0,0,0,36.0,71.0,214.0,71.0,18.0                             5
9,2,0,9,10,0.418,0.418,9.72,10.078,39.60,9.72,5.039                     5
10,2,0,10,11,0.418,0.418,9.72,10.078,39.60,9.72,5.039                   5
11,2,0,11,12,0.418,0.418,9.72,10.078,39.60,9.72,5.039                   5
12,2,0,12,13,0.418,0.418,9.72,10.078,39.60,9.72,5.039                   5
13,2,0,13,14,0.418,0.418,9.72,10.078,39.60,9.72,5.039                   5
14,2,0,14,15,0.418,0.418,9.72,10.078,39.60,9.72,5.039                   5
15,2,0,15,16,0.418,0.418,9.72,10.078,39.60,9.72,5.039                   5
16,2,0,16,17,0.418,0.418,9.72,10.078,39.60,9.72,5.039                   5
17,2,0,17,18,0.418,0.418,9.72,10.078,39.60,9.72,5.039                   5
18,2,0,18,19,0.418,0.418,9.72,10.078,39.60,9.72,5.039                   5
19,2,0,19,20,0.418,0.418,9.72,10.078,39.60,9.72,5.039                   5
20,2,0,20,21,0.418,0.418,9.72,10.078,39.60,9.72,5.039                   5
4000.0,15.0,12.0,6.0E-06                                                6
4000.0,15.0,12.0,6.0E-06                                                6
4000.0,15.0,12.0,6.0E-06                                                6
4000.0,15.0,12.0,6.0E-06                                                6
4000.0,15.0,12.0,6.0E-06                                                6
4000.0,15.0,12.0,6.0E-06                                                6
3400.0,15.0,10.2,6.0E-06                                                6
3400.0,15.0,10.2,6.0E-06                                                6
```

Table 17. (Continued)

30000.0,15.0,36.0,6.5E-06	6
30000.0,15.0,36.0,6.5E-06	6
30000.0,15.0,36.0,6.5E-06	6
30000.0,15.0,36.0,6.5E-06	6
30000.0,15.0,36.0,6.5E-06	6
30000.0,15.0,36.0,6.5E-06	6
30000.0,15.0,36.0,6.5E-06	6
30000.0,15.0,36.0,6.5E-06	6
30000.0,15.0,36.0,6.5E-06	6
30000.0,15.0,36.0,6.5E-06	6
30000.0,15.0,36.0,6.5E-06	6
0.0,1.0,10.0	7
0.0,1.0,10.0	7
0.0,1.0,10.0	7
0.0,1.0,10.0	7
0.0,1.0,10.0	7
0.0,1.0,10.0	7
3.385,3.0,1.45	7
7.147,3.0,4.19	7
0.0,3.0,7.1	7
0.0,3.0,9.54	7
0.0,1.0,0.4	7
0.0,1.0,0.546	7
3.064,1.0,0.766	7
3.888,1.0,0.972	7
15.625,2.0,3.125	7
15.625,2.0,3.125	7
15.625,2.0,3.125	7
15.625,2.0,3.125	7
15.625,2.0,3.125	7
15.625,2.0,3.125	7
0.0,1.0,20.0	8
0.0,1.0,20.0	8
0.0,1.0,20.0	8
0.0,1.0,20.0	8
0.0,1.0,20.0	8
0.0,1.0,20.0	8
0.0,1.0,20.0	8
0.0,1.0,20.0	8
0.0,1.0,0.322	8
0.0,1.0,0.322	8
0.0,1.0,0.322	8
0.0,1.0,0.322	8
12.874,1.0,0.322	8
12.874,1.0,0.322	8
20.57,1.0,0.518	8
20.57,1.0,0.518	8

Table 17. (Continued)

20.57,1.0,0.518	8
20.57,1.0,0.518	8
20.57,1.0,0.518	8
20.57,1.0,0.518	8
12.53,1.0,0.3125	9
3	10
1	11
1	11
1	11
0.01	12
1,20	13
6,20	13
25,20	13
20	14
20	14
20	14
0.0	15
0.0	15
-250.0	15
0.0,0.0	16
60.0,60.0	16
60.0,60.0	16
0.0,0.0	16
60.0,60.0	16
60.0,60.0	16
0.0,0.0	16
60.0,60.0	16
60.0,60.0	16
0.0,0.0	16
60.0,60.0	16
60.0,60.0	16
0.0,0.0	16
60.0,60.0	16
60.0,60.0	16
0.0,0.0	16
60.0,60.0	16
60.0,60.0	16
1	17
1	18
111	19